Bio Mar PT

Instituto Português
do Mar e da Atmosfera

Curso de formação

Introdução ao ICP-MS

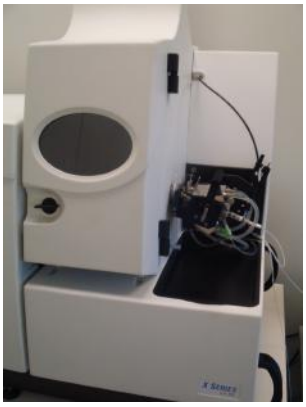
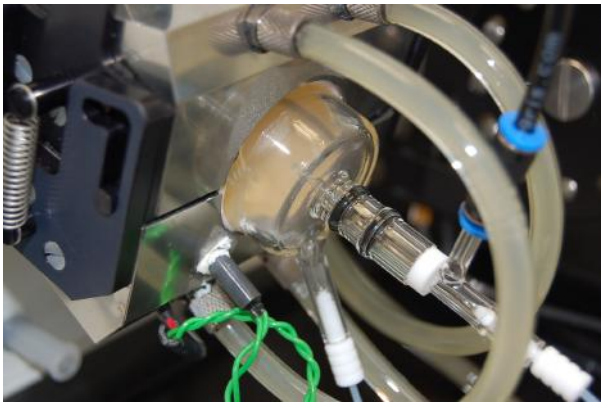


Pedro Brito

eea grants · Governo de Portugal · dgpm Direção-Geral de Política do Mar · ipma · ciimar · emepc

Curso de Introdução ao ICP-MS

Indice

Curso de Introdução ao ICP-MS

Introdução ao ICP-MS

Formador: Pedro Brito (IPMA)

2 a 4 de Novembro de 2016

Instituto Português do Mar e da Atmosfera, I.P. (IPMA)

História e desenvolvimento do ICP-MS

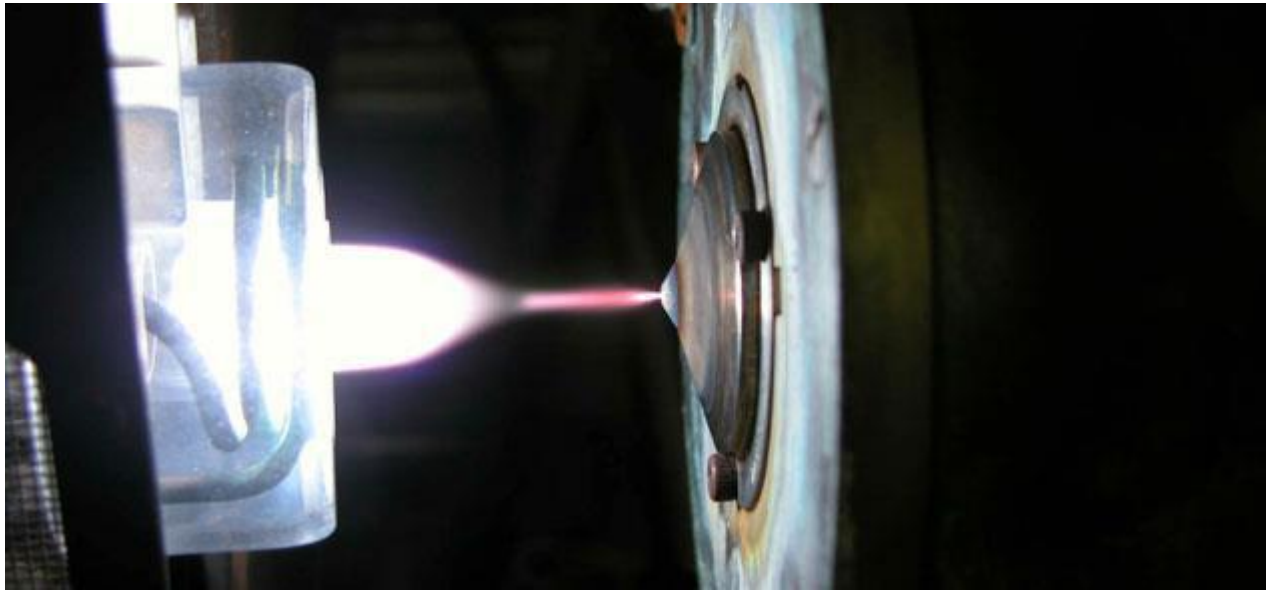

Inductively Coupled Plasma Mass Spectrometry

Espectrometria de Massa com Plasma Acoplado por Indução

- Técnica analítica desenvolvida comercialmente nos anos 80 do século passado;
- Aplicada na determinação de elementos maioritários, minoritários e vestigiais (traço);
- Usada em diversas áreas de investigação e de análise de rotina (geologia, ambiente, medicina, farmacêutica, indústria do petróleo, etc.).

Características do ICP-MS

Larga cobertura elementar

- praticamente todos os elementos da Tabela Periódica

Alta performance

- grande sensibilidade e baixo ruído de fundo -> baixos limiares analíticos (ppt)

Rápido tempo de análise

- 4 minutos por amostra para uma análise de vários elementos

Larga gama de trabalho

- até 9 ordens de grandeza (rectas de calibração de ppt até ppm)

Informação isotópica

Excelente detector cromatográfico


Atomic Number, Symbol
Isotopic Abundance
Most Abundant Isotope
Detection Limit Ranges
< 0.1– 1 ppt
1–10 ppt
10–100 ppt
0.1–1 ppb
1–10 ppb
1 H
2 He
3 Li
4 Be
5 B
6 C
7 N
8 O
9 F
10 Ne
11 Na
12 Mg
13 Al
14 Si
15 P
16 S
17 Cl
18 Ar
19 K
20 Ca
21 Sc
22 Ti
23 V
24 Cr
25 Mn
26 Fe
27 Co
28 Ni
29 Cu
30 Zn
31 Ga
32 Ge
33 As
34 Se
35 Br
36 Kr
37 Rb
38 Sr
39 Y
40 Zr
41 Nb
42 Mo
43 Tc
44 Ru
45 Rh
46 Pd
47 Ag
48 Cd
49 In
50 Sn
51 Sb
52 Te
53 I
54 Xe
55 Cs
56 Ba
57 La
72 Hf
73 Ta
74 W
75 Re
76 Os
77 Ir
78 Pt
79 Au
80 Hg
81 Tl
82 Pb
83 Bi
84 Po
85 At
86 Rn
87 Fr
88 Ra
89 Ac
58 Ce
59 Pr
60 Nd
61 Pm
62 Sm
63 Eu
64 Gd
65 Tb
66 Dy
67 Ho
68 Er
69 Tm
70 Yb
71 Lu
90 Th
91 Pa
92 U
93 Np
94 Pu
95 Am
96 Cm
97 Bk
98 Cf
99 Es
100 Fm
101 Md
102 No
103 Lr

Espectrometria atómica

TÉCNICA	ELEMENTOS	LIMIARES	VANTAGENS	DESVANTAGENS
ICP-MS	Praticamente todos	ppt-ppm	Rápida, sensitiva, multi-elementar, larga gama de trabalho, bom controlo de interferências	TDS
ICP-OES (AES)	Metais e não-metais	ppb-ppm	Rápida, multi-elementar, elevados TDS	Interferências complexas, fraca sensibilidade relativa
GFAAF	Metais	ppt	Sensitiva, poucas interferências	Mono-elementar, gama de trabalho limitada
Hidretos AAS	Elementos que formam hidretos	ppt-ppb	Sensitiva, poucas interferências	Mono-elementar, lenta, complexa
Vapor Frio	Hg	ppt	Sensitiva, simples, poucas interferências	Mono-elementar. lenta

O início...

O primeiro artigo sobre espectrometria de massa com plasma acoplado é publicado em 1975 por Alan Gray (Applied Research Laboratories, Luton, UK), onde o autor descreve o equipamento - *"capillary direct current (DC) arc plasma coupled to a quadrupole mass spectrometer".*

MAY, 1975 Vol. 100, No. 1190

The Analyst

Mass-spectrometric Analysis of Solutions Using an Atmospheric Pressure Ion Source

A. L. Gray

Applied Research Laboratories Limited, Wingate Road, Luton, Bedfordshire

The use of an atmospheric pressure d.c. plasma as an ion source has been explored for the direct analysis of solutions introduced into it from a nebuliser. Ions are extracted from the plasma into a vacuum system and are focused into a quadrupole mass analyser. A high yield of singly charged ions with a small energy spread is obtained and clear spectra of the constituents of the solution are observed.

The method is described and the results observed on simple solutions are given. The sensitivity of the method for a number of elements is indicated and appears to be comparable with other trace-analysis methods.

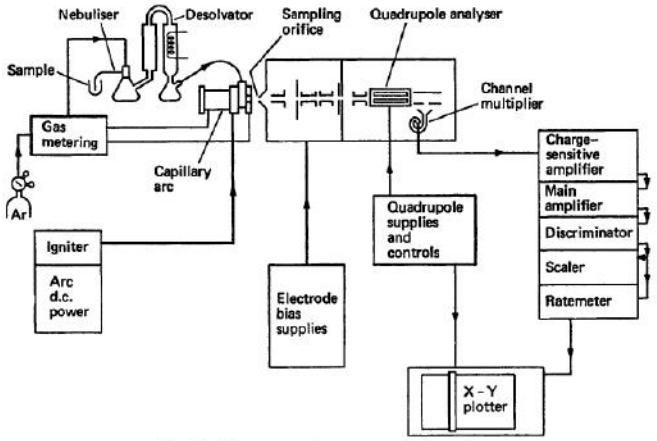

Fig. 1. Plasma sampling mass analysis system.

… e a aventura continuou!

Em 1980 é publicado o primeiro artigo onde se demonstram as possibilidades da técnica de ICP-MS e o primeiro sistema comercial surgiu também nesta década.

Desde o aparecimento dos primeiros sistemas comerciais os maiores desenvolvimentos que ocorreram foram na introdução da amostra, na eficiência do plasma, na transmissão dos iões e na redução de interferências.

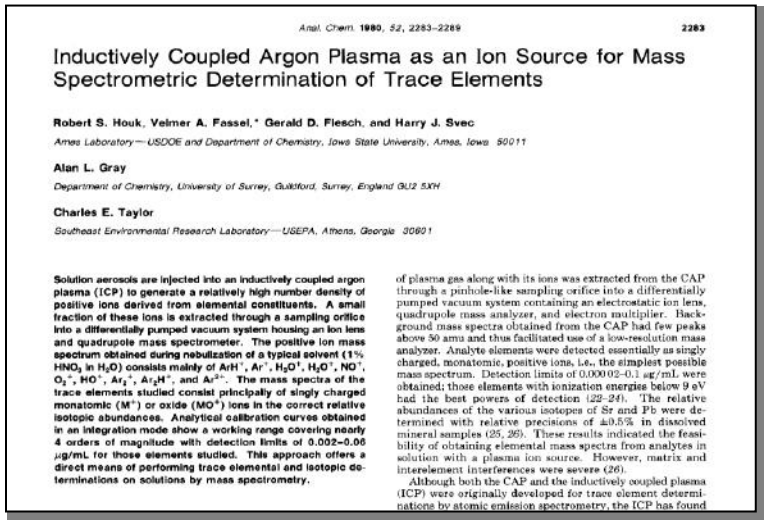

Anal. Chem. 1980, 52, 2283–2289 2283

Inductively Coupled Argon Plasma as an Ion Source for Mass Spectrometric Determination of Trace Elements

Robert S. Houk, Velmer A. Fassel,* Gerald D. Flesch, and Harry J. Svec
Ames Laboratory—USDOE and Department of Chemistry, Iowa State University, Ames, Iowa 50011
Alan L. Gray
Department of Chemistry, University of Surrey, Guildford, Surrey, England GU2 5XH
Charles E. Taylor
Southeast Environmental Research Laboratory—USEPA, Athens, Georgia 30601

Solution aerosols are injected into an inductively coupled argon plasma (ICP) to generate a relatively high number density of positive ions derived from elemental constituents. A small fraction of these ions is extracted through a sampling orifice into a differentially pumped vacuum system housing an ion lens and quadrupole mass spectrometer. The positive ion mass spectrum obtained during nebulization of a typical solvent (1% HNO_3 in H_2O) consists mainly of ArH^+, Ar^+, H_2O^+, H_3O^+, NO^+, O_2^+, HO^+, Ar_2^+, Ar_2H^+, and Ar^{2+}. The mass spectra of the trace elements studied consist principally of singly charged monatomic (M^+) or oxide (MO^+) ions in the correct relative isotopic abundances. Analytical calibration curves obtained in an integration mode show a working range covering nearly 4 orders of magnitude with detection limits of 0.002–0.06 μg/mL for those elements studied. This approach offers a direct means of performing trace elemental and isotopic determinations on solutions by mass spectrometry.

of plasma gas along with its ions was extracted from the CAP through a pinhole-like sampling orifice into a differentially pumped vacuum system containing an electrostatic ion lens, quadrupole mass analyzer, and electron multiplier. Background mass spectra obtained from the CAP had few peaks above 50 amu and thus facilitated use of a low-resolution mass analyzer. Analyte elements were detected essentially as singly charged, monatomic, positive ions, i.e., the simplest possible mass spectrum. Detection limits of 0.00002–0.1 μg/mL were obtained; those elements with ionization energies below 9 eV had the best powers of detection (22–24). The relative abundances of the various isotopes of Sr and Pb were determined with relative precisions of ±0.5% in dissolved mineral samples (25, 26). These results indicated the feasibility of obtaining elemental mass spectra from analytes in solution with a plasma ion source. However, matrix and interelement interferences were severe (26).

Although both the CAP and the inductively coupled plasma (ICP) were originally developed for trace element determinations by atomic emission spectrometry, the ICP has found

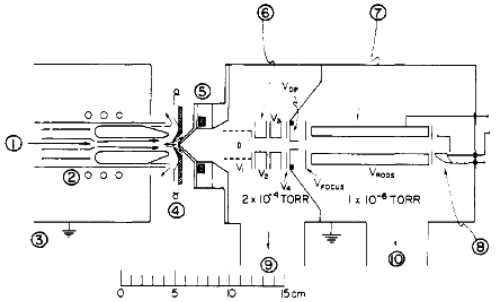

Figure 1. Schematic diagram of ICP, ion sampling interface, and vacuum system: (1) analyte aerosol from nebulizer; (2) ICP torch and load coil; (3) shielding box; (4) skimmer with plasma plume shown streaming through central hole; (5) sampler cone with extraction orifice (detailed diagram in Figure 2); (6) electrostatic ion lens assembly; (7) quadrupole mass analyzer; (8) channeltron electron multiplier; (9) pumping port to slide valve and diffusion pump (first pumping stage); (10) pumping port to slide valve, liquid nitrogen baffle, and diffusion pump (second pumping stage).

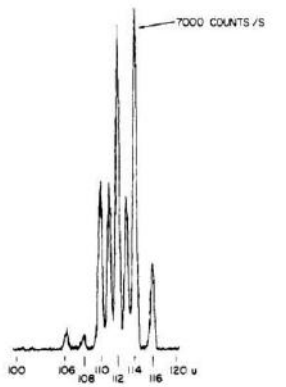

Figure 5. Mass spectrum of Cd at 50 μg/mL in 1% HNO_3.

No entanto, os principais componentes de um ICP-MS moderno continuam a ser idênticos aos dos primeiros sistemas desenvolvidos na década de 80.

Protótipo de ICP-MS
Universidade de Surrey, UK, 1979

Thermo Scientific iCAP RQ
2015

Curso de Introdução ao ICP-MS

Fundamentos de ICP-MS

Formador: Pedro Brito (IPMA)

2 a 4 de Novembro de 2016

Instituto Português do Mar e da Atmosfera, I.P. (IPMA)

Principais componentes do ICP-MS

Um equipamento de ICP-MS é constituído por vários componentes distintos:

- Introdução de amostra
- Geração de iões
- Interface plasma/vácuo
- Focagem de iões
- Separação e quantificação de iões

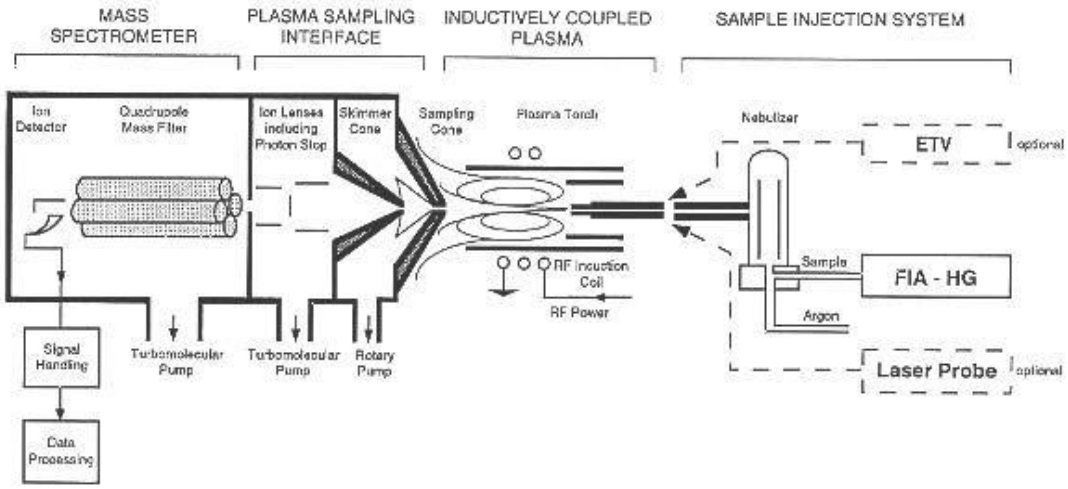

Introdução de amostra

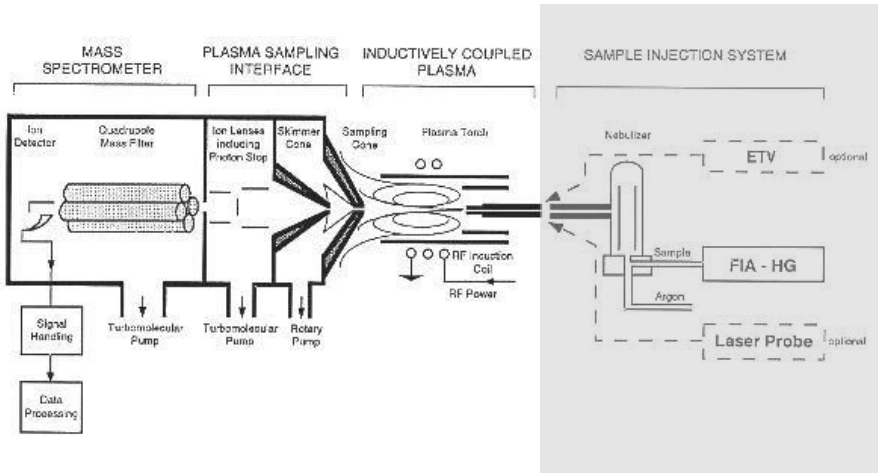

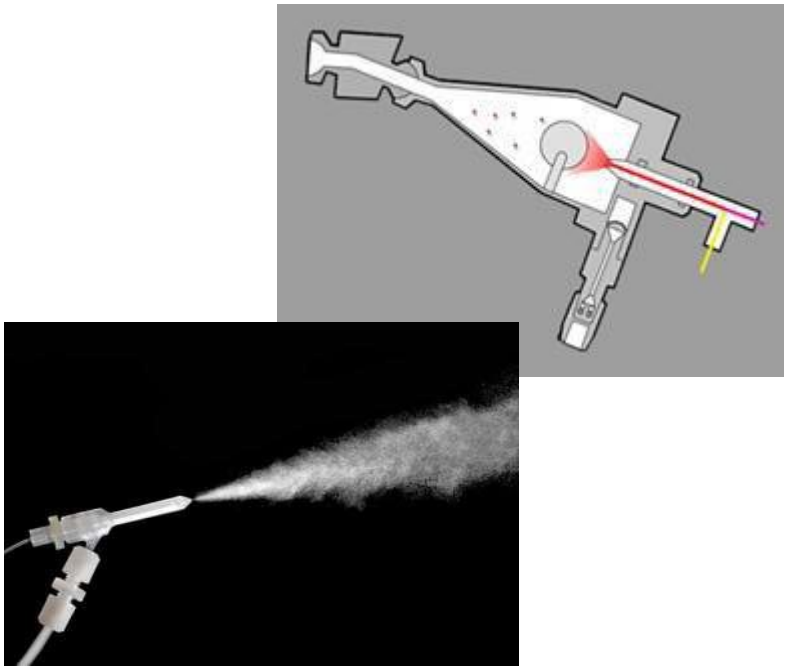

- Tipicamente na forma de aerosol produzido através de um nebulizador
- Remoção de gotículas maiores numa câmara de nebulização
- Controlo de temperatura (*Peltier*) para redução da variabilidade do sinal

Introdução de amostra

Nebulizadores

- Fluxos mais baixos comparativamente ao ICP-OES
- Tipicamente 1 mL/min. → 20 elementos → aprox. 4-5 mL amostra
- Diversos tipos: concêntrico, Babington, micro-nebulizador, V-Groove, etc.
- Micro-nebulizadores → fluxos menores (0,1 mL/min.) igual ou melhor sensibilidade

Introdução de amostra

Câmara de nebulização (*Spray chamber*)

- Temperatura → afecta a estabilidade e eficiência do plasma
- Principal função: remoção das partículas maiores do aerosol
- Diversos designs: Scott, ciclónica, etc.

Geração de iões

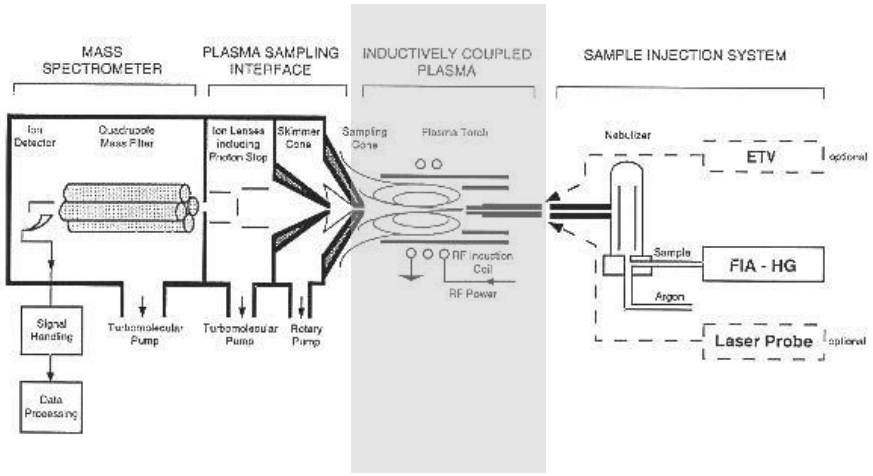

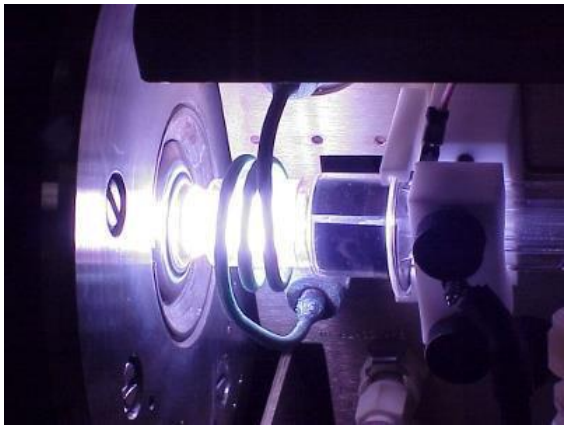

- Uma fonte de ionização - **plasma de argon (Ar)** gerado num torcha de quartzo
- Aplicação de uma corrente eléctrica elevada no "coil" de cobre (1400 W) a partir de um gerador de rádio-frequência (ex. 27.12 MHz)
- Elevada temperatura (cerca de 7500° K no centro do plasma)
  - Secagem; decomposição; vaporização; atomização; ionização

$$M(H_2O)^+ X^- \rightarrow MX \rightarrow M^+ \rightarrow MO^+$$

Interface plasma/vácuo

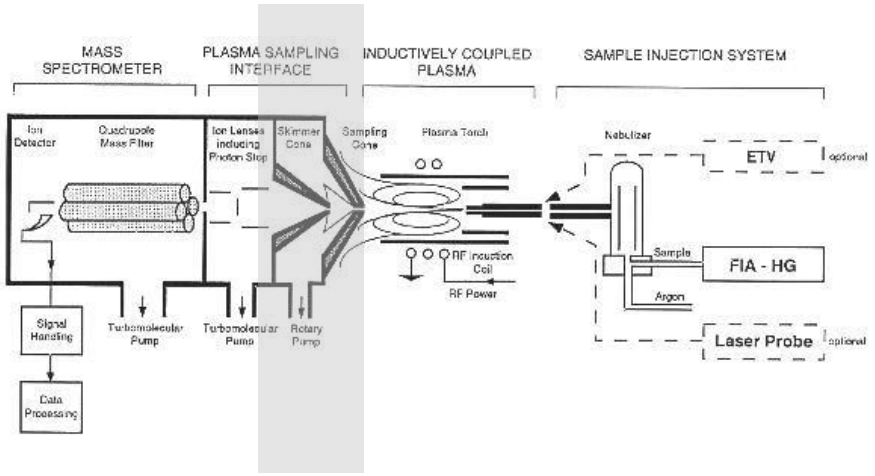

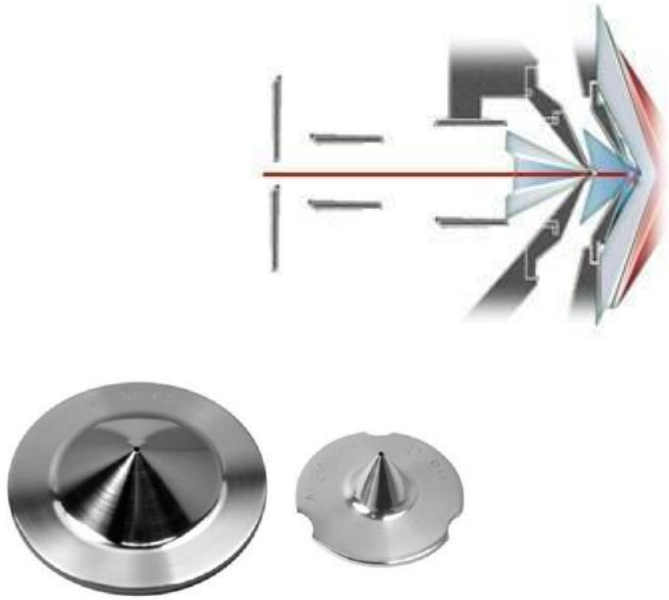

- Extracção dos iões produzidos no plasma para uma zona de vácuo via dois cones de interface (placas de metal com um pequeno orificio central por onde passa o feixe de iões):
  - Sample cone
  - Skimmer cone

Focagem de iões

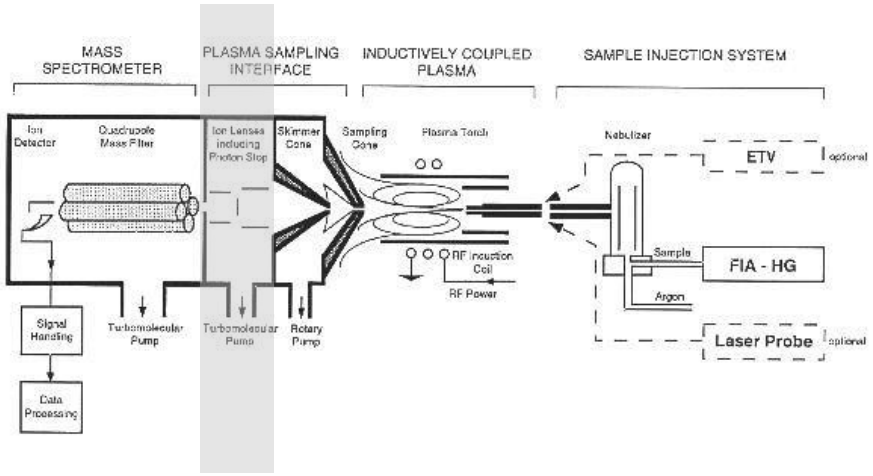

- Lentes electro-estáticas focam o feixe de iões ao longo do sistema de vácuo até à câmara de análise onde se encontra o espectrómetro de massa e o detector.
- Separação dos iões dos fotões e material residual neutral (neutrões) – redução do ruído de fundo (*background*)

Separação e quantificação de iões

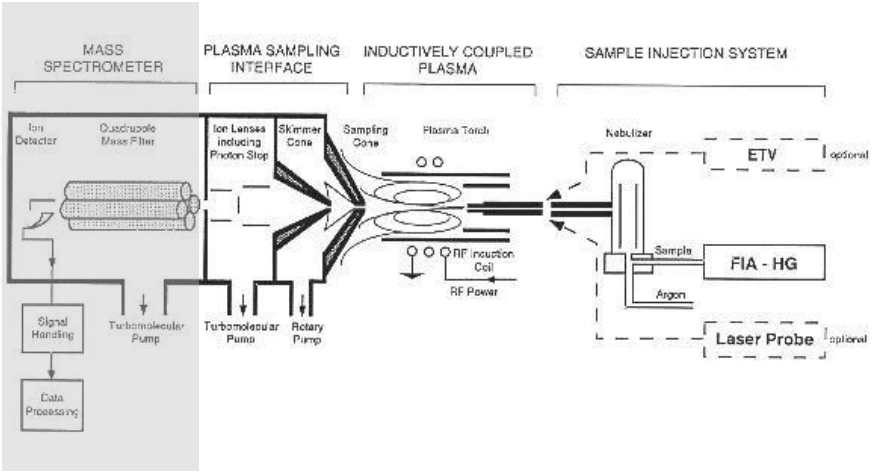

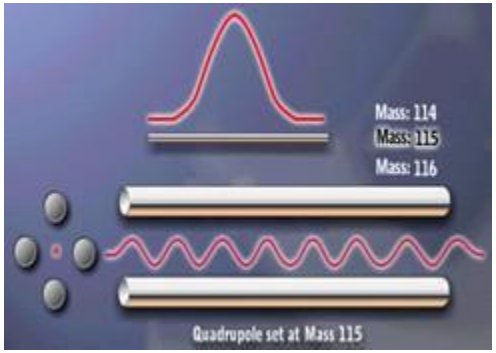

- Espectrómetro de massa – quadrupolo (outros tipos de espectrómetros usados: *magnetic sector* e *time-of-flight*)
- Combinação de campos eléctricos de corrente contínua (DC) e alternada (AC) para separar os iões com base na sua razão massa/carga (m/z).
- Para uma determinada voltagem aplicada no quadrupolo apenas uma determinada razão m/z é estável passando cada massa para o detector.

Separação e quantificação de iões

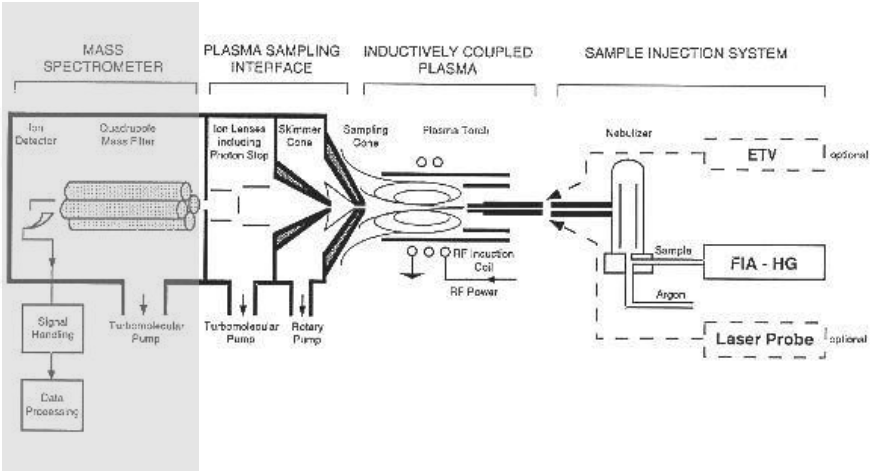

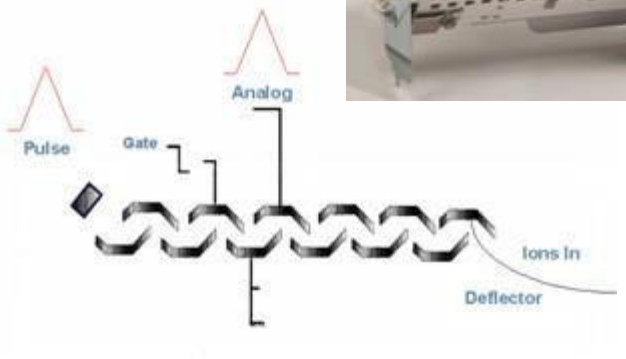

- O detector é um multiplicador de electrões que detecta os iões à saída do quadrupolo contando electronicamente o total do sinal de cada massa (m/z) criando um espectro de massa.
- A magnitude de cada pico é proporcional à concentração do elemento em análise numa amostra.

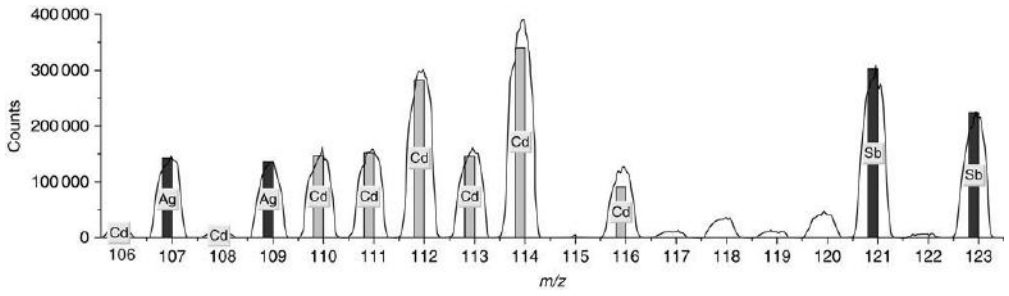

Curso de Introdução ao ICP-MS

Preparação de amostras e controlo de contaminações

Formadores: Joana Raimundo e Pedro Brito (IPMA)

2 a 4 de Novembro de 2016

Instituto Português do Mar e da Atmosfera, I.P. (IPMA)

Matriz

Água

Organismos

Sedimentos

Matéria em Suspensão

Solo

Preparação de amostras

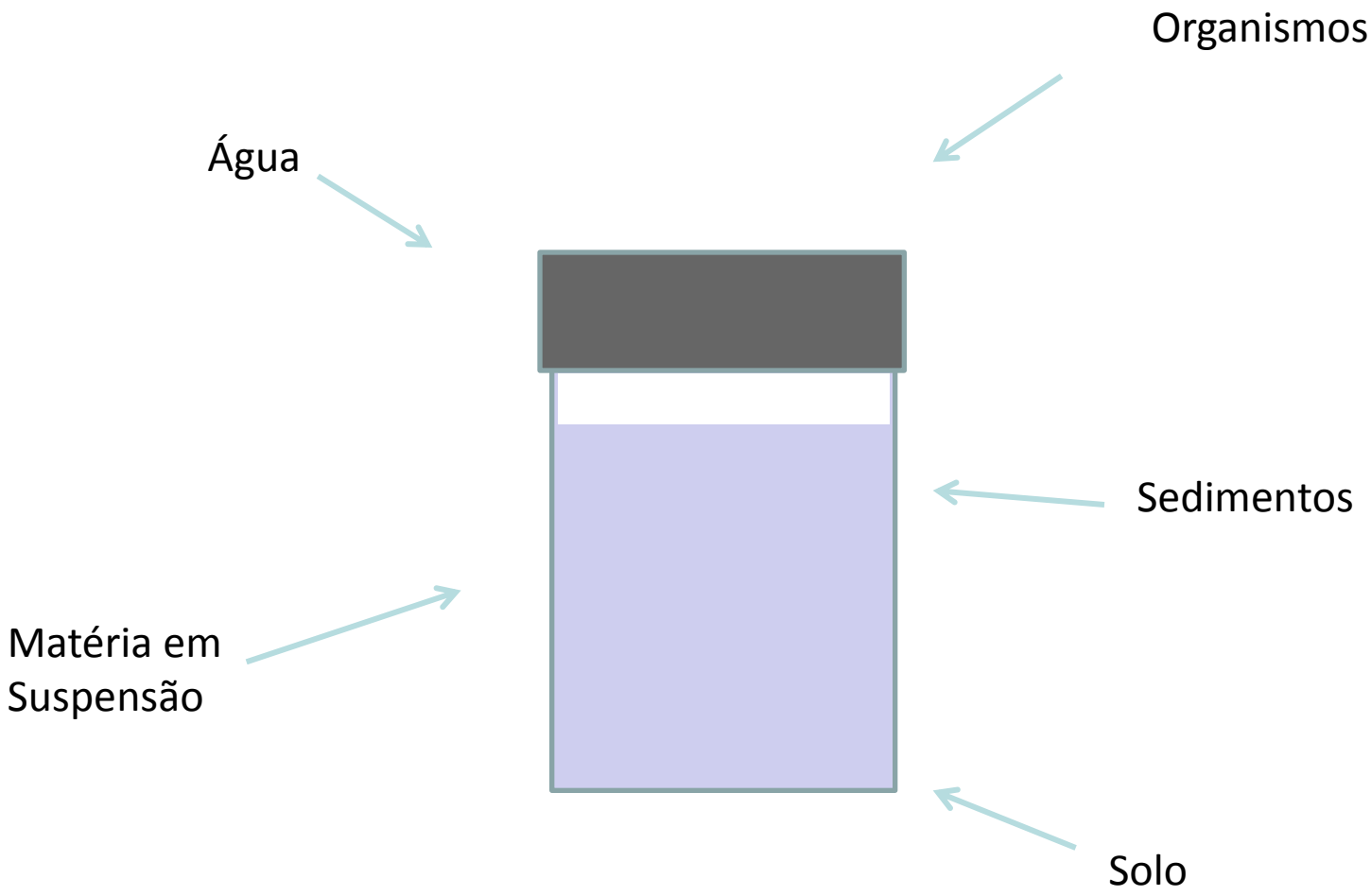

Preparação de amostras

Tabela Periódica dos Elementos

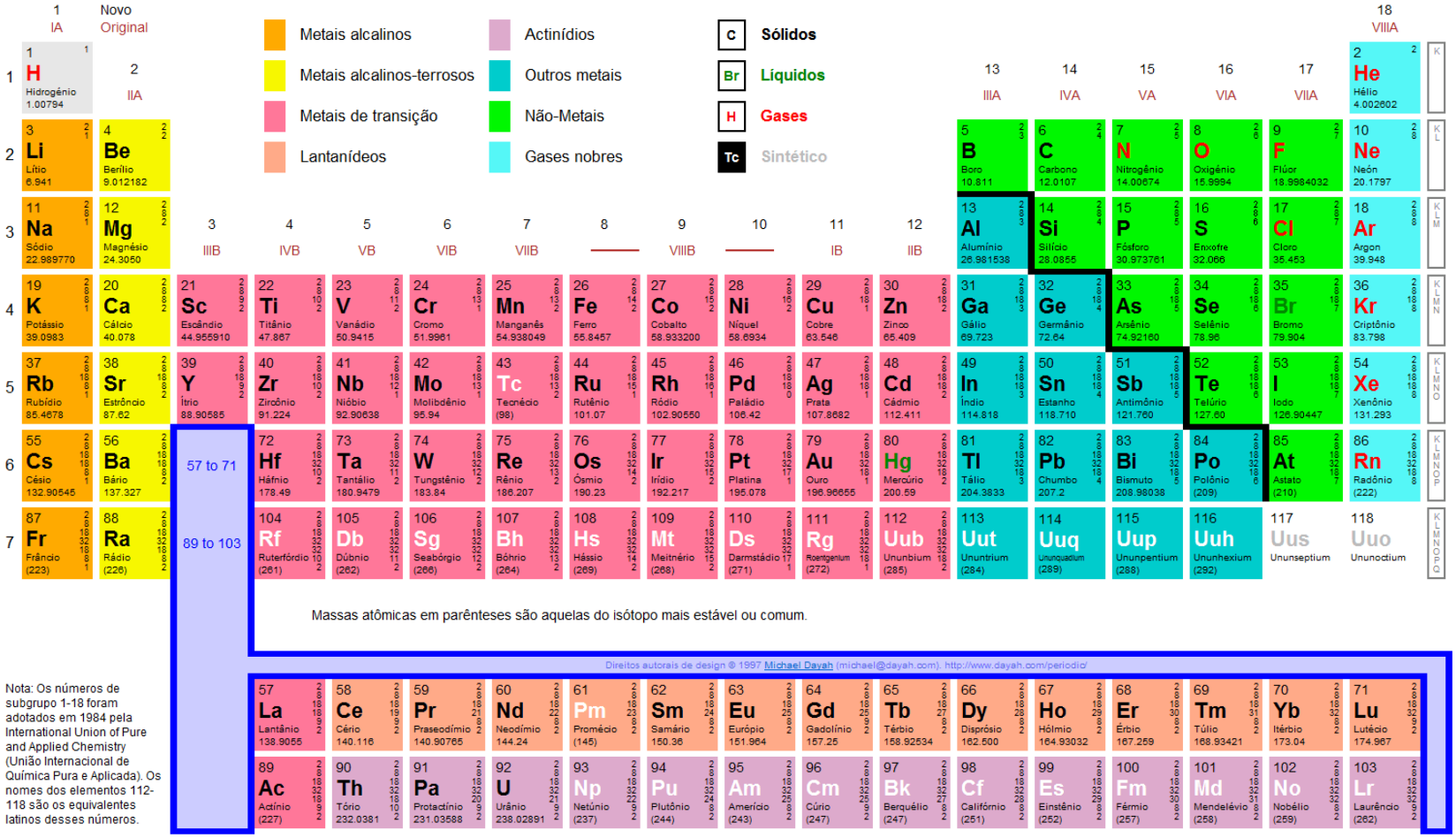

Nota: Os números de subgrupo 1-18 foram adotados em 1984 pela International Union of Pure and Applied Chemistry (União Internacional de Química Pura e Aplicada). Os nomes dos elementos 112-118 são os equivalentes latinos desses números.

Interferentes nas análises

- Quantidade de sólidos totais dissolvidos

  (TDS < 2-3%)

  - Diluição com 1% HNO_3

- Interferências da matriz
  - Cloretos, fósforo, matéria orgânica
  - Exemplo: águas subterrâneas e residuais presenç

    cloretos dificulta a análise de As e V

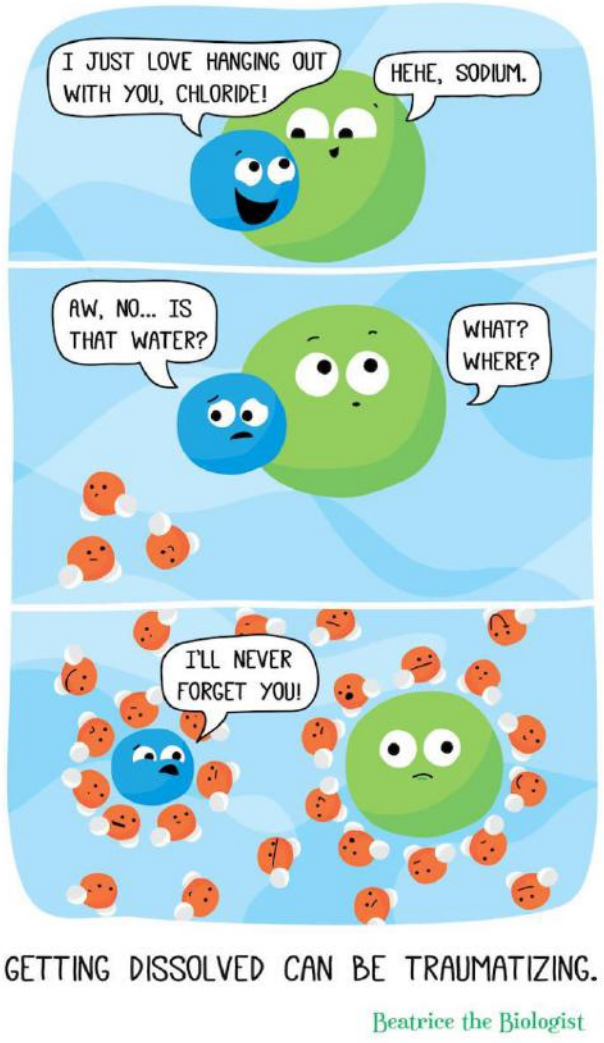

Considerações gerais na prep. das amostras

- A qualidade dos resultados dependem da qualidade dos reagentes

- Redução dos sólidos em suspensão - filtração; centrifugação (alguns problemas)

Prep. de amostras – Água

- Águas doce e de consumo – Análise direta

- Águas residuais e tratamento – filtradas ou digestão

Prep. de amostras – Água

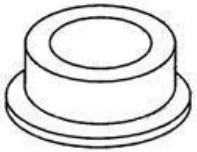

- Água salgada – resinas, passive samplers

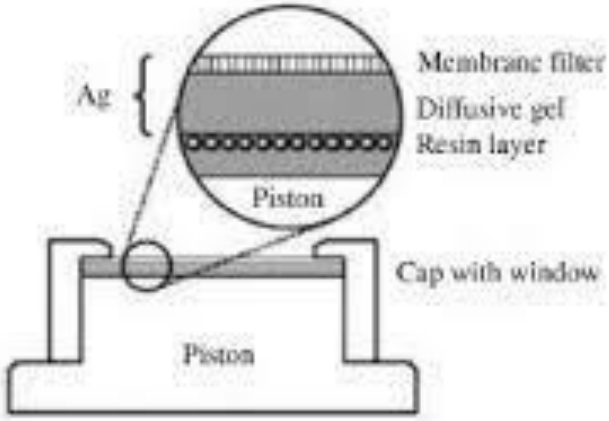

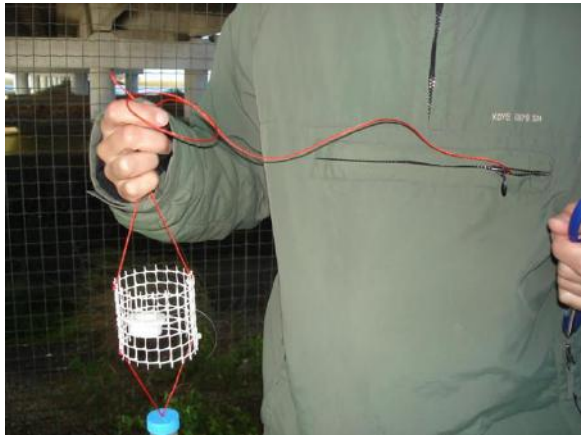

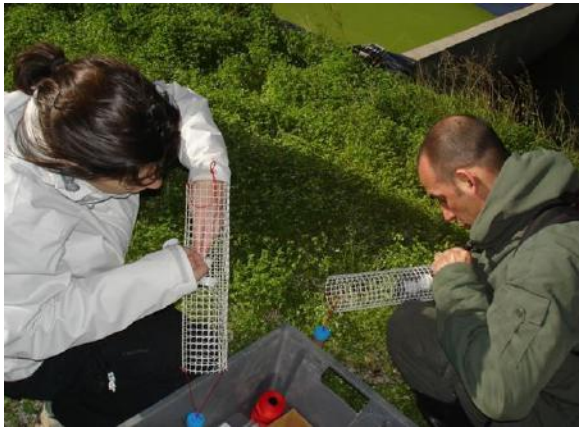

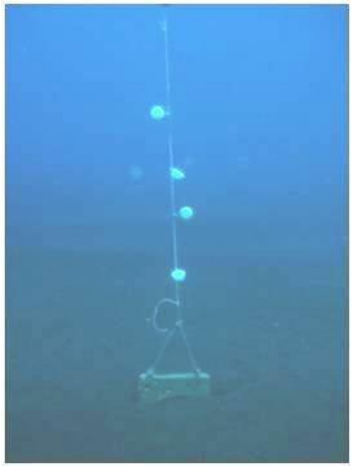

Prep. de amostras – Sedimentos

Prep. de amostras – Sedimentos

- Digestão total
- Digestão parcial
- Digestão sequencial

- Rantala and Loring (1975)
- Rantala+bloco
- Métodos 3050-B EPA

Vantagens e desvantagens

Técnica eficiente e rápida

Prep. de amostras – Matéria em suspensão

- Digestão SPM – digestão sedimentos

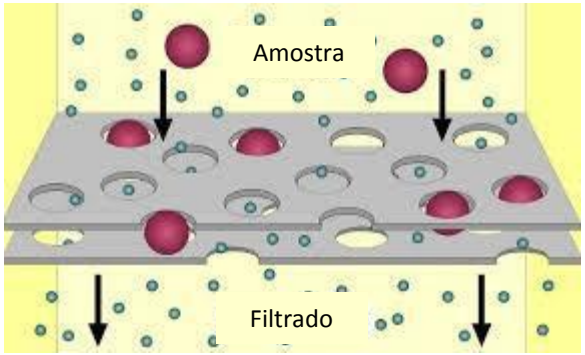

SPM

0.45 µm

Dissolvido

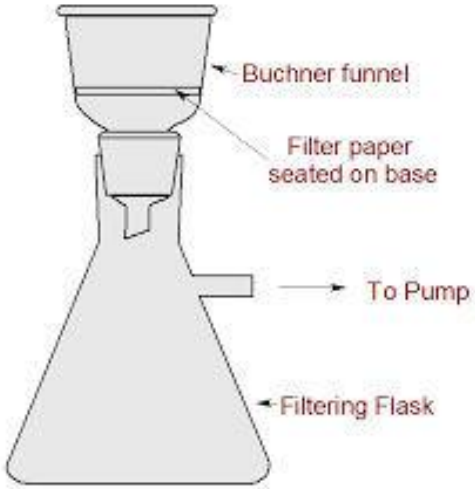

Prep. de amostras – Organismos

Prep. de amostras – Organismos

- Digestão total – HNO_3 e H_2O_2

  HNO_3 e $HClO_4$

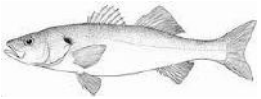

Prep. de amostras – Métodos

- EPA

https://www.epa.gov/measurements/collection-methods

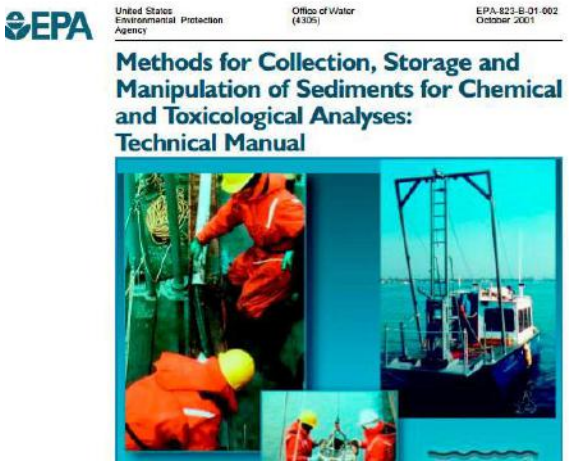

EPA United States Environmental Protection Agency | Office of Water (4305) | EPA-823-B-01-002 October 2001

Methods for Collection, Storage and Manipulation of Sediments for Chemical and Toxicological Analyses: Technical Manual

METHOD 3050B

ACID DIGESTION OF SEDIMENTS, SLUDGES, AND SOILS

1.0 SCOPE AND APPLICATION

1.1 This method has been written to provide two separate digestion procedures, one for the preparation of sediments, sludges, and soil samples for analysis by flame atomic absorption spectrometry (FLAA) or inductively coupled plasma atomic emission spectrometry (ICP-AES) and one for the preparation of sediments, sludges, and soil samples for analysis of samples by Graphite Furnace AA (GFAA) or inductively coupled plasma mass spectrometry (ICP-MS). The extracts from these two procedures are not interchangeable and should only be used with the analytical determinations outlined in this section. Samples prepared by this method may be analyzed by ICP-AES or GFAA for all the listed metals as long as the detecion limits are adequate for the required end-use of the data. Alternative determinative techniques may be used if they are scientifically valid and the QC criteria of the method, including those dealing with interferences, can be achieved. Other elements and matrices may be analyzed by this method if performance is demonstrated for the analytes of interest, in the matrices of interest, at the concentration levels of interest (See Section 8.0). The recommended determinative techniques for each element are listed below:

FLAA/ICP-AES		GFAA/ICP-MS
Aluminum	Magnesium	Arsenic
Antimony	Manganese	Beryllium
Barium	Molybdenum	Cadmium
Beryllium	Nickel	Chromium
Cadmium	Potassium	Cobalt
Calcium	Silver	Iron
Chromium	Sodium	Lead
Cobalt	Thallium	Molybdenum
Copper	Vanadium	Selenium
Iron	Zinc	Thallium
Lead		

Prep. de amostras – Métodos

http://www.standardmethods.org/store/ProductList.cfm

http://www.iso.org/iso/home/search.htm?qt=ICP-MS&sort=rel&type=simple&published=on

Controlo de contaminações

Controlo de contaminações

Controlo de contaminações

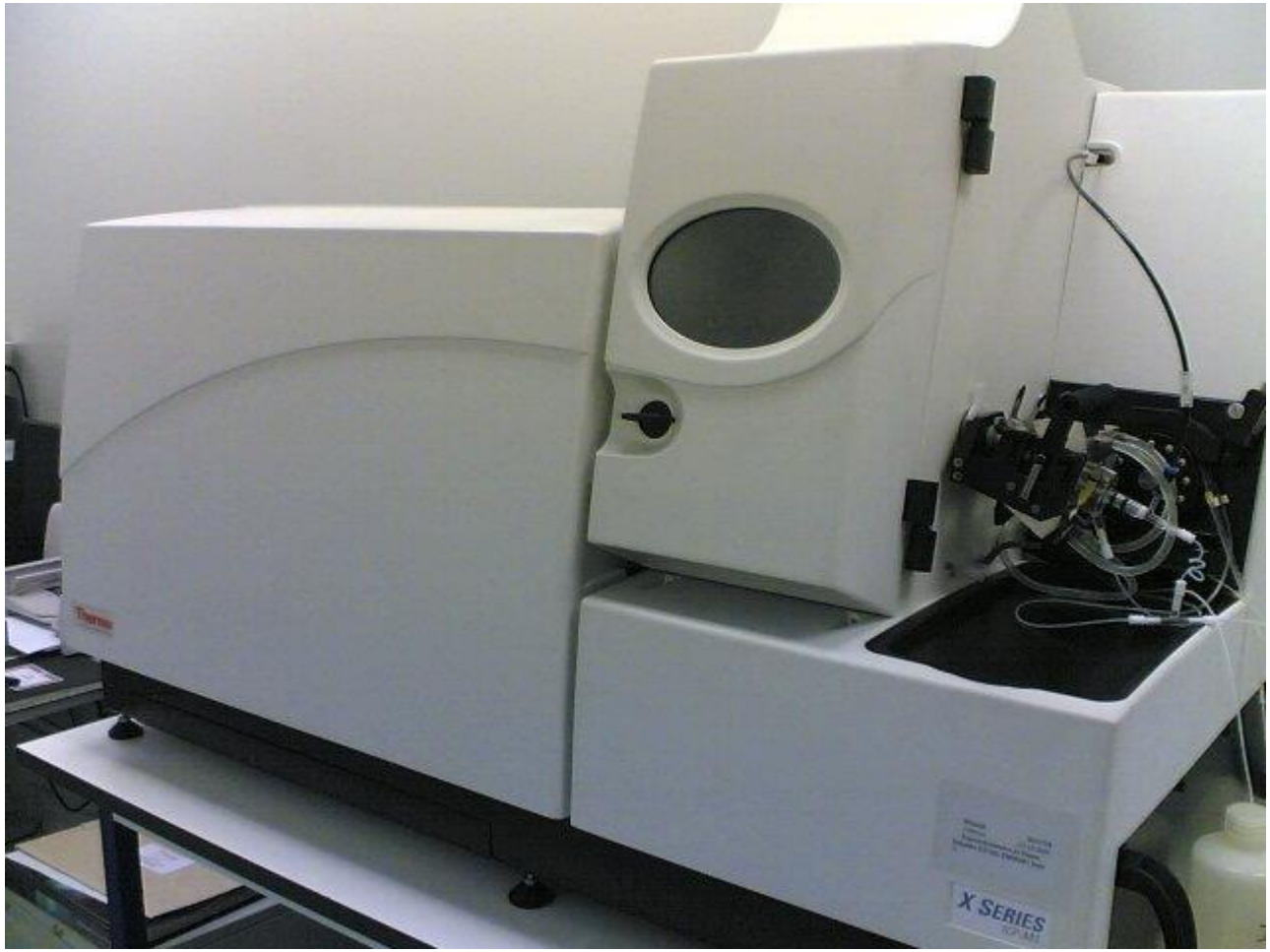

Controlo de contaminações

Instrument detection limit (IDL)

Most analytical instruments produce a signal even when a blank (matrix without analyte) is analyzed. This signal is referred to as the instrument background level. Noise is a measure of the fluctuation of the background level. It is generally measured by calculating the standard deviation of a number of consecutive point measurements of the background signal. The instrument detection limit (IDL) is the analyte concentration required to produce a signal that is distinguishable from the noise level within a particular statistical confidence limit. Approximate estimate of LOD can be obtained from the signal-to-noise ratio (S/N) as described in this document.

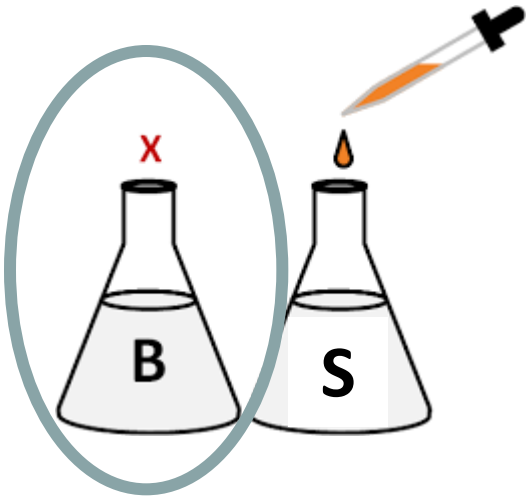

- Leitura dos analitos num Branco (10x)
- Análise de padrões com concentrações conhecidas

IDL = (3 x stdevBr) / (sinal padrão - sinal Br)

Controlo de contaminações

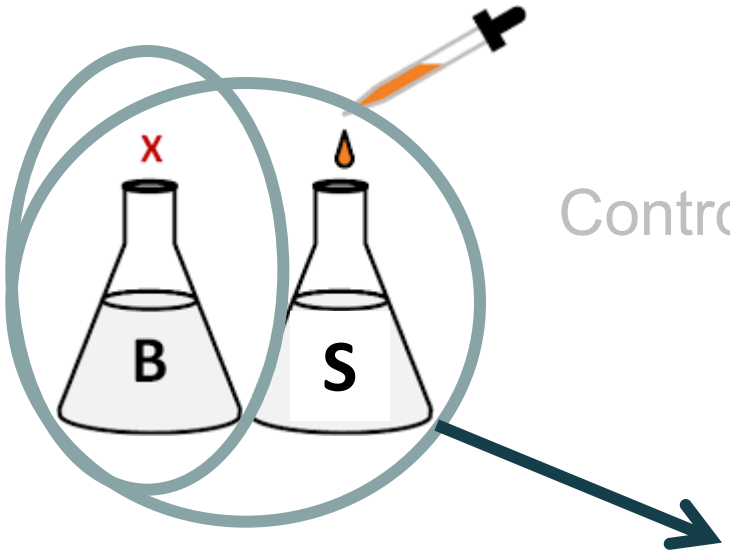

Controlo da exatidão e da precisão das determinações

• Contaminação por:

• via aérea • reagentes e ácidos • material de laboratório •operador

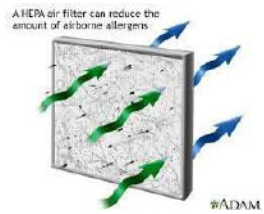

+1

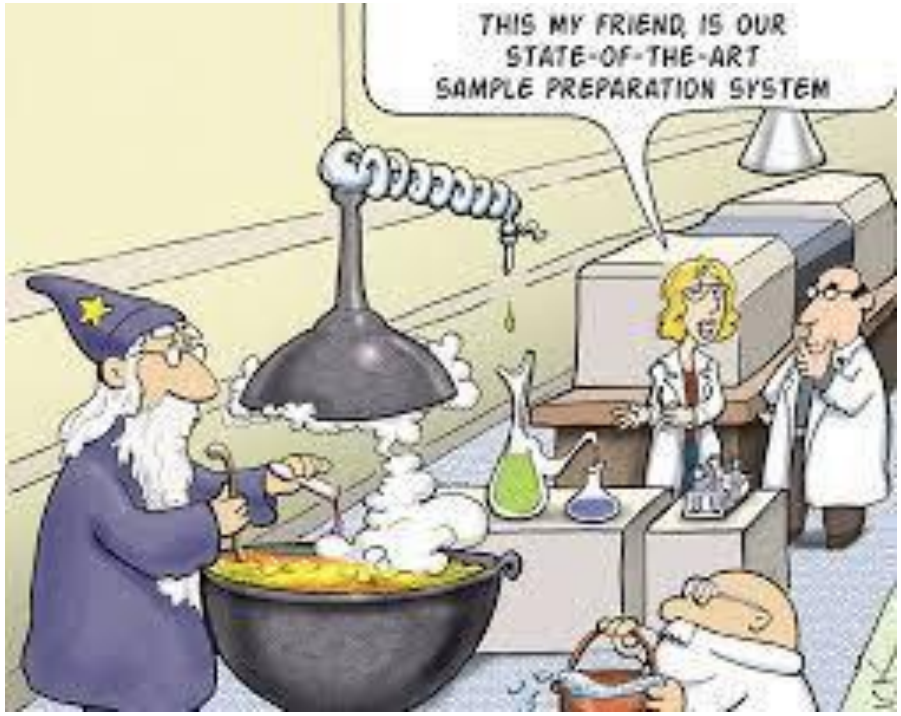
THIS MY FRIEND, IS OUR
STATE-OF-THE-ART
SAMPLE PREPARATION SYSTEM


KEEP
CALM
AND
CLEAN THE
LAB

Curso de Introdução ao ICP-MS

Controlo de interferências no ICP-MS

Formador: Pedro Brito (IPMA)

2 a 4 de Novembro de 2016

Instituto Português do Mar e da Atmosfera, I.P. (IPMA)

As fontes de interferências no ICP-MS

- Interferências não-espectrais
  - Depósitos no ICP-MS
  - Matriz das amostras

- Interferências espectrais
  - Isobáricas
  - Poliatómicas (ou moleculares)

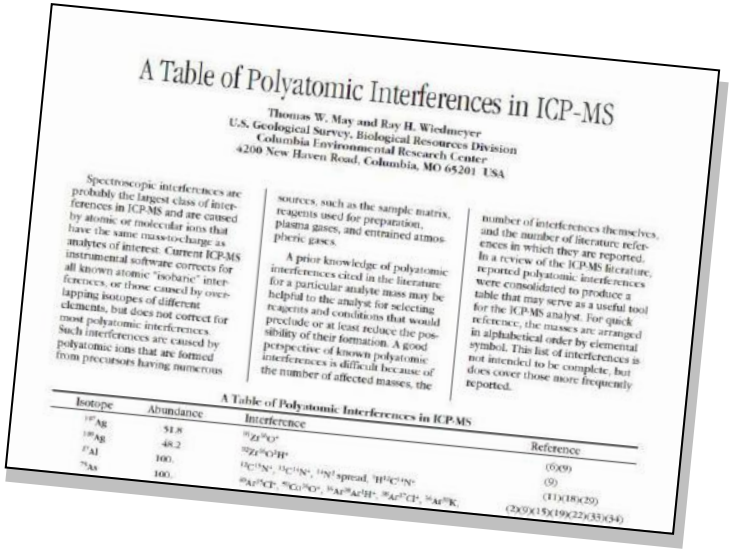

A Table of Polyatomic Interferences in ICP-MS

Thomas W. May and Ray H. Wiedmeyer
U.S. Geological Survey, Biological Resources Division
Columbia Environmental Research Center
4200 New Haven Road, Columbia, MO 65201 USA

Spectroscopic interferences are probably the largest class of interferences in ICP-MS and are caused by atomic or molecular ions that have the same mass-to-charge as analytes of interest. Current ICP-MS instrumental software corrects for all known atomic "isobaric" interferences, or those caused by overlapping isotopes of different elements, but does not correct for most polyatomic interferences. Such interferences are caused by polyatomic ions that are formed from precursors having numerous sources, such as the sample matrix, reagents used for preparation, plasma gases, and entrained atmospheric gases.

A prior knowledge of polyatomic interferences cited in the literature for a particular analyte mass may be helpful to the analyst for selecting reagents and conditions that would preclude or at least reduce the possibility of their formation. A good perspective of known polyatomic interferences is difficult because of the number of affected masses, the number of interferences themselves, and the number of literature references in which they are reported. In a review of the ICP-MS literature, reported polyatomic interferences were consolidated to produce a table that may serve as a useful tool for the ICP-MS analyst. For quick reference, the masses are arranged in alphabetical order by elemental symbol. This list of interferences is not intended to be complete, but does cover those more frequently reported.

A Table of Polyatomic Interferences in ICP-MS

Isotope	Abundance	Interference	Reference
^{107}Ag	51.8	$^{91}Zr^{16}O^{+}$	(6)(9)
^{109}Ag	48.2	$^{93}Zr^{16}O^{1}H^{+}$	(9)
^{27}Al	100.	$^{13}C^{14}N^{+}$, $^{13}C^{15}N^{+}$, $^{14}N^{2}$ spread, $^{14}N^{1}H^{13}C^{+}$	(11)(18)(29)
^{75}As	100.	$^{40}Ar^{35}Cl^{+}$, $^{59}Co^{16}O^{+}$, $^{59}Al^{16}Ar^{1}H^{+}$, $^{38}Ar^{37}Cl^{1}H^{+}$, $^{36}Ar^{39}K^{+}$	(2)(9)(15)(19)(22)(33)(34)

Interferências não-espectrais

- Depósitos no ICP-MS
  - Partículas em suspensão (ex. digestões incompletas)
    - ✓ Boas práticas de laboratório
    - ✓ Procedimentos adequados

- Matriz da amostra
  - TDS (<0,2%) – H2O oceânicas, estuarines, etc.
    - ✓ Eliminação da matriz (DGT, SPE, SeaFast, etc.)

Interferências espectrais

- Isobáricas
  - Elementos com a 'mesma' massa isotópica – ex. ^{48}Ca e ^{48}Ti

Z	Name	Symbol	Mass of Atom (u)	% Abundance
20	Calcium	^{40}Ca	39.962591	96.941
		^{42}Ca	41.958618	0.647
		^{43}Ca	42.958767	0.135
		^{44}Ca	43.955481	2.086
		^{46}Ca	45.953693	0.004
		^{48}Ca	47.952534	0.187
21	Scandium	^{45}Sc	44.955910	100
22	Titanium	^{46}Ti	45.952629	8.25
		^{47}Ti	46.951764	7.44
		^{48}Ti	47.947947	73.72
		^{49}Ti	48.947871	5.41
		^{50}Ti	49.944792	5.18

Diferença <0,1 u.m.a.(0,004587)

✓ HR-ICP-MS (quando disponível)

Interferências espectrais

- Isobáricas
  - Elementos com a 'mesma' massa isotópica – ex. ^{48}Ti e ^{48}Ca
    - ✓ Correcção matemática (equações de correcção)

Exemplo:

Quantificar o titânio (Ti) através do isótopo ^{48}Ti(

(existe sobreposição do sinal do isótopo ^{48}Ca no ^{48}Ti)

- Corrigir através da medição de outro isótopo do elemento interferente (Ca) → ^{44}Ca
- Medir o isótopo ^{44}Ca e subtrair o factor **0,089645 x ^{44}Ca** ao valor do ^{48}Ti

Table of Isotopic Masses and Natural Abundances

Calcium	^{40}Ca	39.962591	96.941
	^{42}Ca	41.958618	0.647
	^{43}Ca	42.958767	0.135
	^{44}Ca	43.955481	2.086
	^{46}Ca	45.953693	0.004
	^{48}Ca	47.952534	0.187

•O factor 0,089645 é o valor da razão das abundâncias naturais dos isótopos do Ca envolvidos no cálculo ($^{48}Ca/^{44}Ca$)

•Deve existir pelo menos uma massa isotópica perfeitamente limpa do elemento interferente (ex. poliatómicas)

^{58}Ni (^{58}Fe) → ^{56}Fe → ^{40}Ar $^{16}O^{+}$

Interferências espectrais

- Poliatómicas ou moleculares
  - Do fluxo iónico produzido no plasma de Ar (ruído de fundo)
    - ✓ Iões simples e poliatómicos do Ar, água e do ar circundante do plasma
    - ✓ O^+, N_2^+, NO^+, O_2^+, Ar^+ ArO^+ e Ar_2^+
  - Gama das massas baixas
    - ✓ $^{28}Si^+$ (N_2^+)
    - ✓ $^{31}P^+$ (NOH^+)
    - ✓ $^{32}S+$ (O_2^+)
    - ✓ $^{40}Ca^+$ (Ar^+)
    - ✓ $^{56}Fe^+$ (ArO^+)
    - ✓ $^{80}Se^+$ (Ar_2^+)

Interferências espectrais

- Da matriz da amostra
  - Iões simples e poliatómicos com origem em soluções a 5% de HCl e H_2SO_4
  - Cl^+, ClO^+, ClN^+, Cl_2^+, $ArCl^+$

Exemplo:

$^{35}Cl^{16}O^+$ → massa 51 (35+16)

Vários elementos da primeira série de transição

^{51}V → isótopo alternativo ^{50}V → menor sensibilidade, duas isobáricas ($^{50}Ti^+$ e $^{50}Cr^+$) e uma poliatómica ($^{35}Cl^{15}N^+$)

Z	Name	Symbol	Mass of Atom (u)	% Abundance
23	Vanadium	^{50}V	49.947163	0.250
		^{51}V	50.943964	99.750

Interferências espectrais

Exercício prático

Pretende-se quantificar arsénio (As) em amostras com teores de Cl^- elevados.

1. Que tipo de interferência é? **Poliatómica**
2. Que isótopo escolhemos para estimar a contribuição do interferente?
3. Calcular o factor para a equação de correcção.

O arsério é um elemento mono-isotópico → ^{75}As

Z	Name	Symbol	Mass of Atom (u)	% Abundance
33	Arsenic	^{75}As	74.921596	100

Interferência no ^{75}As → $^{75}ArCl$ ($^{40}Ar^{35}Cl$) → $^{77}ArCl$ ($^{40}Ar^{37}Cl$)

Interferência no $^{77}ArCl$ ($^{40}Ar^{37}Cl$) → ^{77}Se → ^{82}Se

Interferência no ^{82}Se → ^{82}Kr → ^{83}Kr

Interferências espectrais

1. Medir o sinal de ^{75}M, ^{77}M, ^{82}M e ^{83}M.
2. Assumir que o sinal de ^{83}M vem do ^{83}Kr e estimar o sinal de ^{82}Kr.
3. Subtrair a contribuição estimada do ^{82}Kr do sinal de ^{82}M; a diferença corresponde ao sinal de ^{82}Se.
4. Usar o sinal estimado de 82Se para estimar o sinal de ^{77}Se na ^{77}M.
5. Subtrair a contribuição estimada do ^{77}Se a ^{77}M; a diferença corresponde ao sinal de $^{77}ArCl$.
6. Usar o sinal estimado de $^{77}ArCl$ para estimar a contribuição de ^{75}M de $^{75}ArCl$.
7. Subtrair a contribuição estimada de $^{75}ArCl$ a ^{75}M; a diferença corresponde ao sinal de ^{75}As.

Interferências espectrais

Exercício prático

Pretende-se quantificar arsénio (As) em amostras com teores de Cl^- elevados.

1. Medir o sinal de ^{75}M, ^{77}M, ^{82}M e ^{83}M.
2. Assumir que o sinal de ^{83}M vem do ^{83}Kr e estimar o sinal de ^{82}Kr.

   $^{82}Se = {}^{82}M - 1{,}0078 * {}^{83}Kr$
3. Subtrair a contribuição estimada do ^{82}Kr do sinal de ^{82}M; a diferença corresponde ao sinal de ^{82}Se.
4. Usar o sinal estimado de 82Se para estimar o sinal de ^{77}Se na ^{77}M.

   $^{77}ArCl = {}^{77}M - 0.8740 * {}^{82}Se$
5. Subtrair a contribuição estimada do ^{77}Se a ^{77}M; a diferença corresponde ao sinal de $^{77}ArCl$.
6. Usar o sinal estimado de $^{77}ArCl$ para estimar a contribuição de ^{75}M de $^{75}ArCl$.

   $^{75}As = {}^{75}M - 3{,}1288 * {}^{77}ArCl$
7. Subtrair a contribuição estimada de $^{75}ArCl$ a ^{75}M; a diferença corresponde ao sinal de ^{75}As.

Curso de Introdução ao ICP-MS

Manutenção e diagnóstico de problemas básicos no ICP-MS

Formadores: Joana Raimundo e Pedro Brito (IPMA)

2 a 4 de Novembro de 2016

Instituto Português do Mar e da Atmosfera, I.P. (IPMA)

Manutenção e diagnóstico

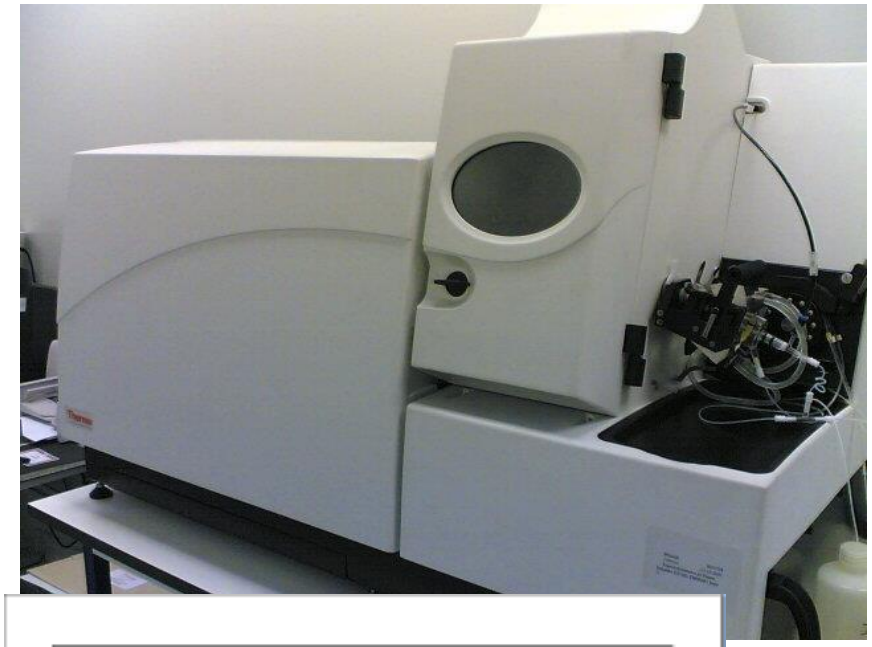

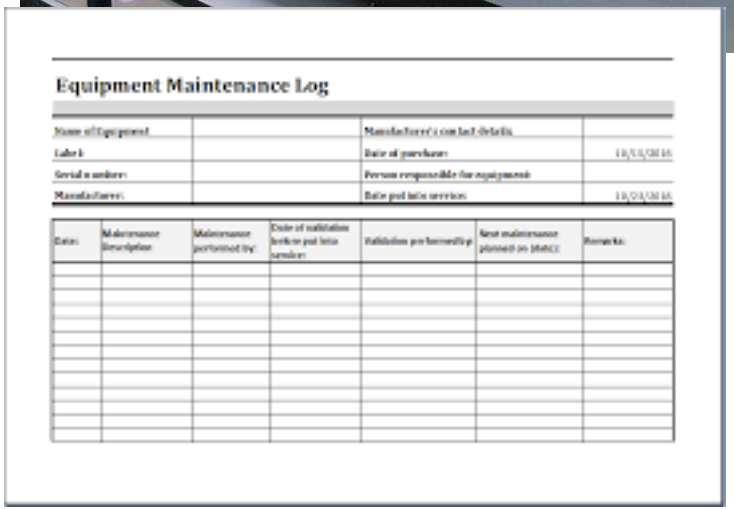

Equipment Maintenance Log

- Utilizador
- Horas de trabalho
- Condições de trabalho
- Operação de verificação
- Alterações ao aparelho
- Número de amostras analisadas
- Tipo de matriz analisada
- Número de elementos analisados
- ...

Manutenção e diagnóstico

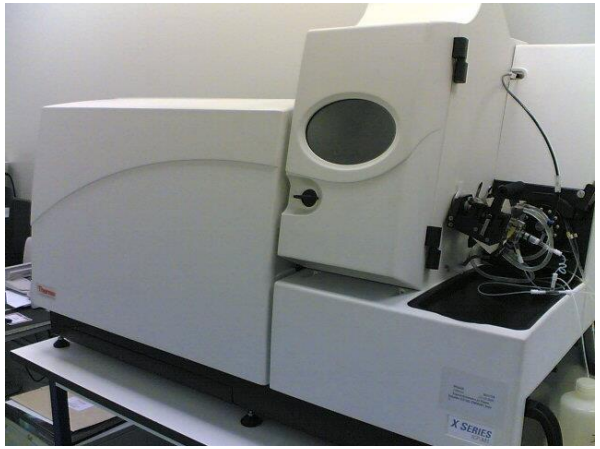

Scheduling Maintenance

Table 9 Maintenance Schedule

Frequency	Component	Task/Action	Remarks
Daily (As a matter of routine, check daily before starting work and over the course of daily analysis)	Argon gas	Check argon gas pressure and volume	
	Drain vessel	Check, empty if required	Refer to note in Chapter 2, "Precautions"
	Peristaltic pump tubing	Check for damage/deterioration	
Weekly	Sampling cone, Skimmer cone	Check orifice for foreign matter, deformation and enlargement	Clean if required
Monthly	Rotary pump	Check oil level and color. Check mist filter for presence of oil	
	Nebulizer	Run Nebulizer test, take appropriate action as indicated	For the Nebulizer Test refer to the MassHunter Workstation Operator's Manual (or ChemStation Operator's Manual), Chapter 3
	RF return strips and shield bar	Clean	
	Cooling water	Check water level and condition	
3 – 6 Months	Extraction Lenses*	Clean	7500a
	Extraction/Omega Lenses*	Clean	7500cs, 7500cx
6 Months	Einzel/Omega Lenses*	Clean	7500a
	Entrance Lens, Exit Lens, Plate Bias / Cell Entrance, QP Focus*	Clean	7500cs, 7500cx
	Rotary pump	Change oil	
Annually	Rotary pump oil mist filter	Check / replace mist filter	
	Penning gauge	Clean	Replace or clean
	Water strainer	Check and clean	
	Octopole*	Clean	7500cs, 7500cx

Manutenção e diagnóstico

Bomba peristáltica e tubos

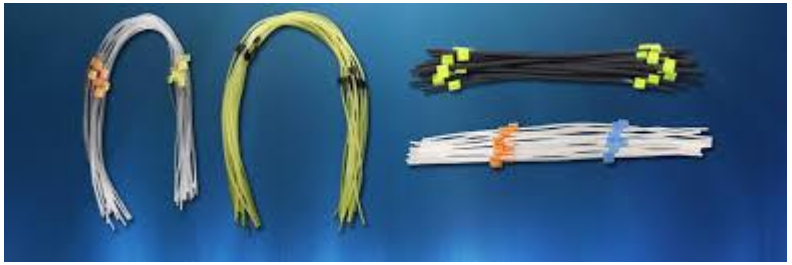

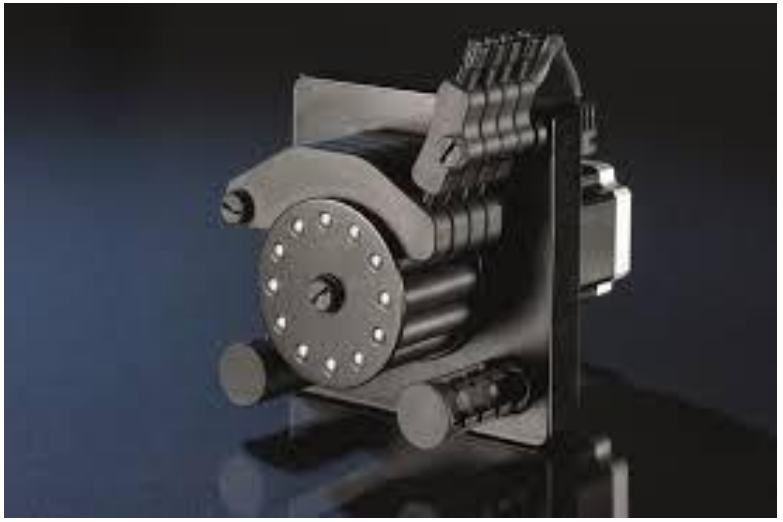

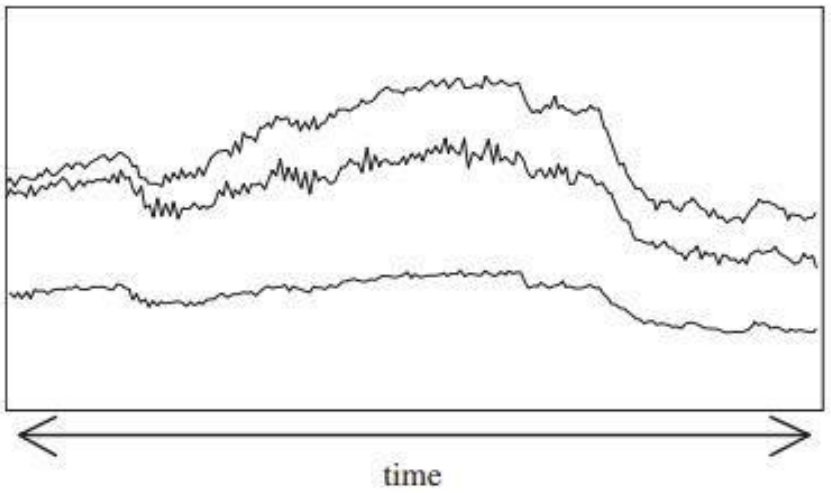

- Instabilidade do sinal
- Menor sensibilidade

Manutenção e diagnóstico

Spray chamber
Nebulizer

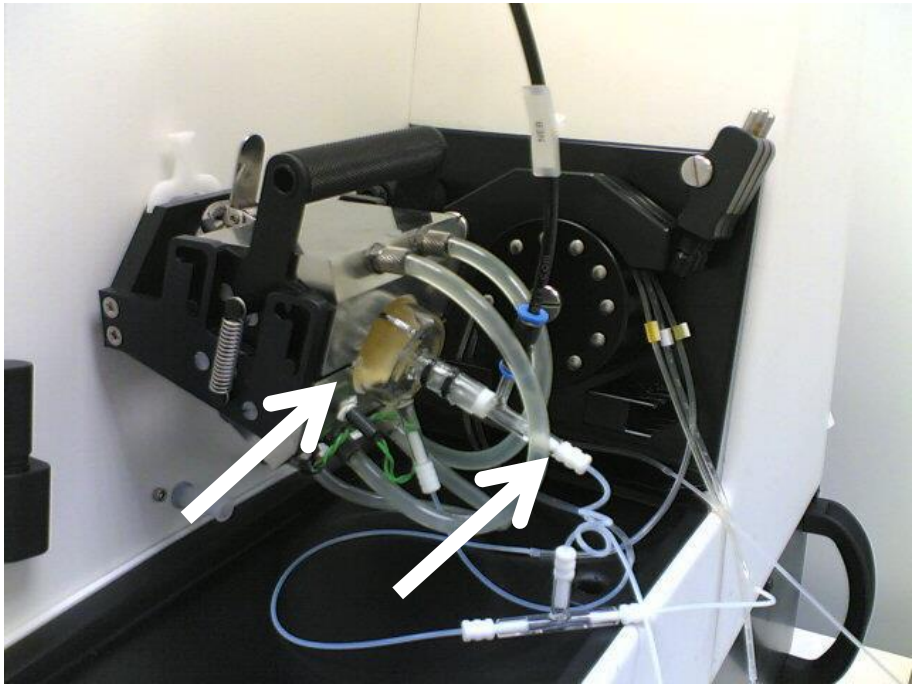

- Alteração na pressão e fluxo do gás
- Instabilidade do sinal
- TDS - Entupir

Manutenção e diagnóstico

Cones

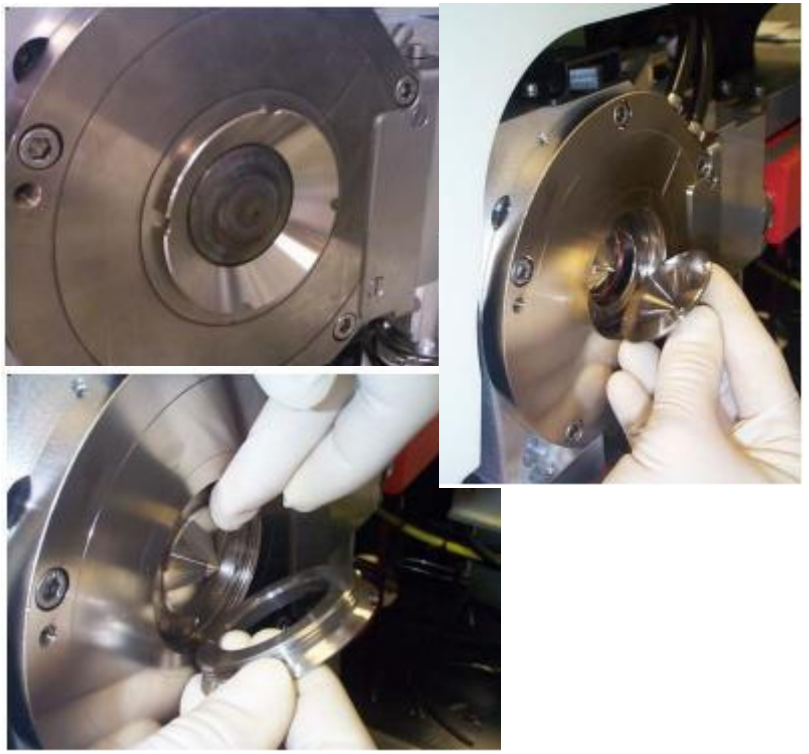

- Instabilidade do sinal
- Diminuição da sensabilidade
- Aumento do sinal de background
- Aumento do sinal dos Brancos

Manutenção e diagnóstico

Torch

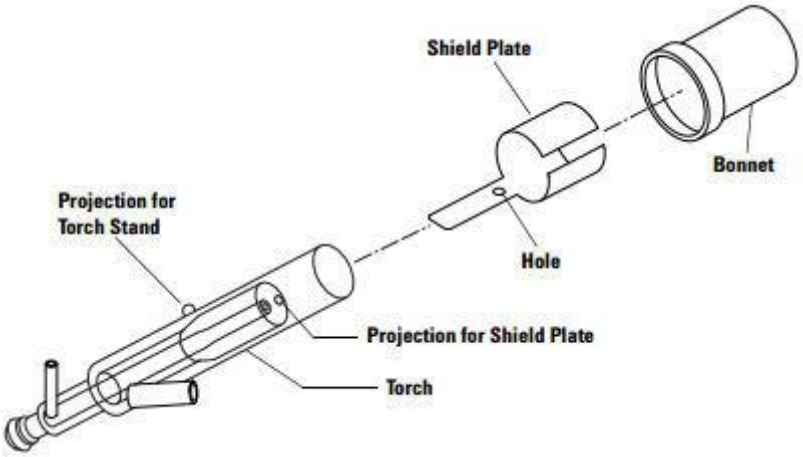

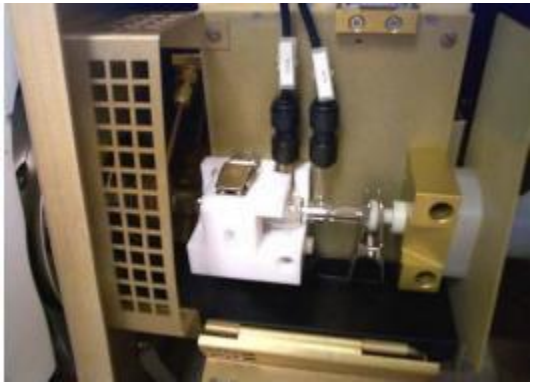

- Aumento do sinal de background
- Aumento do sinal dos Brancos

Manutenção e diagnóstico

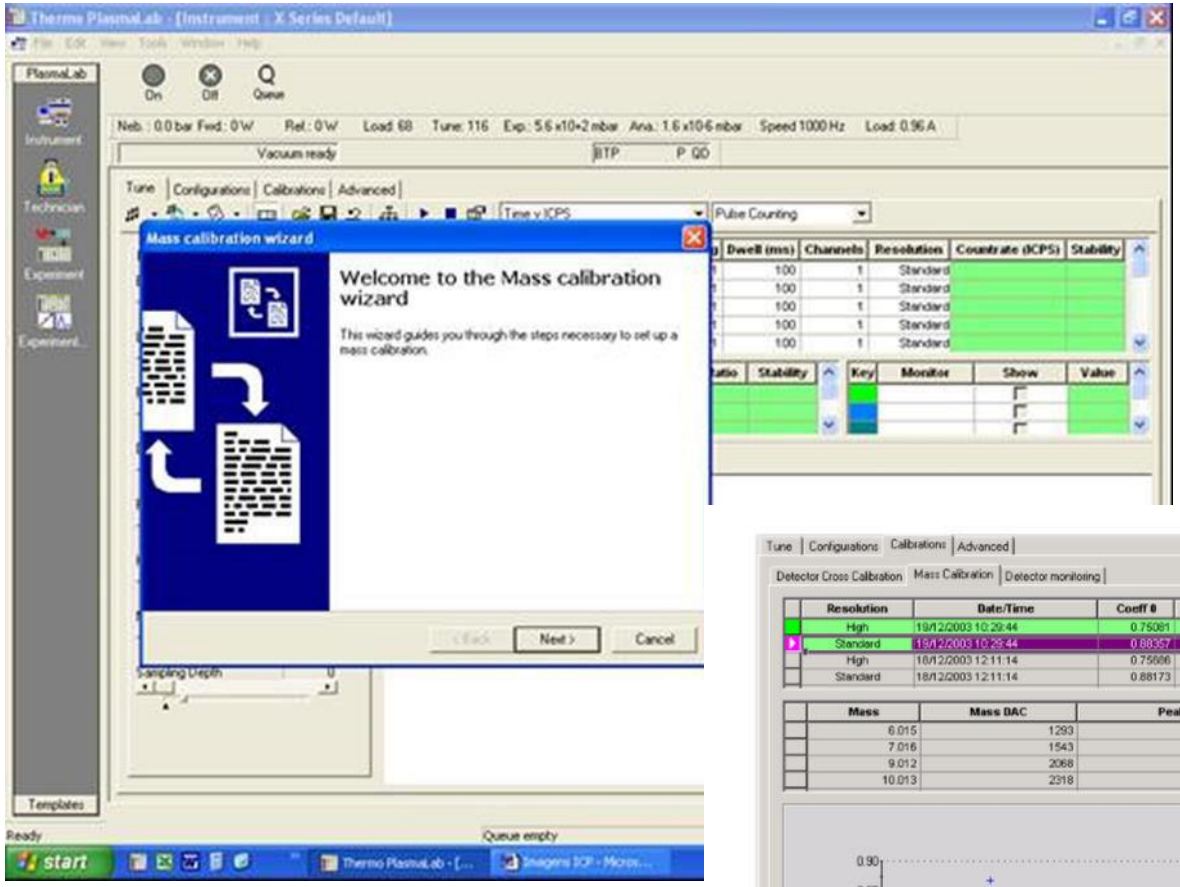

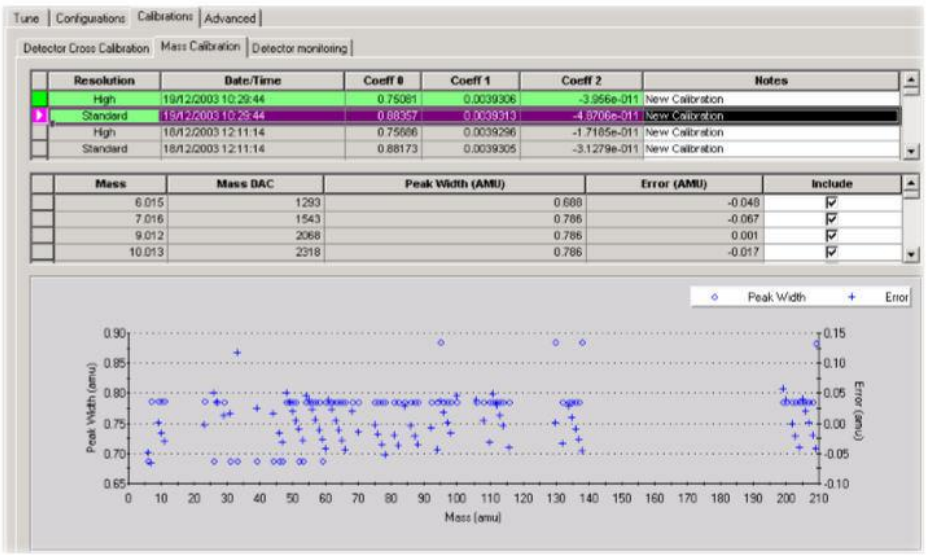

Manutenção e diagnóstico

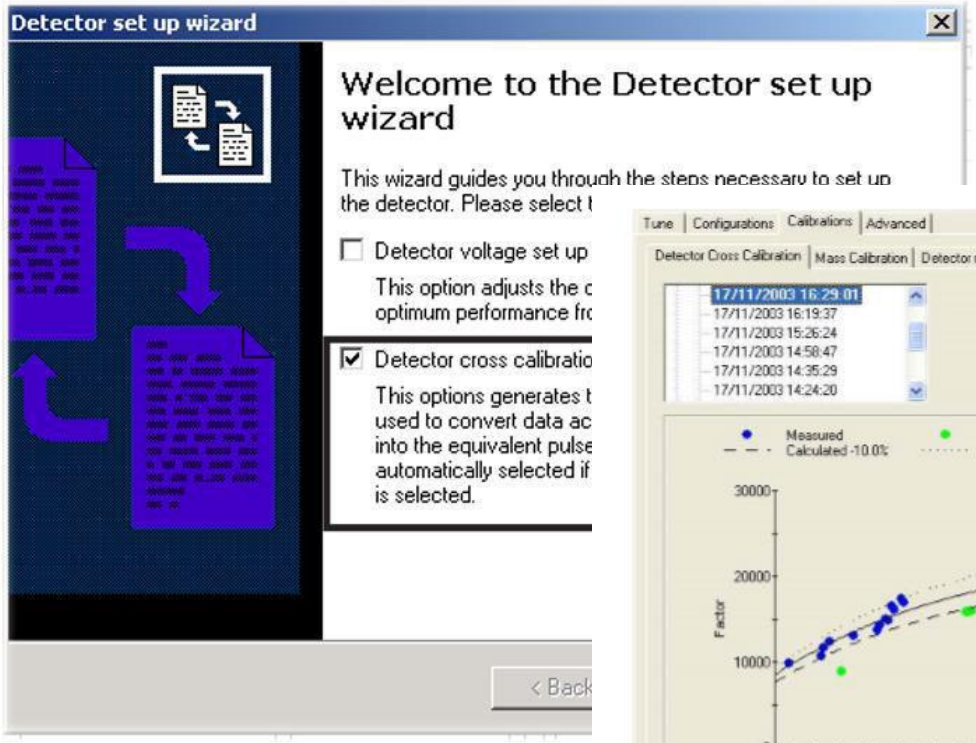

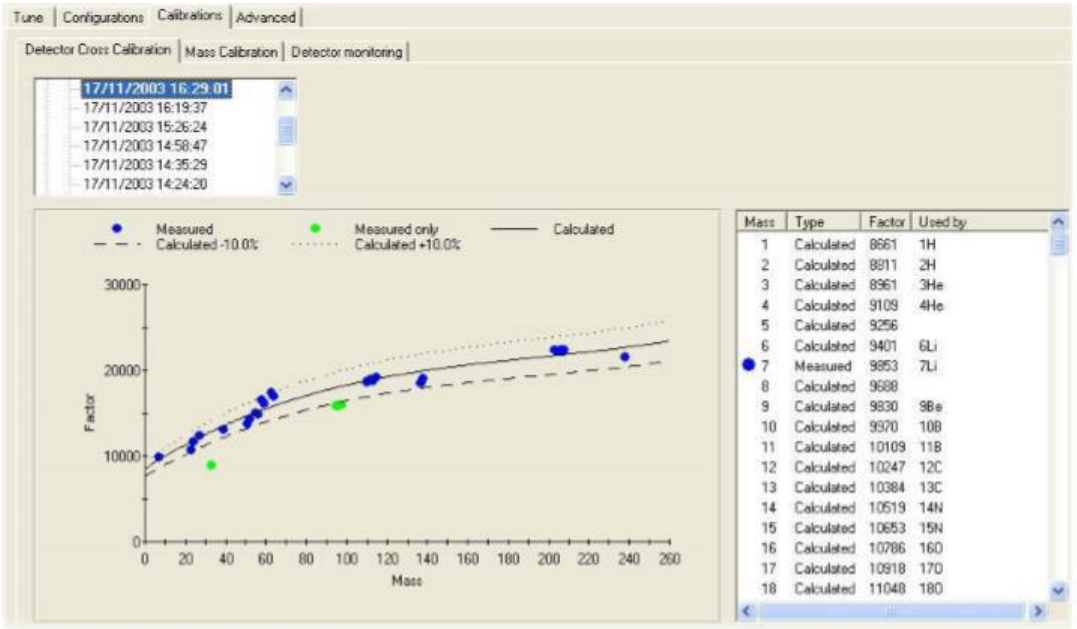

The detector cross calibration is used to convert the data acquired using the analog detector mode into the equivalent pulse counting data. The results of a successful calibration are shown on the *Detector Cross Calibration* page. This page is shown in both the *experiment* and the *instrument* views.

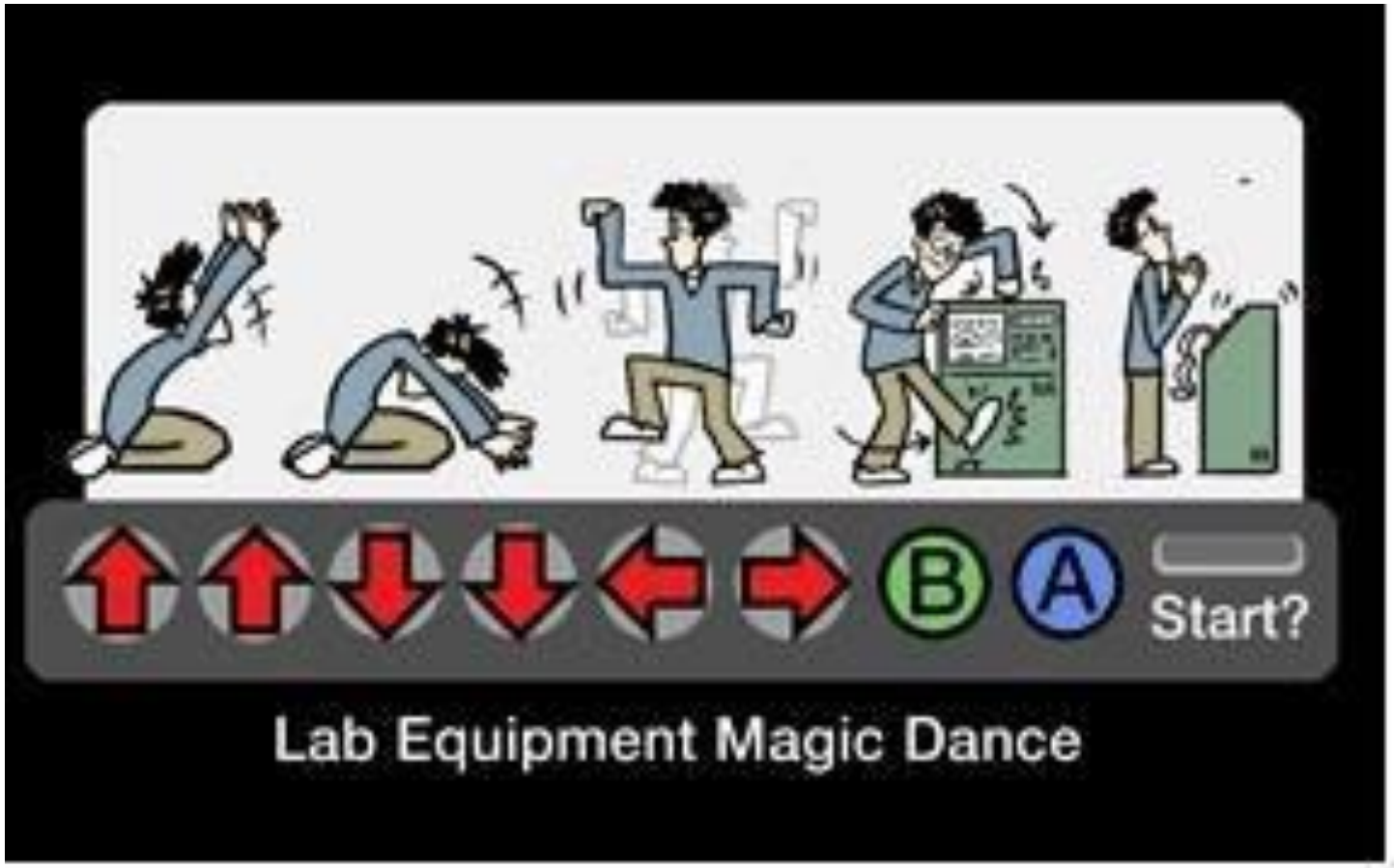
B
A
Start?
Lab Equipment Magic Dance


KEEP
CALM
AND
CALL A
TECHNICIAN

Curso de Introdução ao ICP-MS

"Um dia no ICP-MS (IPMA)"

Formadores: Joana Raimundo e Pedro Brito (IPMA)

2 a 4 de Novembro de 2016

Instituto Português do Mar e da Atmosfera, I.P. (IPMA)

ICP-MS Thermo X-Series

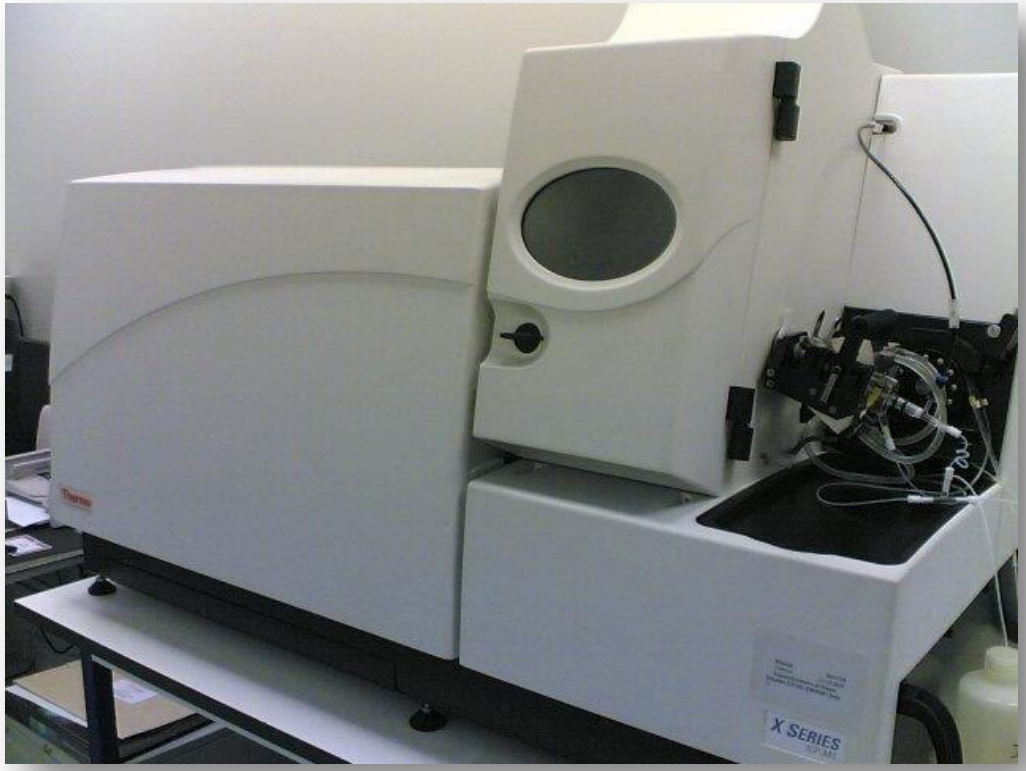

- Primeiras verificações
  - Condições sala
  - Tubos
  - Nebulizador
- Ligar aparelho
- Estabilização ±40 minutos

ICP-MS Thermo X-Series

Soluções

- Solução de limpeza (HNO_3)
- Padrão Interno (In)
- Soluções de calibração (Tune)
- Curvas de calibração

Otimização do sinal

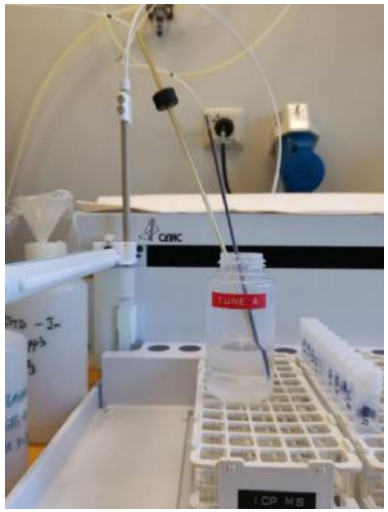

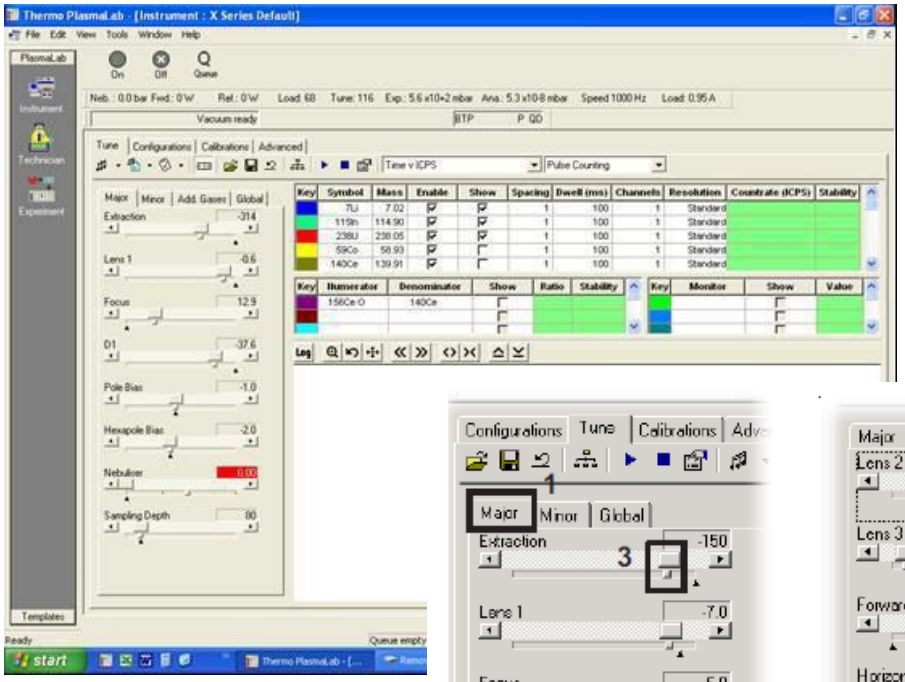

Performance report

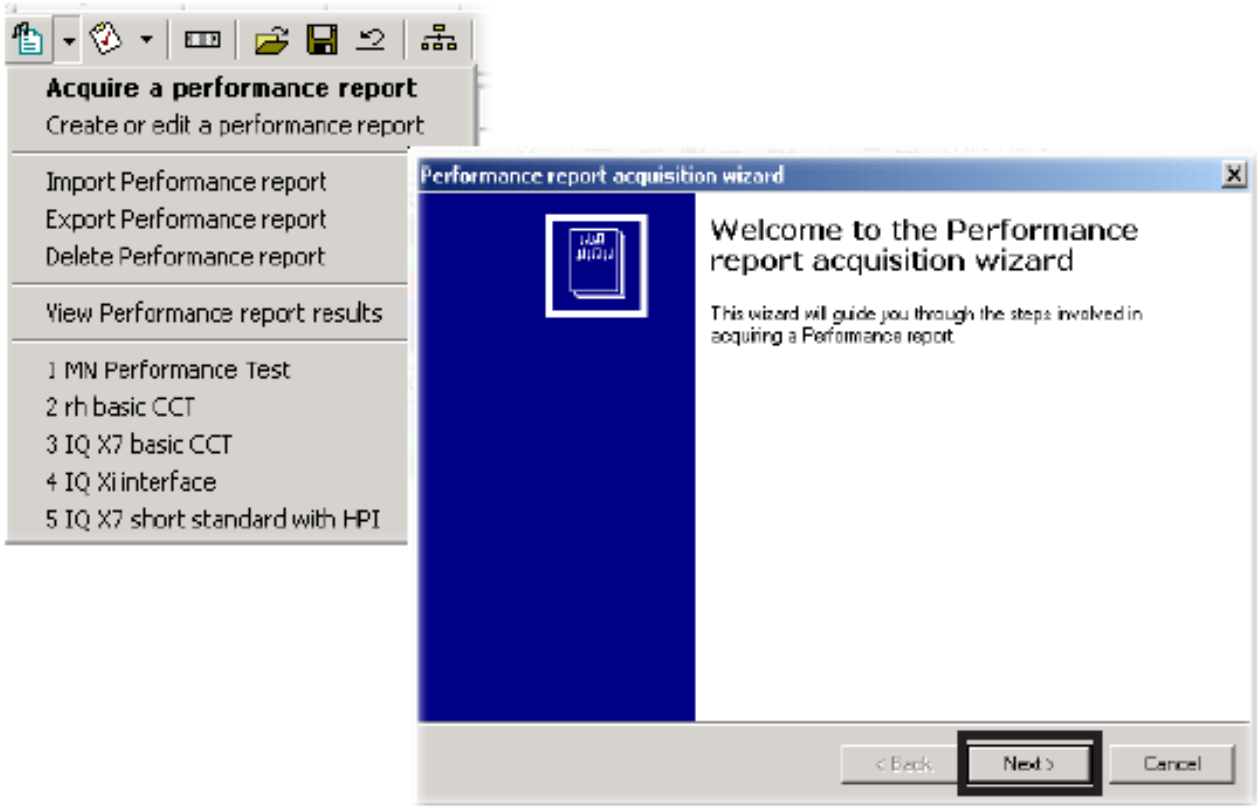

Performance Report

Autotune Report

Performance Report

Acquired at : 09/25/2002 03:13:04 PM
Report name : XS
Report version : 09/17/2002 10:51:11 AM

All failed criteria are highlighted in red.

Tune conditions

Major		Minor		Global		Add. Gases	
Extraction	-70	Lens 2	-20.0	Standard resolution	120	1% NH3 / He	0.00
Lens 1	-1.0	Lens 3	-45.0	High resolution	120	8% H2 / He	0.00
Focus	10.0	Forward power	1404	Analogue Detector	2490	AddGas	n/a
D1	-36.0	Horizontal	70	PC Detector	3770		
Pole Bias	-0.5	Vertical	475				
Hexapole Bias	-1.0	D2	-150				
Nebulizer	1.09	D4	-100.0				
Sampling Depth	90	Cool	13.0				
		Auxiliary	0.80				

Sensitivity and stability results

Run	Time	7Li	9Be	56Ar O	59Co	138Ba++	140Ce+	115In	138Ba	140Ce
1	03:13:04 PM	6601.525	1019.634	20893.45	11520.724	716.601	178.81	26310.135	17815.625	4280.777
x		6601.525	1019.634	20893.45	11520.724	716.601	178.81	26310.135	17815.625	4280.777
σ		0.00	0.00	0.00	0.00	0.00	0.00	0.00	0.00	0.00
%RSD		0.000	0.000	0.000	0.000	0.000	0.000	0.000	0.000	0.000

Run	Time	154Ba O	156Ce O	220Bkg	238U
1	03:13:04 PM	692.382	17744.682	0.101	6812.177
x		692.382	17744.682	0.101	6812.177
σ		0.00	0.00	0.00	0.00
%RSD		0.000	0.000	0.000	0.000

Ratio results

Run	Time	56Ar O/59Co	138Ba++/138Ba	140Ce++/140Ce	154Ba O/138Ba	156Ce O/140Ce
1	03:13:04 PM	20.910	0.040	0.042	0.039	4.194
x		20.910	0.040	0.042	0.039	4.194

Mass calibration

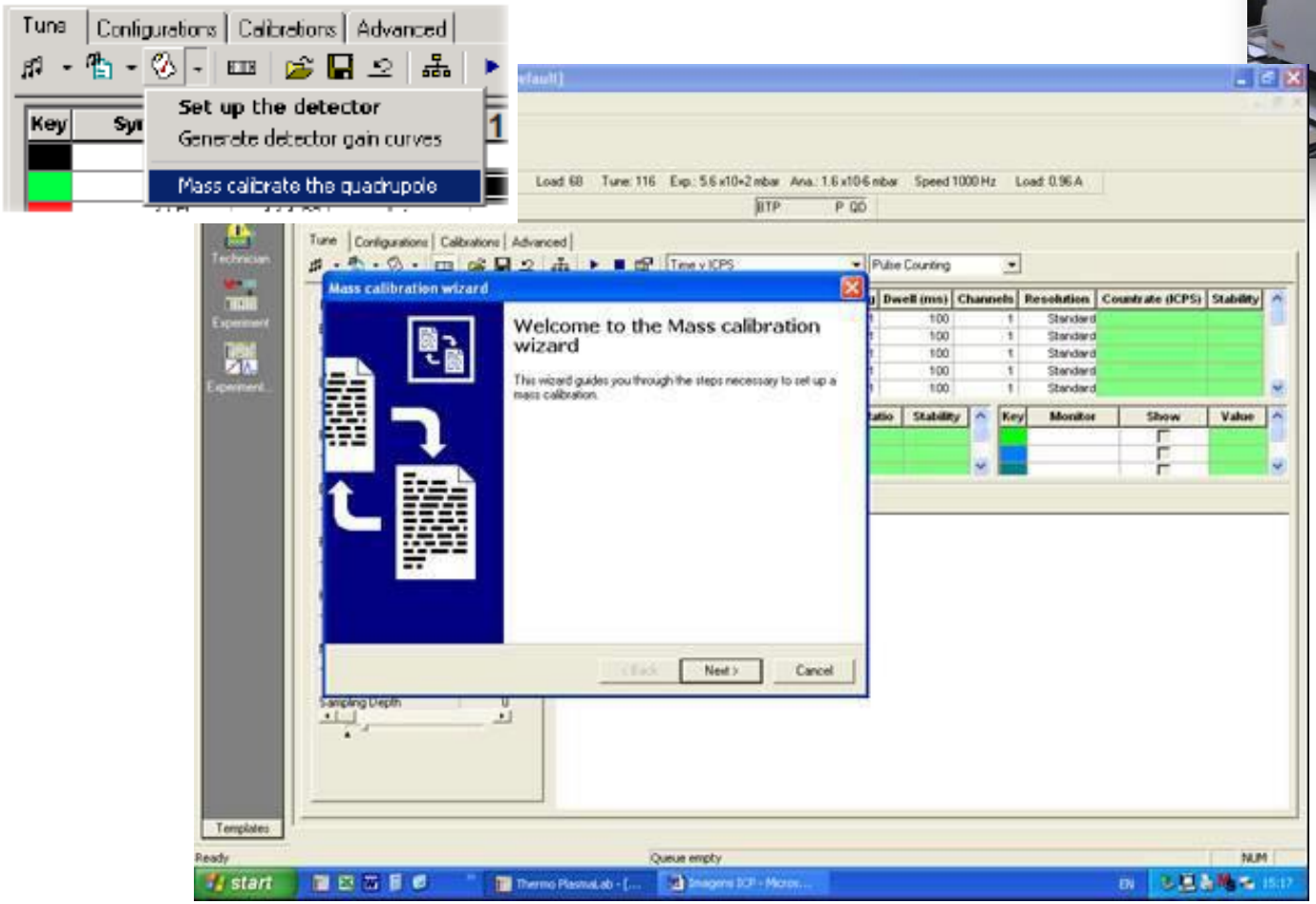

Performance report

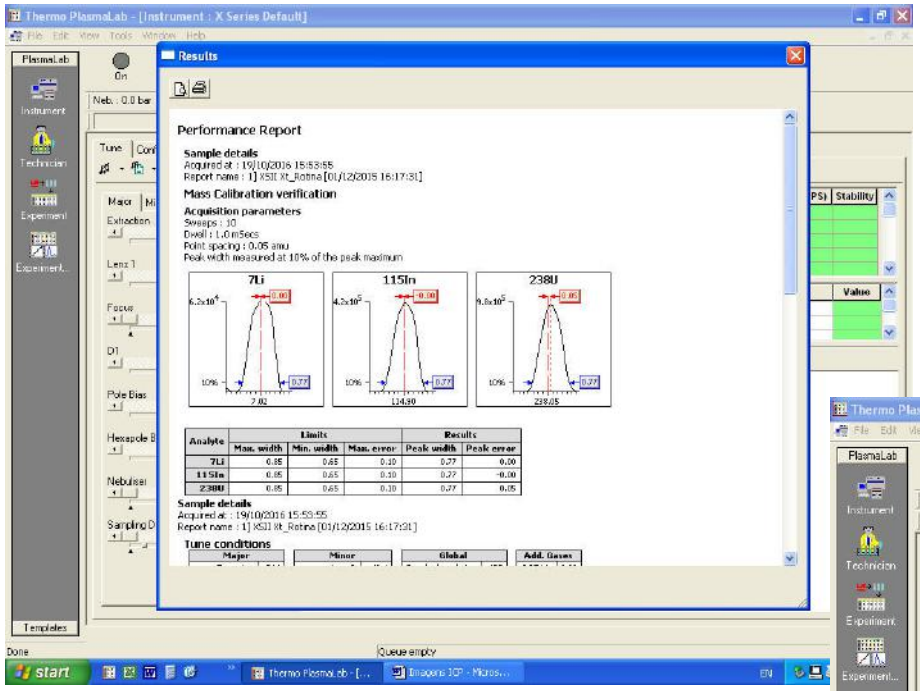

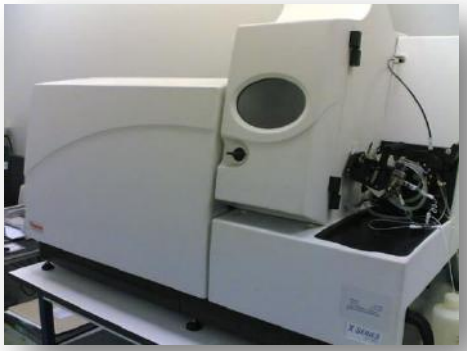

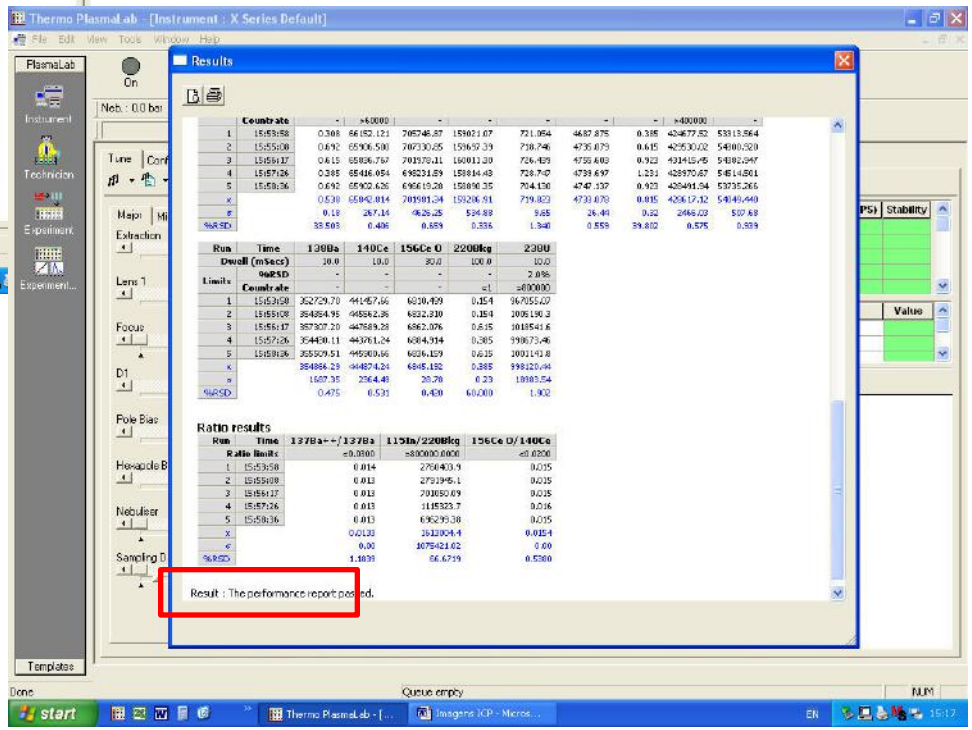

Seleção de analitos

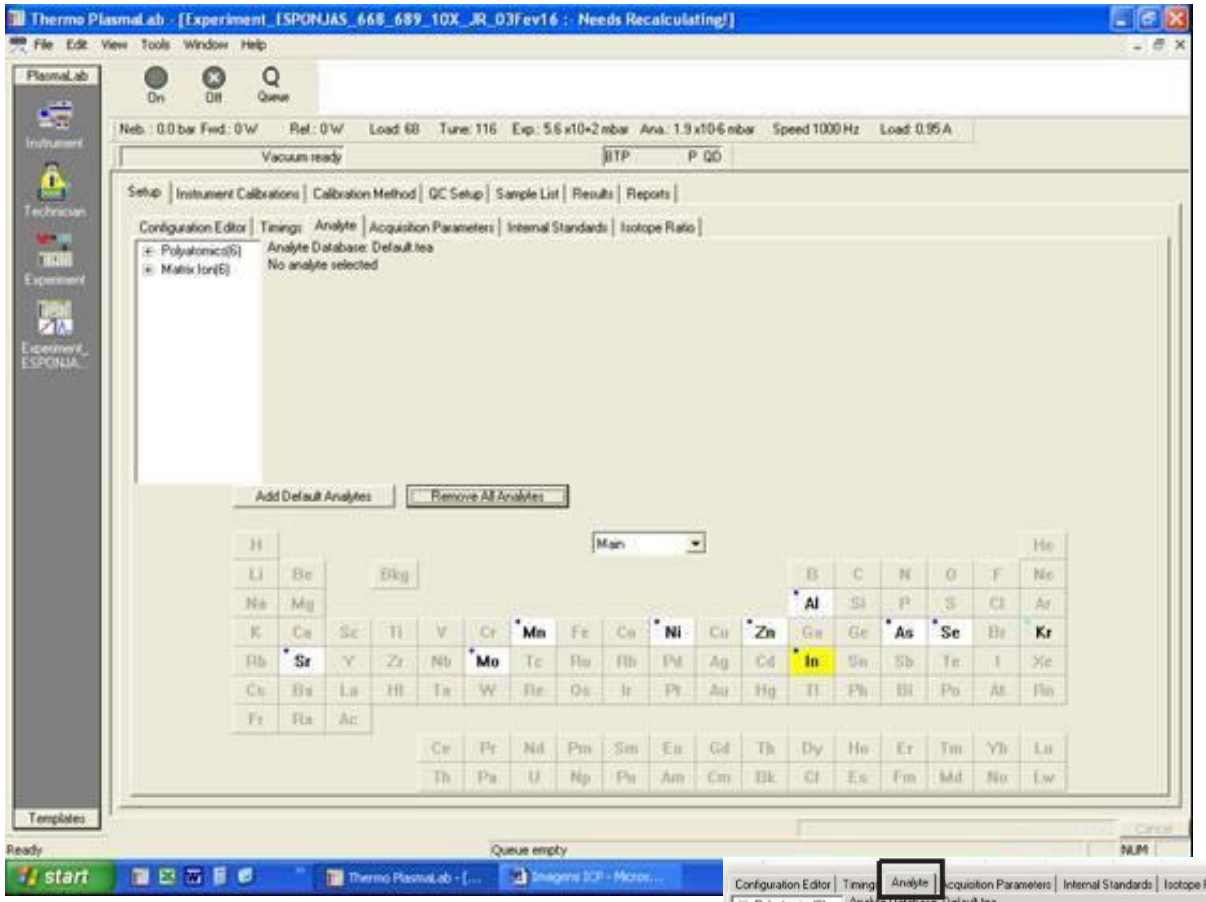

Identificação do padrão interno

Thermo PlasmaLab - [Experiment_ESPONJAS_668_689_10X_JR_03Fev16 :- Needs Recalculating!]

File Edit View Tools Window Help

PlasmaLab

On Off Queue

Instrument

Technician

Experiment

Experiment_ESPONJA...

Templates

Neb. : 0.0 bar Fwd.: 0 W Ref.: 0 W Load: 68 Tune: 117 Exp.: 5.6 x10+2 mbar Ana.: 1.9 x10-6 mbar Speed 1000 Hz Load: 0.94 A

Vacuum ready BTP P QD

Setup | Instrument Calibrations | Calibration Method | QC Setup | Sample List | Results | Reports

Configuration Editor | Timings | Analyte | Acquisition Parameters | Internal Standards | Isotope Ratio

Internal standard set

115In[Default] New

Internal dilution standard

None Concentration: 1000000 ppq

Standardisation techniques

Symbol	Technique	1st ion.pot.
27Al	Interpolate	5.9860
55Mn	Interpolate	7.4350
60Ni	Interpolate	7.6350
66Zn	Interpolate	9.3940
75As	Interpolate	9.8100
77Ar Cl	Interpolate	
82Se	Interpolate	9.7520
83Kr	Interpolate	13.9990
88Sr	Interpolate	5.6950
95Mo	Interpolate	7.0990

>> <<

Internal standards

Symbol	Concentration	Units	Profile
115In	1	ppb	☑

Cancel

Ready Queue empty NUM

start Thermo PlasmaLab - [... Imagens ICP - Micros... EN 15:13

Lista de amostras

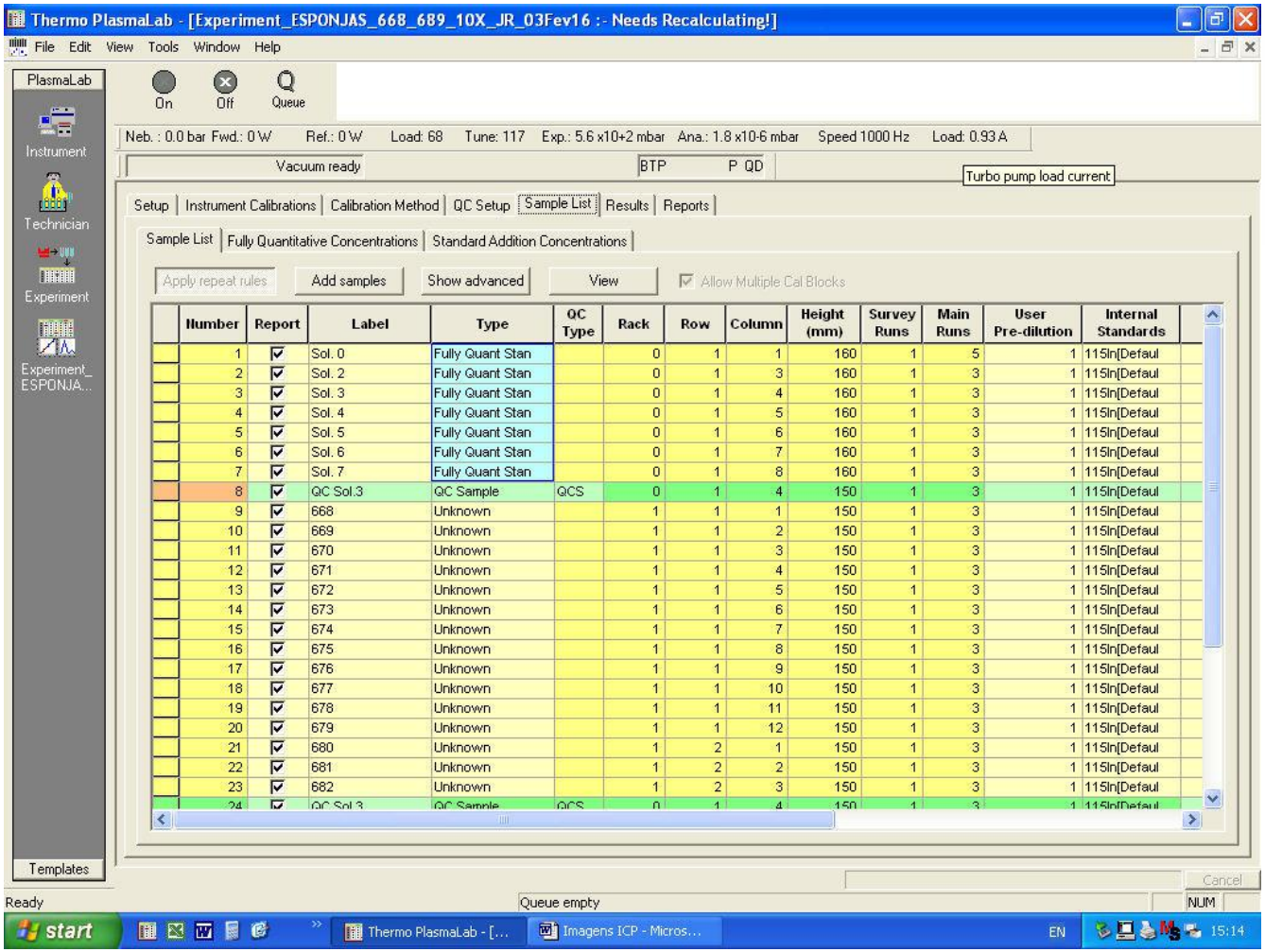

Number	Report	Label	Type	QC Type	Rack	Row	Column	Height (mm)	Survey Runs	Main Runs	User Pre-dilution	Internal Standards
1	☑	Sol. 0	Fully Quant Stan		0	1	1	160	1	5	1	115In[Defaul
2	☑	Sol. 2	Fully Quant Stan		0	1	3	160	1	3	1	115In[Defaul
3	☑	Sol. 3	Fully Quant Stan		0	1	4	160	1	3	1	115In[Defaul
4	☑	Sol. 4	Fully Quant Stan		0	1	5	160	1	3	1	115In[Defaul
5	☑	Sol. 5	Fully Quant Stan		0	1	6	160	1	3	1	115In[Defaul
6	☑	Sol. 6	Fully Quant Stan		0	1	7	160	1	3	1	115In[Defaul
7	☑	Sol. 7	Fully Quant Stan		0	1	8	160	1	3	1	115In[Defaul
8	☑	QC Sol.3	QC Sample	QCS	0	1	4	150	1	3	1	115In[Defaul
9	☑	668	Unknown		1	1	1	150	1	3	1	115In[Defaul
10	☑	669	Unknown		1	1	2	150	1	3	1	115In[Defaul
11	☑	670	Unknown		1	1	3	150	1	3	1	115In[Defaul
12	☑	671	Unknown		1	1	4	150	1	3	1	115In[Defaul
13	☑	672	Unknown		1	1	5	150	1	3	1	115In[Defaul
14	☑	673	Unknown		1	1	6	150	1	3	1	115In[Defaul
15	☑	674	Unknown		1	1	7	150	1	3	1	115In[Defaul
16	☑	675	Unknown		1	1	8	150	1	3	1	115In[Defaul
17	☑	676	Unknown		1	1	9	150	1	3	1	115In[Defaul
18	☑	677	Unknown		1	1	10	150	1	3	1	115In[Defaul
19	☑	678	Unknown		1	1	11	150	1	3	1	115In[Defaul
20	☑	679	Unknown		1	1	12	150	1	3	1	115In[Defaul
21	☑	680	Unknown		1	2	1	150	1	3	1	115In[Defaul
22	☑	681	Unknown		1	2	2	150	1	3	1	115In[Defaul
23	☑	682	Unknown		1	2	3	150	1	3	1	115In[Defaul
24	☑	QC Sol.3	QC Sample	QCS	0	1	4	150	1	3	1	115In[Defaul

Curvas de calibração

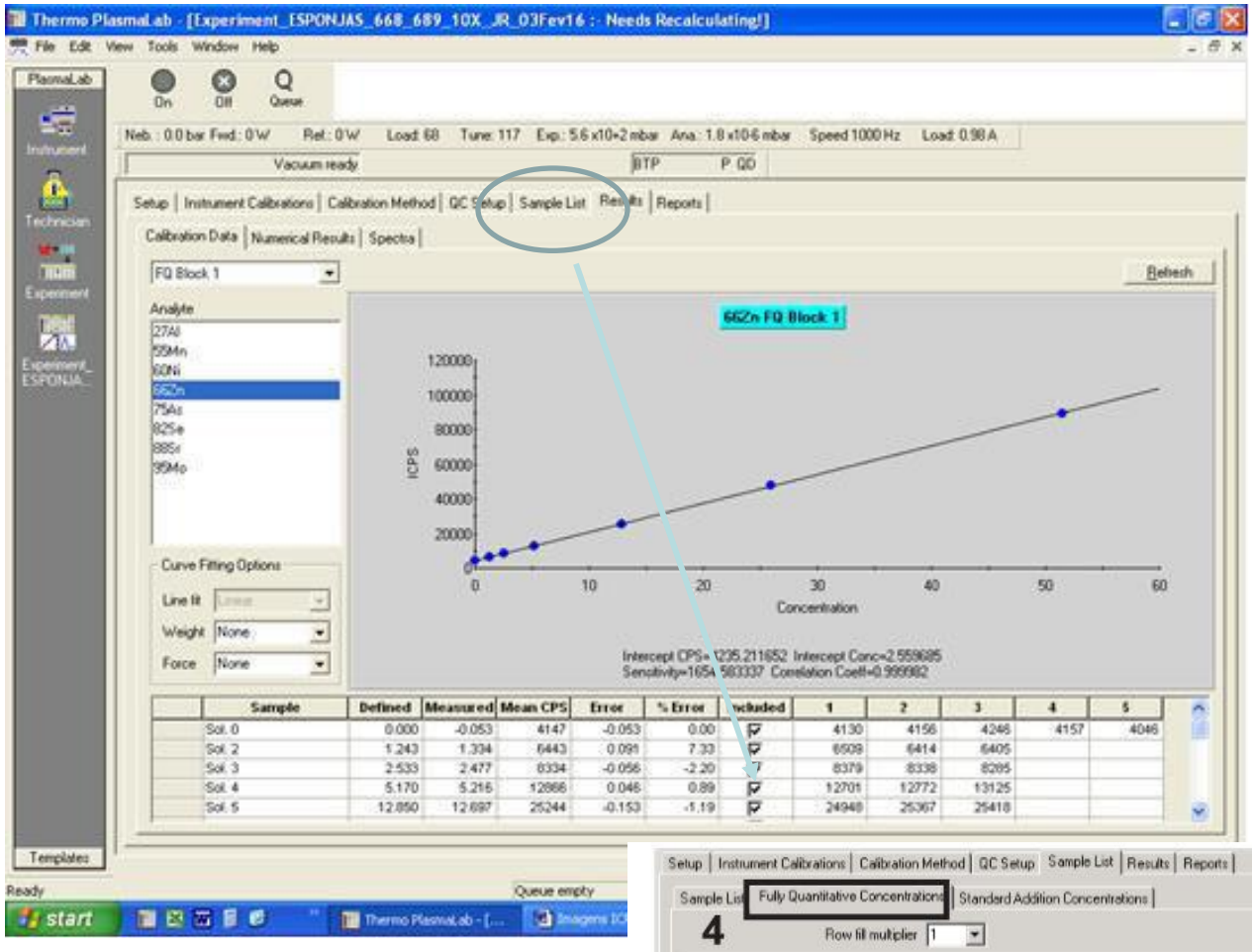

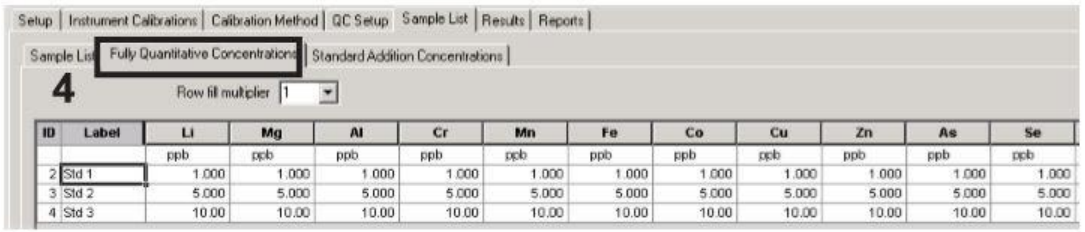

Resultados

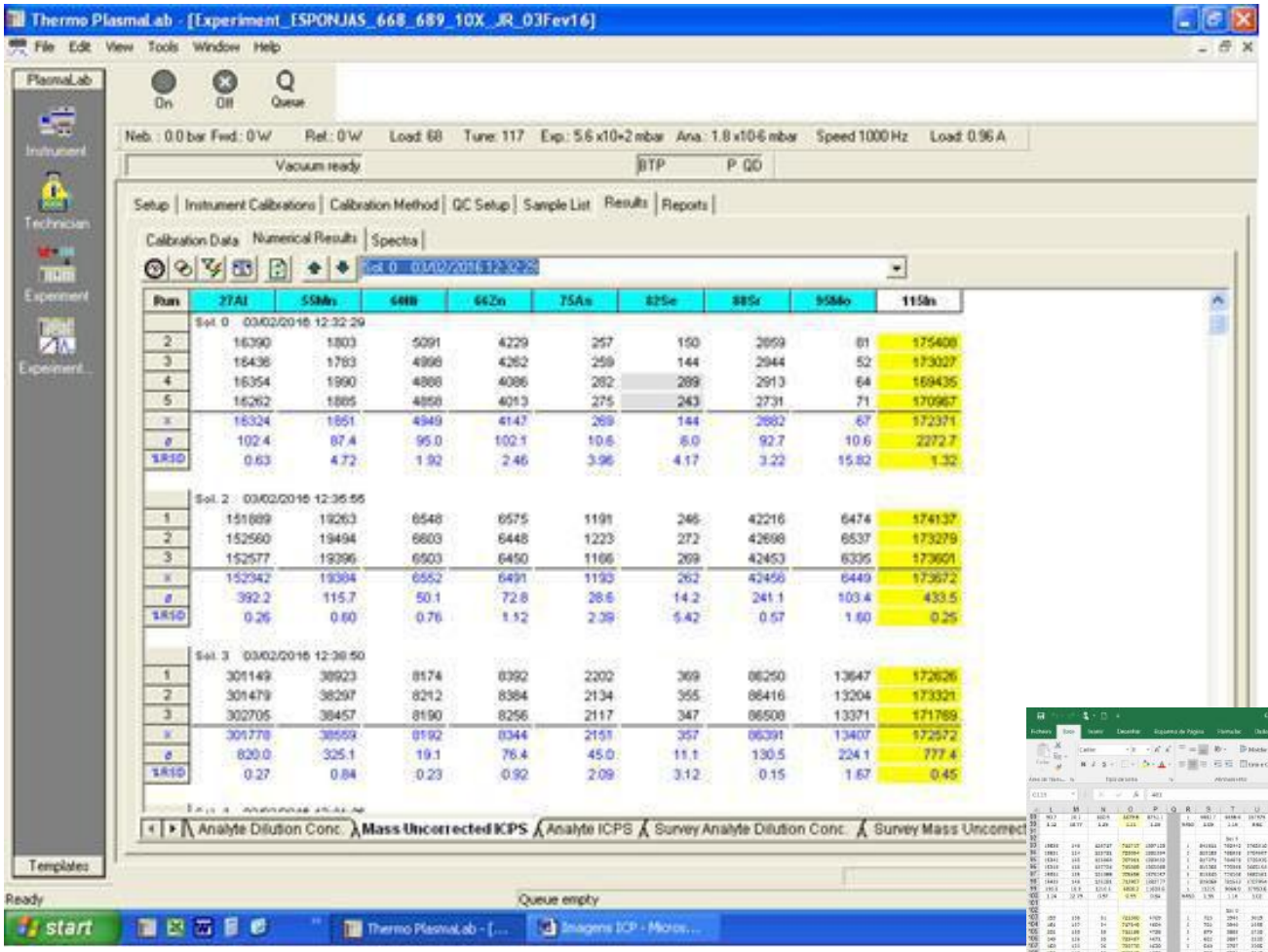
Thermo PlasmaLab - [Experiment_ESPONJAS_668_689_10X_JR_03Fev16]
File Edit View Tools Window Help
PlasmaLab
On
Off
Queue
Vacuum ready
Setup | Instrument Calibrations | Calibration Method | QC Setup | Sample List | Results | Reports
Calibration Data | Numerical Results | Spectra
Templates
Ready
Queue empty
start

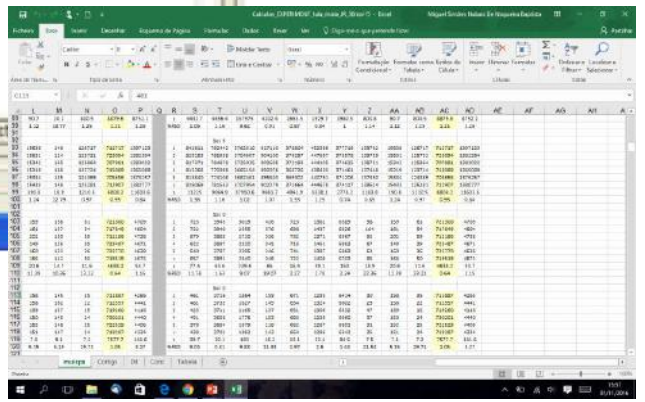

ICP-MS – Tratamento de resultados

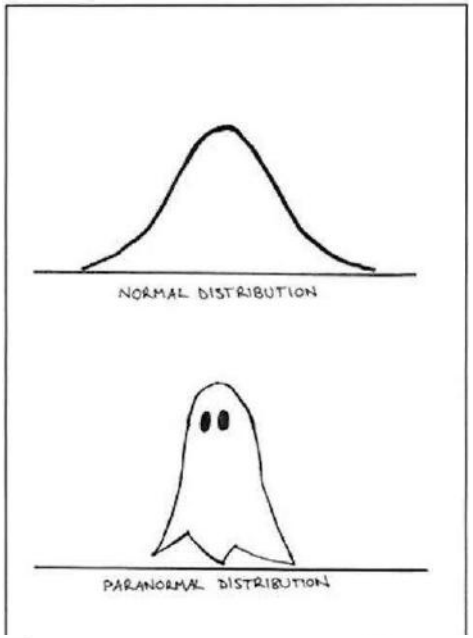

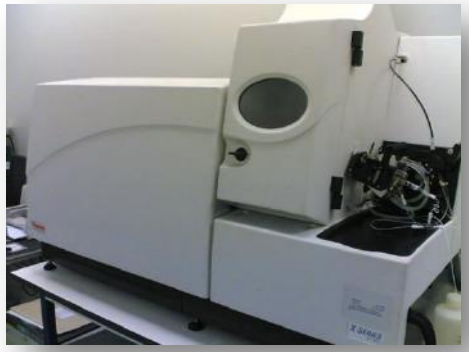

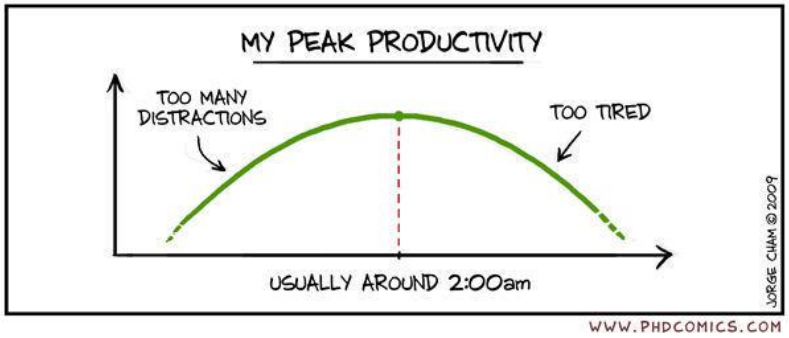

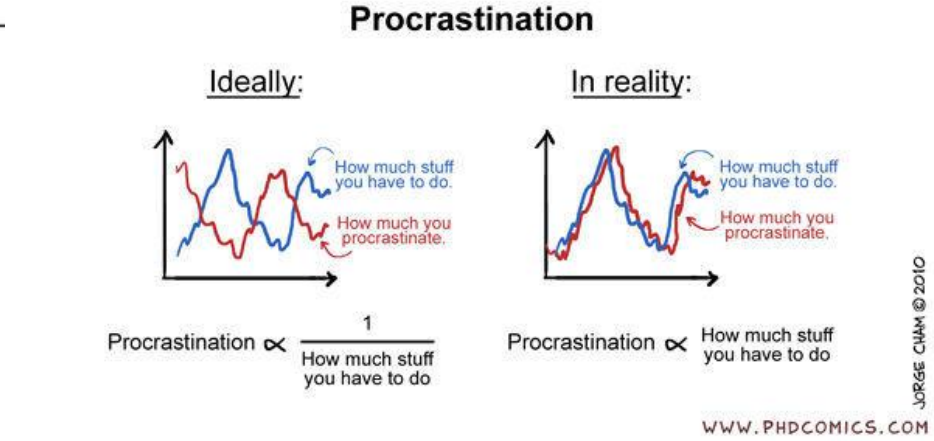

Curso de Introdução ao ICP-MS

Anexos

MAY, 1975 Vol. 100, No. 1190

The Analyst

Mass-spectrometric Analysis of Solutions Using an Atmospheric Pressure Ion Source

A. L. Gray

Applied Research Laboratories Limited, Wingate Road, Luton, Bedfordshire

The use of an atmospheric pressure d.c. plasma as an ion source has been explored for the direct analysis of solutions introduced into it from a nebuliser. Ions are extracted from the plasma into a vacuum system and are focused into a quadrupole mass analyser. A high yield of singly charged ions with a small energy spread is obtained and clear spectra of the constituents of the solution are observed.

The method is described and the results observed on simple solutions are given. The sensitivity of the method for a number of elements is indicated and appears to be comparable with other trace-analysis methods.

The determination of trace elements in solutions by instrumental analysis has become an important requirement and a number of different methods have come into use, prominent among which is atomic-absorption spectrometry. More recently much attention has been paid to optical emission methods involving plasma excitation. Both of these methods enable low limits of detection to be achieved in routine applications. Atomic absorption, in the form in which instruments are at present marketed, is primarily a single-element technique, thus for multi-element routine analysis the use of an emission source for excitation combined with a conventional scanning or direct-reading spectrometer is attractive. A variety of plasma sources have been reported[1–3] and one of these sources is now commercially marketed.[4] Although the high temperatures achieved in the most suitable of these plasmas lead to low limits of detection and relative freedom from inter-element effects and interferences, there are still requirements for higher sensitivity and flexibility that are not ideally met.

Many of the most difficult problems that arise in trace analysis have been solved by recourse to mass spectrometry. The only suitable ion sources at present available for the determination of most elements in the Periodic Table are the ion bombardment and spark sources, and in order to use either of these sources sample preparation into the preferred solid form is necessary. Although adequate methods are available for this purpose, neither source is well suited to routine analysis at large sample throughputs, and mass analysers compatible with these sources are necessarily costly.

Consideration of possible ways in which sample introduction and analyser design could both be simplified while retaining the wide capability and sensitivity of the mass spectrometer for element determinations led to the examination of the ionisation process that occurs in the atmospheric pressure electrical plasmas that were concurrently being studied as optical emission sources.

The most convenient of these sources for this initial investigation was a small wall-stabilised d.c. plasma source that had been found to be very stable and reproducible as an optical source for the analysis of steels.[5] It was concluded that this plasma, when fed with the sample in a suitable form, produced substantial ion populations of the sample elements at atmospheric pressure and that if these ions could be representatively transferred to a mass analyser at its much lower operating pressure a useful technique might be developed. In particular, the possibility of direct introduction of the sample at atmospheric pressure into the plasma, for example by means of a solution nebuliser, was thought to be especially attractive. Techniques of mass-spectrometric sampling of flames used in studies of combustion processes have been well established for some years[6,7] and although rather higher temperatures occur in plasmas, it seemed reasonable to attempt sampling of this small d.c. plasma in the same way. This paper describes the production of ions in a plasma and the equipment used for the investigation, and presents the results obtained so far.

The Production of Sample Ions

A wide variety of physical processes can be used to produce ions from sample atoms. Among these processes some of the best known are electron bombardment, photo-ionisation, field ionisation and thermal ionisation, and ion sources that involve the use of all these mechanisms are well known. In all of the sources commonly used, however, it is necessary for the sample, usually in the form of a gas, to be introduced into the vacuum system. When a solid sample is used two established methods are available for producing ions directly from it, either by bombardment by a primary ion beam, or by making the sample one electrode of a spark gap and initiating a discharge in the gap.

The characteristics of the different ion source methods are extensively discussed in the literature, but it is sufficient to mention here that apart from requiring the sample to be inside the vacuum, those most useful for the analysis of solids and liquids produce ions with a wide distribution of energies and containing many ions with multiple charges. Both of these properties of the resulting ions require the use of a rather complex mass analyser system for their successful analysis, as high resolution is necessary to resolve the multiply charged ion peaks from the wanted spectrum and an energy analysing stage is required in order to restrict the energy range of the incoming ions so as to enable high resolution to be achieved.

Ionisation at atmospheric pressure has recently been reported by Caroll *et al.*[8] for organic vapours. Molecular ionisation is achieved in this source mainly by the addition or removal of protons as a result of ion - molecule reactions, and its attraction lies particularly in the high yield of M^+, MH^+ or $(M-H)^+$ ions, which is obtained because of the small excess of energy available for fragmentation. Such a source, although of interest for organic applications, cannot be used for elemental analysis without some additional mechanism to enable the sample to be transformed into the dissociated vapour state before ionisation.

One of the most convenient methods for vaporising and dissociating a sample, introduced either as liquid droplets or fine solid particles, is to feed it in a gas stream to a high-temperature plasma, and this is done in the plasmas used for optical excitation. At atmospheric pressure these plasmas may, under favourable electrical conditions, attain core conditions that approach thermal equilibrium, thus favouring rapid vaporisation and dissociation. Typically, in a small discharge in argon the core temperature may reach 5000 K or more. Under these conditions a small amount of fine solid particles or liquid droplets introduced into the carrier gas will, on entering the core, be vaporised and most molecules dissociated.

The extent to which the resulting atoms become ionised is described by the Saha equation, which defines the ionisation constant at the given temperature for each component of the system. The degree of ionisation of each element present is then dependent on the relationship of the ionisation constant and the partial pressure of the atom in the plasma. A fuller discussion of this subject is not possible here but it is well treated by Boumans.[9] However, in practical terms, for a component in solution at 100 μg ml^{-1} concentration, giving a partial pressure in the core of about 10^{-6} atm at a core temperature of 5000 K, the degree of ionisation ranges from 100 per cent. for an element of ionisation potential of 5 V or less down to 15 per cent. for a potential of 10 V. At this partial pressure, even 15 per cent. ionisation represents an enormous number of ions, and as the partial pressure is reduced the degree of ionisation rapidly approaches 100 per cent. All but 13 elements of the Periodic Table have first ionisation potentials below 11 V and only one, barium, has a second ionisation potential below this level. Thus, such a plasma represents a plentiful source of ions with single charges and contains very few ions with more than one charge.

An additional advantage of operating at atmospheric pressure is that the ions produced very rapidly reach equilibrium with the surrounding gas molecules, mostly argon, and thus have kinetic energies of between 0·5 and 1 eV, corresponding to those of the gas molecules in thermal equilibrium in the plasma. The low electric field of about 50 V cm^{-1} in the plasma is insufficient to affect their energies significantly, thus resulting in a low ion energy spread. The ions produced at atmospheric pressure have to be transferred from the hot core to the mass analyser in a vacuum without significantly affecting their relative concentrations. The flow of carrier gas through the plasma core leaves the outlet of the arc as a small flame, carrying the ions with it.

The transit time from core to flame is short enough for little ion recombination to occur, even though the gas cools considerably during this time. Techniques for sampling flame

gases at temperatures of up to 3000 K have been developed by several workers[6,7] who have studied combustion processes in flames, and such techniques can also be used here. During the course of the work described, the suggestion was also made by Alkemade[10] that a flame of the type used for atomic absorption should be a useful analytical source of ions. In such flames, however, the rather lower temperatures obtained and the highly reactive species present may give rise to more complex spectra that are beyond the capability of a simple mass analyser to resolve.

The process of sampling a flame or plasma through a small orifice in a boundary wall into a region of low pressure is complex and has been extensively studied.[11] Provided that sampling conditions are correctly chosen, it is possible to avoid both mass selective effects in the flow through the orifice and distortion of the spectrum due to ion - molecule reactions in the boundary layer in front of the orifice, so that the sample expanded into the low-pressure region can be representative of the plasma composition. Once they are inside the vacuum system the mean free path of the ions is sufficiently large to freeze the composition effectively, and ions can be separated from the accompanying molecules and directed into the mass analyser.

Experimental

Apparatus

The experimental system used for this investigation is shown in schematic form in Fig. 1. It consists of three main functional groups:

the capillary arc plasma, its power and gas supplies, and nebuliser for introduction of the sample and desolvator;
the sampling orifice, ion-beam forming system and mass analyser;
the ion detector, pulse counting system and signal read-out.

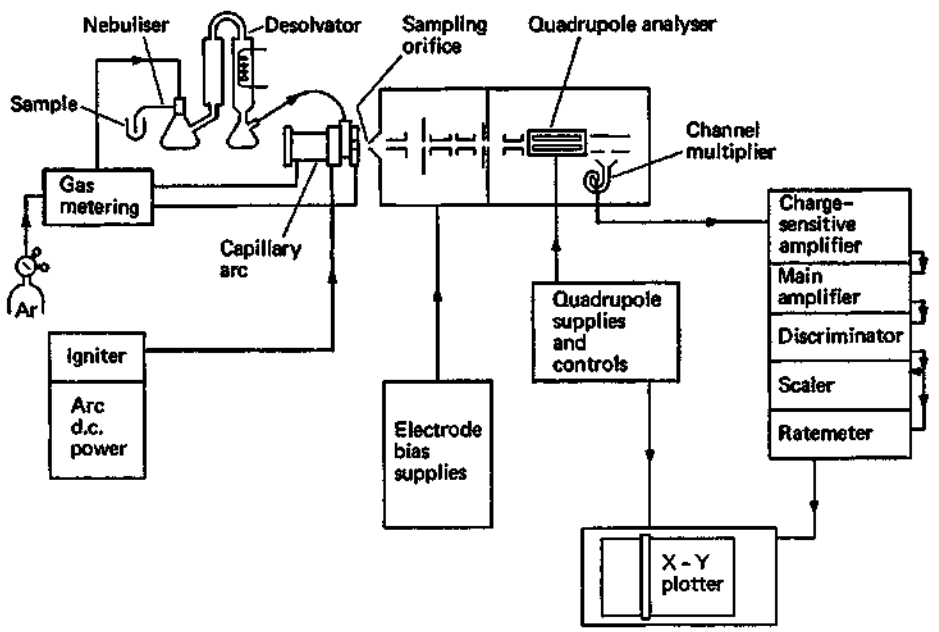

Fig. 1. Plasma sampling mass analysis system.

Plasma and Sample Introduction

The capillary arc plasma unit used for this work has been described,[1,12] and is shown in Fig. 2. The discharge occurs in the bore of the main insulator and is approximately 1 cm long and less than 3 mm in diameter. The tantalum cathode and copper anode are recessed so as to minimise contamination. Three separate argon flows metered by capillary tubes are fed to the arc: a small flow to cool the cathode; a main flow along the discharge channel; and the sample flow, which is introduced tangentially into the centre of the discharge. The main

body of the arc, which also forms the anode, and the block supporting the cathode, through which the tail flame emerges, are water cooled. The arc is fed from a well smoothed d.c. supply of 300 V through a ballast resistor of about 20 Ω. It is started by a high-voltage igniter. Spectroscopic measurements of the core temperature show that it rises from 2500 K

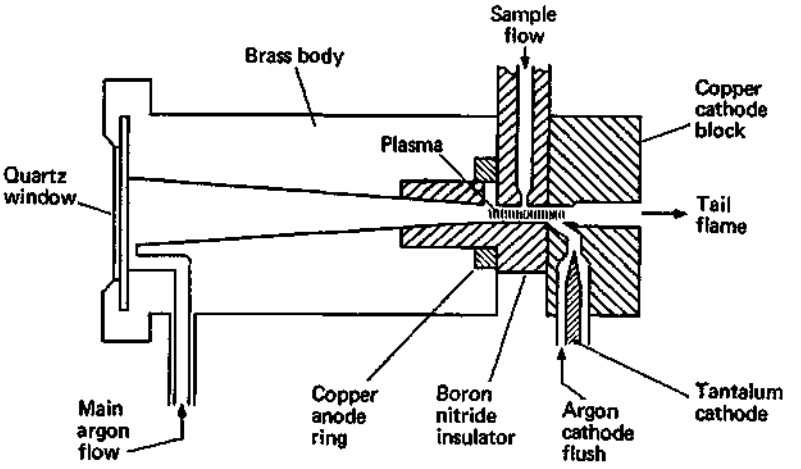

Fig. 2. Capillary arc plasma unit.

at 6 A to 5700 K at 12 A. The arc is typically operated at between 10 and 12 A. Operation is very stable and quiet and it will run for long periods without the need for attention.

Aqueous solutions are introduced into the sample stream by direct nebulisation. Both pneumatic and ultrasonic nebulisers are used, as convenient. The ultrasonic nebuliser is similar to that described by Hoare and Mostyn,[13] except that a concave crystal is used to agitate the surface of the sample, which is contained in a sample cell with a thin Mylar window that admits the energy from the transducer. The sample carrier gas is passed across the liquid surface and the mist is carried to the plasma. The ultrasonic nebuliser, although less convenient to use than the pneumatic type, allows the sample gas flow to be varied without affecting the nebulisation efficiency. Whichever nebuliser is used the gas stream containing the sample droplets is passed through a glass chamber heated to about 470 K and then through a water-cooled condenser. This condenses and removes much of the water from the sample. Typical operating conditions for the whole system are shown in Table I.

TABLE I

TYPICAL OPERATING CONDITIONS

Orifice diameter	75 μm	Sample size	5 ml
Operating pressures		Sample consumption	0·25 ml min^{-1}
1st chamber	5×10^{-4} torr	Electrode potentials	
2nd chamber	2×10^{-6} torr	*1st chamber*	
Gas flows to plasma		Collector electrode	−200 V
Main flow	1 l min^{-1}	Cylinder 1	−60 V
Sample flow	1·5 l min^{-1}	Cylinder 2	0 V
Cathode purge	0·1 l min^{-1}	*2nd chamber*	
Plasma current	12 A	Cylinder 3	−20 V
Pneumatic nebuliser		Quadrupole body	−7 V
Sample uptake	3 ml min^{-1}	Quadrupole rods	−10 V mean d.c. level
Efficiency	5% approx.		
Ultrasonic nebuliser		Channel electron multiplier	
Frequency	1 MHz	Type, Mullard	B 318 AL
Power to transducer	15 W	EHT at mouth	−2800 V

Ion Sampling, Focusing and Analysis

Optimum sampling conditions from the plasma are obtained with an orifice diameter of between 75 and 125 μm and an orifice at the lower end of this range is usually used. This orifice admits a gas flow into the first vacuum stage (Fig. 3), which is pumped by a 9-in oil diffusion pump that maintains a pressure of less than 10^{-3} torr.

The orifice, which is drilled in a platinum insert, opens on the low-pressure side into a cone, which enables the effective wall thickness at the orifice to be comparable with the diameter of orifice. The insert is itself mounted in the tip of a metal cone, which projects into the tail flame and is mounted at its base on a small gate valve, which enables the cone to be isolated from the vacuum chamber for cleaning. Immediately inside the gate valve, ions are collected by a cylindrical electrode maintained at a negative potential of a few hundred volts and then focused into a beam so as to pass through a 2-mm aperture into the second chamber, the pressure in which is pumped to below 10^{-5} torr by a 4-in diffusion pump. A further cylindrical electrode ensures that the ion beam is co-axial with the quadrupole mass analyser system, which is mounted in this chamber.

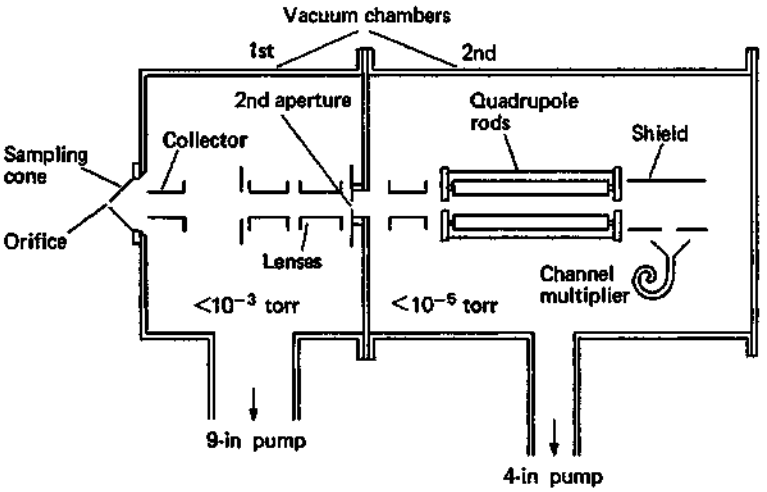

Fig. 3. Ion sampling, focusing and analysis system.

The quadrupole mass analyser or filter consists of four cylindrical electrodes mounted parallel to and equidistant from the beam axis. By means of appropriately controlled a.c. and d.c. potentials applied to the electrodes, the field along the axis is arranged so that for any particular field only ions of one mass to charge ratio (m/e) have a stable trajectory and emerge from the end of the system.

All other ions are deflected away from the axis and are lost. The ratio of a.c. to d.c. field determines the "window" of ion mass that is transmitted and the a.c. level the mass centre of the window. This analyser is very compact and simple, and its operating parameters are set by purely electrical levels. The electrode system used has rods that are 6 mm in diameter and 12·5 cm long. A mass range of 0–300 a.m.u. is covered with a resolution up to 300 ($\frac{M}{\Delta M}$, 10 per cent. valley). A useful review of these analysers is given by Dawson and Whetten.[14] A variety of such instruments are commercially available, although, as in the prototype used, long-term stability and reproducibility do not always meet the full requirement for quantitative measurements. However, short-term stability has been found adequate to explore the potential of the method, and the scope for improvement in quadrupole performance is being studied.

Those ions which are transmitted by the analyser emerge on the axis and can be passed directly into the detector. However, because in the equipment constructed the quadrupole axis is directly on a line of sight from the aperture, and the plasma forms a very intense ultraviolet light source, it is found necessary to mount the detector off the axis and to deflect the ions into it. Even this arrangement is not sufficient to reduce the photon count to zero if the plasma core is located on the system axis because of the light scattered in the electrode system. However, the plasma can also be displaced slightly from the axis, provided that the tail flame plays on the sampling orifice, and this adjustment reduces the photon count to zero.

Ion Detection and Signal Handling

The ion detector used is a channel electron multiplier. This detector, unlike other types of electron multiplier, tolerates the relatively poor vacuum of the second stage and can repeatedly be exposed to the atmosphere. Ions striking the mouth of the detector release electrons that are attracted along the conducting inside surface of the tube by the high electric field. Each time they strike the wall they release further electrons until an average gain of about 10^8 is achieved. The multiplier is operated in the saturated mode so that the output pulse height obtained for each incident ion is approximately the same. The pulses are fed to a charge-sensitive amplifier and the main amplifier and then through a conventional pulse height discriminator, thus rejecting electrical noise and presenting standardised output pulses to a linear rate meter and scaler. These instruments enable the arrival rate of pulses to be displayed on a meter over a range of 10–10^6 pulses s^{-1} and also the total number of pulses in a defined time interval to be integrated.

The pulse rate at any given mass setting is a measure of the rate at which ions of that mass are entering the system. If this pulse rate is displayed as the Y deflection of an X - Y recorder and the X deflection made proportional to the mass setting, then a mass spectrum is obtained when the mass analyser is set to scan through the mass range, thus providing a very convenient display for a qualitative examination of the ions present in the plasma. Alternatively, quantitative measurements can be made by integrating counts on the scaler for known periods at each mass of interest.

These two modes of operation represent the simplest available. Because of the simplicity of electrical control, the quadrupole mass analyser and counting system permit electrical programming and data handling to be used in order to enhance greatly the operational convenience.

Operation

The operation of the system described has been explored on aqueous solutions. The vacuum pumps are usually left running so that start up is determined by the warm-up time of the counting electronics and of the heater of the desolvator. The arc can be started after briefly purging to clear the air from it and samples introduced as soon as the desolvator is hot. Samples can be exchanged in less than 1 min by using a pneumatic nebuliser but a slightly longer time is required in order to clean and change the window of the ultrasonic nebuliser.

During operation the tip of the arc cathode becomes white hot and forms a molten hemispherical tip to the tantalum pin. The latter is usually replaced with a fresh, sharply pointed pin after operating for about 4 h. Longer periods of operation can usually be achieved on one electrode but the arc tends to burn unstably at the end of the life of the electrode. The change is made earlier in order to avoid the occurrence of this effect at the most interesting part of the day's run.

The orifice needs to be cleaned at intervals, depending on the material being analysed. With trace solutions cleaning is required after operation for about 10–20 h and can easily be performed in an ultrasonic cleaning bath. Sampling closer to the arc core, however, is thought to increase the interval between cleaning as this is also related to the incidence of atmospheric dust.

It has been found to be convenient to position the orifice as close to the tail flame outlet of the arc cathode block as possible and, as described above, to incline the arc axis slightly to the system axis. Because of the use of a high-voltage igniter, it is necessary to withdraw the arc unit when striking it; it can, however, be quickly re-set. Positioning the orifice by eye in the centre of the tail flame is found to give a yield of ions close to the optimum; further transverse adjustment across the flame usually effects little improvement. The effective electrical potential in the tail flame is intermediate between the plasma electrode potentials. The ion yield is optimised by adjusting a bias potential between the earthed orifice and the arc supply.

Results and Discussion

The performance of the system on aqueous solutions was studied by running test solutions of a range of convenient elements in distilled and de-ionised water at levels of 100, 10 and 1 $\mu g\ ml^{-1}$. Simple mixtures were also prepared from these solutions. A typical spectrum plotted on the X - Y recorder from a solution prepared by mixing equal volumes of aluminium

and lead solutions, each containing 1 μg ml^{-1} of solute, is shown in Fig. 4. In such a solution, containing 0·5 μg ml^{-1} of lead in total, the concentration of the isotope lead-204, which has an abundance of 1·48 per cent., is therefore 0·0075 μg ml^{-1}. The peak due to this isotope can be clearly seen as the first of the lead peaks. On the scale shown, the height of this peak represents 400 counts s^{-1} and it can be seen that the background is extremely small; the ultimate sensitivity for lead is clearly very high.

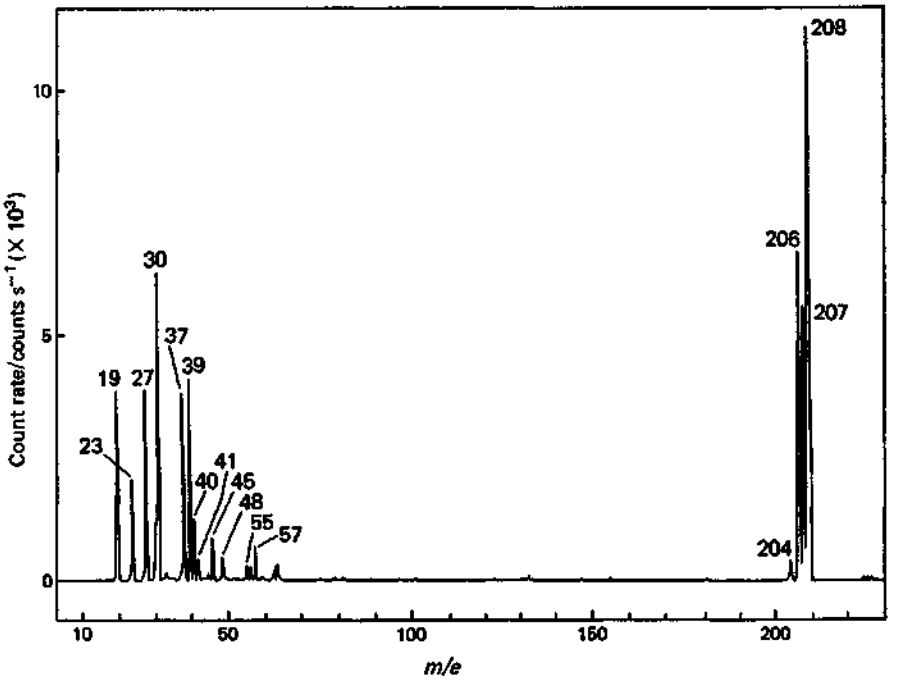

Fig. 4. Spectrum of solution containing 0·5 μg ml^{-1} of aluminium and 0·5 μg ml^{-1} of lead.

Metal	Isotope	Abundance, per cent.
Aluminium	27	100
Lead	204	1·48
	206	23·6
	207	22·6
	208	52·3

At the low mass end of the spectrum a complex collection of peaks occurs, but among them a substantial isolated peak of about 3000 counts s^{-1} is seen for $^{27}Al^+$. Contaminant peaks from sodium ($^{23}Na^+$) and potassium ($^{39}K^+$ and $^{41}K^+$; these are close to the correct isotopic ratio) are also clearly seen. The other peaks arise from a variety of causes and considerable assistance towards their identification can be obtained by comparing them with similar spectra obtained by other workers when sampling electrical discharges[15] in which similar reactions are to be expected. They can most conveniently be examined on an expanded mass scale and Fig. 5 (*b*) shows such a spectrum obtained from AnalaR water. On the larger peaks the rate meter has become saturated so that they appear with square tops.

The largest peak is due to NO^+ at mass 30, which has so far always been found and is attributed to the presence of nitrogen in the argon used and possibly to slight air leakage. The large peak at mass 19 is identified as OH_3^+, an ion very familiar to mass spectroscopists. It is produced from trace amounts of water in the argon even when water is not being introduced. Trace amounts of sodium and potassium can again be seen and $^{40}Ar^+$ is present, at a relatively low level owing to its high ionisation potential. Peaks of O_2^+ and NH_4^+ are also evident at masses 32 and 18 and there is a very small peak at mass 36, which is probably due to NH_4^+ with a water molecule attached.

Major peaks are found at masses 37 and 45, that at mass 37 being attributed to hydrated OH_3^+ and that at 45 to N_2OH^+, an ion that is commonly found in discharges. Other small peaks (with mass numbers in parentheses) arise from HNO^+ (31), N_2O^+ (44), $NO^+.H_2O$ (48) and $OH_3^+.2H_2O$ (55). The conflict between these peaks and those due to atomic ions of interest is less serious than might at first be thought. The peak due to OH_3^+ at *m/e* 19 would obscure any due to fluorine although, because of its high ionisation potential, the sensitivity for fluorine would be expected to be low, especially in the inevitable presence of elements of lower ionisation potential. The peak at *m/e* 30 of NO^+ does not cause difficulty by direct coincidence with an ion of interest. Both of these peaks are, however, very large and could potentially cause interference on adjacent mass numbers owing to overlapping of peak fringes, which can occur because of faulty alignment or incorrect operation of the quadrupole. Some indication of this effect can be seen at the leading edge of some of the peaks in Fig. 5. With good design and correct operation, however, the overlap contribution between adjacent mass numbers should be reduced to below 10^{-5}.

Interferences with P^+ and S^+ ions are caused by the peaks at masses 31 and 32. Phosphorus has no other isotope but sulphur has an isotope with 4 per cent. abundance at mass 34, which can be used for its detection at lower sensitivity and which is not subject to interference. Similarly calcium-40 coincides with the small argon peak but has an isotope at mass 42 with an abundance of 0·6 per cent., which is free from interference. Further peaks at masses 45, 48 and 55 interfere to some extent with scandium, titanium and manganese.

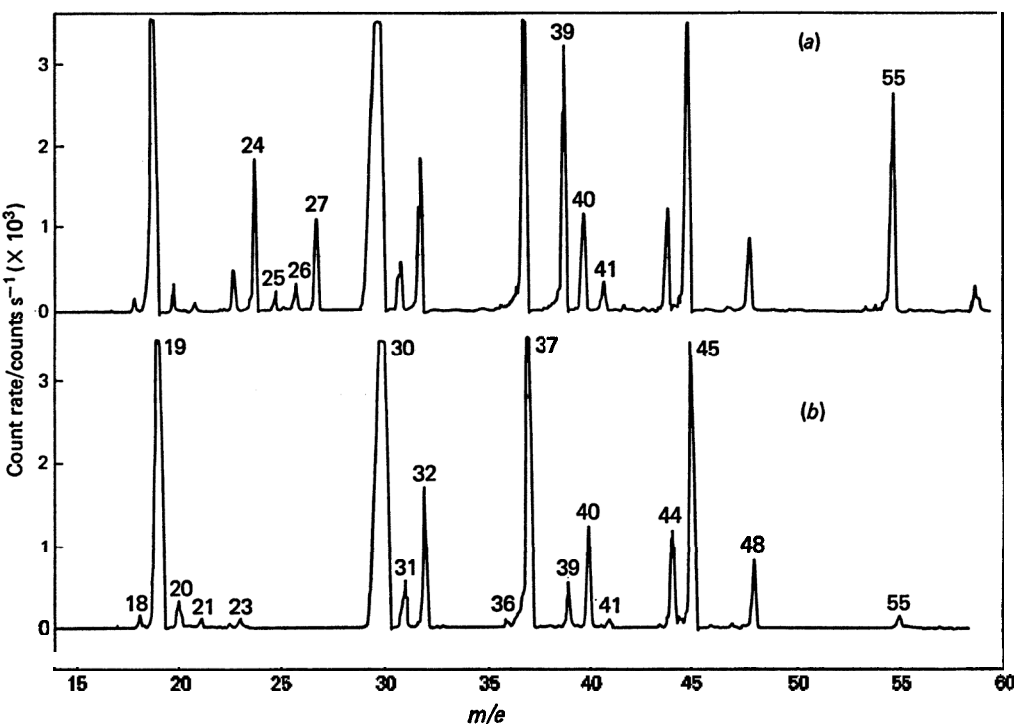

Fig. 5. Comparative spectra of solution and water: (*a*), solution containing Al 0·46, Mg 0·46, K 0·27 and Mn 0·38 μg ml⁻¹; and (*b*), AnalaR water.

Apart from these seven elements, the presence of the undissociated and molecular ions causes little significant interference, as can be seen in Fig. 5 (*a*), where the spectrum of a solution containing aluminium (0·46 μg ml⁻¹), magnesium (0·46 μg ml⁻¹), potassium (0·27 μg ml⁻¹) and manganese (0·38 μg ml⁻¹) is shown. This spectrum can be compared with the spectrum of AnalaR water [Fig. 5 (*b*)] where the peaks of $^{24}Mg^+$, $^{25}Mg^+$, $^{26}Mg^+$, $^{27}Al^+$, $^{39}K^+$ and $^{41}K^+$ are clearly distinguishable. The peak for Mn^+ coincides with that for $OH_3^+.2H_2O$ although it is much larger. A small peak is evident at mass 57, probably due to $^{39}K^+.H_2O$.

Above mass 55 the background is very small (Fig. 4) and no evidence is seen of doubly ionised lead at mass 104, nor do there appear to be any ions corresponding to hydrocarbons from the vacuum pumps.

A spectrum was obtained from a solution of cadmium at 100 μg ml^{-1} concentration (shown in Fig. 6) with the mass analyser set at a rather lower resolution than that used for the spectrum in Fig. 4 and the cadmium peaks are not fully resolved. In addition, at this lower resolution the analyser transmission is higher and the molecular peaks at the lower masses are consequently larger. A small group of peaks is also visible at about mass 206 due, presumably, to a trace amount of lead. Although such spectra are useful for qualitative purposes, they are not suitable for quantitative measurements under the conditions used to plot these examples.

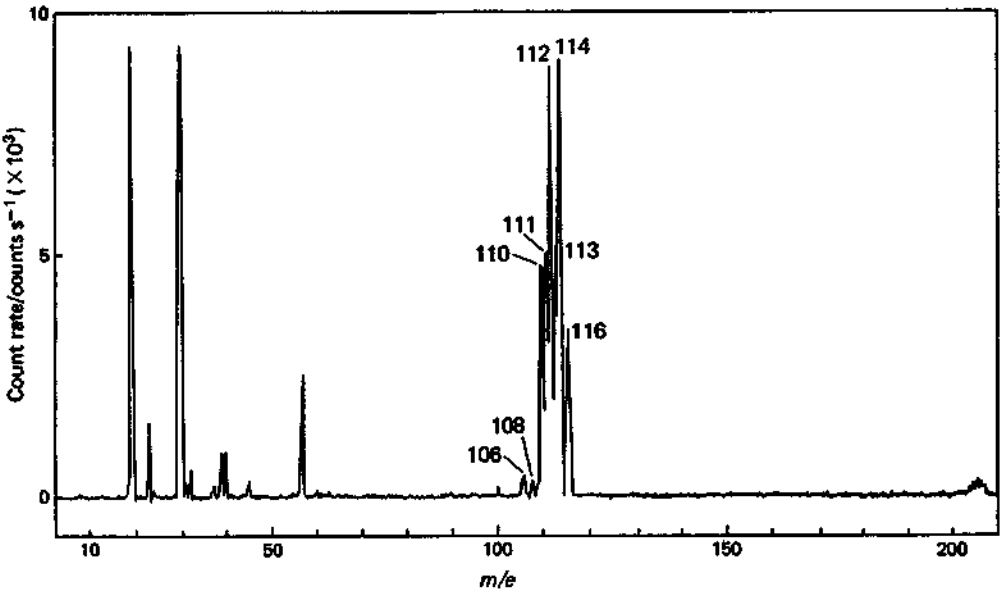

Fig. 6. Spectrum of 100 μg ml^{-1} cadmium solution.

Cadmium isotope	Abundance, per cent.
106	1·22
108	0·88
110	12·39
111	12·75
112	24·07
113	12·26
114	28·86
116	7·58

At the scan rate employed (approximately 1 a.m.u. s^{-1}) the dwell time on each peak is correspondingly short. It has been found that there is a significant fluctuation in the plasma flame, thought to be caused by fluctuations in the sample gas flow, with a period of rather less than 1 s and with such a short dwell time on the centre of each peak that it results in a significant fluctuation in peak height. In addition, the response required from the X - Y plotter for a large peak approaches the limit of its performance at this scan rate and therefore the peak may not be fully developed. For both of these reasons large peaks do not show the correct ratios for elements with several isotopes.

Although both of these effects can be greatly reduced by limiting the scan to a smaller mass range and by increasing the dwell time, it has been found to be more convenient to set the analyser manually to the peak of interest and integrate the signal obtained on the scaler. A counting period of 30 s has been found to provide satisfactory reproducibility. Successive measurements can be made on the unknown and then on a blank water sample at the same mass setting so as to provide a measure of the background level. The background signal, in the absence of the element concerned, in the blank water is small and mostly non-ionic,

arising from such sources as stray photons, electrical noise of all sorts and random multiplier noise pulses. Ionic contributions to the background may arise from sources such as memory effects or contamination, which can provide ions of the mass of interest, or from ions of a mass other than that selected, which are still transmitted by the analyser owing to inadequate resolution or significant contributions from the fringes of the analyser response. Interference signals may also arise from molecular ions, as shown in Fig. 5, although so far the effect of these interferences has been found to be limited to only a few elements.

Measurements of the integrated count obtained for a series of standard solutions can be used to give a measure of the sensitivity of the method, which can conveniently be expressed for the element concerned as the count-rate obtained for a solution of 1 μg ml^{-1} concentration. With the equipment at present used these sensitivities depend on a number of variables in the system, among which are the nebuliser efficiency, the position of the sampling orifice in the flame, the analyser transmission related to resolution settings and the ion mass and ion optics settings chosen.

The over-all ion transmission from the vacuum side of the sampling orifice to the detector is determined by the electrical parameters, which can reproducibly be set so as to optimise the over-all performance. The performance of the nebuliser and behaviour during the plasma sampling are less predictable at the present stage of the investigation and require the most attention in order to make the over-all system satisfactorily reproducible over long periods. However, even in its present experimental form, reasonably stable quantitative performance is obtained during a working day and can be repeated on successive occasions.

The sensitivities obtained when using an ultrasonic nebuliser for a range of elements under constant operating conditions is shown in Table II. The isotopes observed are listed in order of decreasing ionisation potential and the sensitivity in thousands of counts per second for a solution of 1 μg ml^{-1} concentration is shown, first as S_T, the mean count-rate observed on the chosen isotope over a 30-s integration period for 1 μg ml^{-1} of the naturally occurring element. This level is the practical sensitivity that can be used, the most abundant isotope normally being selected. The second value shown, S_I, is the sensitivity normalised to 100 per cent. abundance of the selected isotope, a more convenient parameter for comparing the performance on different elements. For elements of ionisation potential below 8·0 V a high count-rate is achieved.

TABLE II

SENSITIVITIES FOR A RANGE OF ELEMENTS

Isotope measured	Ionisation potential/V	Abundance, per cent.	Count-rate sensitivity*		Effective detection limit†/μg ml^{-1}
			S_T	S_I	
^{75}As	9·81	100	1·30	1·30	0·002
^{80}Se	9·75	49·8	0·10	0·21	0·03
^{112}Cd	8·99	24·1	1·24	5·14	0·003
^{56}Fe	7·87	91·7	182·2	198·7	0·000 02
^{59}Co	7·86	100	68·14	68·14	0·000 05
^{24}Mg	7·64	78·7	232·3	295·2	0·000 02
^{107}Ag	7·57	51·8	16·92	32·6	0·0002
^{208}Pb	7·42	52·3	34·27	65·5	0·0001

* S_T,count-rate, in counts s^{-1} × 1000 for 1 μg ml^{-1} concentration of element; S_I,count-rate, in counts s^{-1} × 1000 for 100% abundance of isotope at 1 μg ml^{-1} concentration.

† Effective detection limit (2σ value), assuming uniform background standard deviation of 50 counts over 30 s, expressed in micrograms per millilitre of the element.

The sensitivity is, however, influenced by reference to a fixed solution concentration because for elements of higher relative atomic mass proportionately fewer atoms are present to be ionised and the lower count-rates for lead and silver partly reflect this fact. For the three elements of high ionisation potential the lower sensitivity suggests that incomplete ionisation occurs.

Although the signals obtained are high, their usefulness for detection of trace levels is related to the background achieved and therefore the usual definition of limit of detection is difficult to apply because of the low background levels obtained. In all these measurements the integrated background was below 1000 counts and in some instances below 200 counts. At these very low levels the background counts depend more on random electrical noise pulses and stray photons than on true background ions and it is thought to be unrealistic to

use the standard deviation of background as a basis for the detection limit. This is especially so as the standard deviation values obtained over ten successive background integrations show σ values that vary from 9 to 40 counts for the various elements, as illustrated by the 95 per cent. confidence limits of detection shown in the final column of Table II, which were calculated from the measured levels for the isotopes shown (at the natural abundance) and a uniform value for background σ of 50 counts in each instance. When the element concerned is normally absent in the blank, so that the background is very low, the performance can be more usefully judged from the count-rate sensitivity. The limit of detection can then be reserved strictly for particular analytical problems in which the background level due to ionic background, arising either from isotopic interference or the level of the element in the blank, is at least one order of magnitude greater than the noise.

Lower sensitivities are shown in Table II for the elements with ionisation potentials above 8 V, suggesting that incomplete ionisation occurs, possibly associated with less effective penetration of the plasma by the sample, but more probably as a result of the effect on the ionisation equilibrium of the presence of a significant concentration of nitric oxide, which has an ionisation potential of 9·4 V. At present, no steps are taken to purify the argon, but clearly this should be investigated in order to increase the ionisation of these elements.

Conclusion

The investigation of the technique of plasma sampling mass analysis[16] has reached a stage at which it appears to have considerable interest for trace analysis. Direct introduction of solution samples into the plasma is practicable by use of conventional nebulisers and the transfer of ions from the plasma to a mass analyser in order to produce qualitative spectra has been demonstrated. Satisfactory quantitative performance requires further development of ion production and sampling techniques and also of mass analyser stability but the sensitivity appears potentially to be very high and the background low. The instrumental configuration necessary to realise the potential performance, while retaining the simple sample handling and rapid throughput of the plasma source, is being studied.

From the initial concept to the practical realisation of the system described invaluable help and advice has been generously given by many people working in the field of flame and plasma mass spectrometry.

In particular, the author gratefully acknowledges the advice and assistance given by Dr. A. N. Hayhurst, University of Sheffield, Dr. P. F. Knewstubb, University of Cambridge, Dr. J. L. Moruzzi, University of Liverpool, and Professor F. M. Page, University of Aston, and also the practical assistance of colleagues at Applied Research Laboratories Limited, especially that of Mr. D. Hagger, in achieving the results reported above.

References

1. Greenfield, S., Jones, I. L., and Berry, C. T., *Analyst*, 1964, **89**, 713.
2. de Boer, F. J., and Boumans, P. W. J. M., *Acta Colloq. Spectrosc. Int. XVII*, 1973, **1**, 107.
3. Fassel, V. A., and Knisely, R. N., *Analyt. Chem.*, 1974, **46**, 1110A.
4. Jones, J. L., Dahlquist, R. L., Knoll, J. W., and Hoyt, R. E., Paper presented at the 1974 Pittsburg Conference, Cleveland, Ohio.
5. Jones, J. L., Dahlquist, R. L., and Hoyt, R. E., *Appl. Spectrosc.*, 1971, **25**, 628.
6. Knewstubb, P. F., "Mass Spectrometry of Organic Ions," Academic Press, New York, 1963, Chapter 6, pp. 255–307.
7. Hayhurst, A. N., and Sugden, T. M., *Proc. R. Soc.*, 1966, **A293**, 36.
8. Caroll, D. I., Dzidic, I., Stillwell, R. N., Horning, M. G., and Horning, E. C., *Analyt. Chem.*, 1974, **46**, 706.
9. Boumans, P. W. J. M., "Theory of Spectrochemical Excitation," Adam Hilger Ltd., London, 1966, Chapter 7, pp. 156–232.
10. Alkemade, C. Th. J., *Proc. Soc. Analyt. Chem.*, 1973, **10**, 130.
11. Hayhurst, A. N., and Telford, N. R., *Proc. R. Soc.*, 1971, **A332**, 483.
12. Applied Research Laboratories Ltd., British Patent 1,261,596, 1969.
13. Hoare, H. C., and Mostyn, R. A., *Analyt. Chem.*, 1967, **39**, 1153.
14. Dawson, P. H., and Whetten, N. R., *Adv. Electronics Electron Phys.*, 1969, **27**, 58.
15. Knewstubb, P. F., "Mass Spectrometry and Ion Molecule Reactions," Cambridge University Press, Cambridge, 1969.
16. Applied Research Laboratories Ltd., British Patent 1,371,104, 1971.

Received *June 17th*, 1974
Amended *December 9th*, 1974
Accepted *December 16th*, 1974

Inductively Coupled Argon Plasma as an Ion Source for Mass Spectrometric Determination of Trace Elements

Robert S. Houk, Velmer A. Fassel,* Gerald D. Flesch, and Harry J. Svec

Ames Laboratory—USDOE and Department of Chemistry, Iowa State University, Ames, Iowa 50011

Alan L. Gray

Department of Chemistry, University of Surrey, Guildford, Surrey, England GU2 5XH

Charles E. Taylor

Southeast Environmental Research Laboratory—USEPA, Athens, Georgia 30601

Solution aerosols are injected into an inductively coupled argon plasma (ICP) to generate a relatively high number density of positive ions derived from elemental constituents. A small fraction of these ions is extracted through a sampling orifice into a differentially pumped vacuum system housing an ion lens and quadrupole mass spectrometer. The positive ion mass spectrum obtained during nebulization of a typical solvent (1% HNO_3 in H_2O) consists mainly of ArH^+, Ar^+, H_3O^+, H_2O^+, NO^+, O_2^+, HO^+, Ar_2^+, Ar_2H^+, and Ar^{2+}. The mass spectra of the trace elements studied consist principally of singly charged monatomic (M^+) or oxide (MO^+) ions in the correct relative isotopic abundances. Analytical calibration curves obtained in an integration mode show a working range covering nearly 4 orders of magnitude with detection limits of 0.002–0.06 μg/mL for those elements studied. This approach offers a direct means of performing trace elemental and isotopic determinations on solutions by mass spectrometry.

Despite the demonstrated utility of mass spectrometry for the analysis of a wide variety of gaseous or solid samples, this technique is scarcely used for the routine determination of elemental constituents in aqueous solutions. Commonly used ion sources are not suitable for the rapid, direct examination of aqueous samples because extensive sample preparation procedures are required (*1*, *2*). Thus, the sample is evaporated onto a filament for thermal ionization or incorporated into an electrode for spark ionization before the sample-containing substrate is physically mounted in the vacuum system. The associated time requirement for these operations renders the routine analysis of large numbers of solutions impractical.

Elemental constituents in solution samples are commonly determined by atomic absorption or emission spectrometry. In these techniques solution aerosols are injected directly into a variety of high-temperature atomization cells at atmospheric pressure for vaporization, atomization, and excitation. These flames and plasmas often provide significant populations of positive ions, which can be extracted through an appropriate sampling orifice into a vacuum system for mass analysis and detection (*3–20*). Ions derived from elemental constituents of injected solution aerosols should also be extractable by a similar approach. Thus the analytical capabilities of mass spectrometry can, in principle, be combined with the convenience and efficiency of solution introduction into an appropriate plasma ion source.

A.L.G. has previously evaluated a system for trace element determinations based on the introduction of solution aerosols into a dc capillary arc plasma (CAP) (*21*). A small fraction of plasma gas along with its ions was extracted from the CAP through a pinhole-like sampling orifice into a differentially pumped vacuum system containing an electrostatic ion lens, quadrupole mass analyzer, and electron multiplier. Background mass spectra obtained from the CAP had few peaks above 50 amu and thus facilitated use of a low-resolution mass analyzer. Analyte elements were detected essentially as singly charged, monatomic, positive ions, i.e., the simplest possible mass spectrum. Detection limits of 0.000 02–0.1 μg/mL were obtained; those elements with ionization energies below 9 eV had the best powers of detection (*22–24*). The relative abundances of the various isotopes of Sr and Pb were determined with relative precisions of ±0.5% in dissolved mineral samples (*25*, *26*). These results indicated the feasibility of obtaining elemental mass spectra from analytes in solution with a plasma ion source. However, matrix and interelement interferences were severe (*26*).

Although both the CAP and the inductively coupled plasma (ICP) were originally developed for trace element determinations by atomic emission spectrometry, the ICP has found much wider application. Most of the characteristics of the ICP that have vaulted it to supremacy as an excitation source for atomic emission spectrometry are also highly desirable in an ion source for mass spectrometry (*27–29*). In particular, a high number density of trace element ions is implied by the common use of emission lines from excited ions for the determination of trace elements by atomic emission spectrometry. For example, cadmium, despite its relatively high ionization energy (8.99 eV), is often determined by using an ion line (*30*). Also, the ICP as an excitation source is remarkably free from such interferences as (a) incomplete solute vaporization and atomization and (b) ionization suppression or enhancement caused by changes in the solution concentration of easily ionized concomitant elements, e.g., Na (*31–34*). The objective of the present work is to present results that demonstrate the feasibility of inductively coupled plasma–mass spectrometry (ICP-MS) for the determination of elemental concentrations and isotopic abundance ratios in solutions.

APPARATUS AND PROCEDURES

The ICP-MS apparatus used in the present work is shown schematically in Figure 1. The components and operating conditions are listed in Table I. The apparatus has been described in greater detail elsewhere (*35*).

Inductively Coupled Plasma. The ICP was generated in a horizontal torch fitted with an extended outer tube as shown in Figure 1. The tube extension merely elongated the ICP relative to its dimensions in torches of conventional length. As viewed from its end, the extended ICP had the usual toroidal appearance. Thus, the injected aerosol particles remained localized in the central or axial channel of the ICP, where vaporization, atomi-

0003-2700/80/0352-2283$01.00/0

Table I. Instrumental Facilities

Component description manufacturer	Operating conditions	Component description manufacturer	Operating conditions
Plasma generator: Type HFP-2500D with impedance matching network Plasma-Therm, Inc. Kresson, NJ	Forward power 1000 W, reflected power <10 W, 27.12 MHz	Ion lens voltage supply: Model 275-L25 Extranuclear Laboratories, Inc. Pittsburgh, PA	Operated in atmospheric pressure ionization mode (electron impact ionizer off)
Plasma torch: all quartz Ames Laborabory design and construction (*29*) with outer tube extended 50 mm above tip of aerosol tube	Argon flow rates: plasma flow 12 L/min aerosol carrier flow 1 L/min auxiliary flow used only during ignition	Quadrupole mass spectrometer: Model 100C Uthe Technologies, Inc. (UTI) Sunnyvale, CA	Minor modifications described in text
Ultrasonic nebulizer: Model UNS-1 Plasma Therm, Inc. Kresson, NJ similar to Ames Laboratory design (*36*) modified Margoshes-Veillon desolvation system (*37*)	Sample introduction rate 2.5 mL/min by peristaltic pump, transducer power ~50 W, transducer and condenser ice water cooled	Detector: Channeltron electron multiplier Model 4717 Galileo Electro-Optics Corp. Sturbridge, MA Supplied by UTI	Cathode bias −4 kV, gain ≈ 10^6, anode electrically isolated from channel
Orifice disk: molybdenum disk Agar Aids Stansted, Essex, England	Two mm o.d. 0.5 mm nominal thickness, orifice length ≈ orifice diameter, 50 μm orifice diameter	Pulse counting system: Model 1121 preamplifier-discriminator Model 1109 counter EG&G Princeton Applied Research Princeton, NJ	Single discriminator mode, threshold 3 mV
Vacuum system: welded stainless steel assembly, differentially pumped Ames Laboratory construction	First stage pressure: 1×10^{-3} torr (air, 1 atm, 25 °C), 4×10^{-4} torr (ICP sampling); second stage pressure: 1×10^{-6} torr (ICP sampling)	Data acquisition (scanning mode): active low pass filter-amplifier Model 1020 Spectrum Scientific Corp. Newark, NJ	Spectrum recorded on X-Y recorder: *Y* axis, filtered and amplified dc voltage (proportional to count rate from counter); *X* axis, dc voltage (0 to +10 V) from mass spectrometer controller (proportional to transmitted mass)
Ion lens elements: stainless steel, based on Model 275-N2 Extranuclear Laboratories, Inc. Pittsburgh, PA	Voltage values: $V_1 = -200$ V, $V_2 = -80$, $V_3 = -95$, $V_4 = -60$, $V_{DP} = -60$, $V_{FOCUS} = -18$, $V_{RODS} = -11$	Data acquisition and handling (integration mode): Counter interfaced to teletype for paper tape, hard copy record	Mass spectrometer manually peaked on mass of interest, count period 10 s, 5–10 count periods recorded and averaged at each mass and for each solution

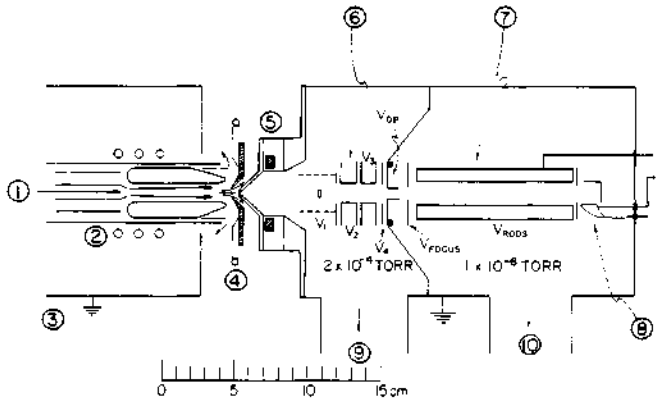

Figure 1. Schematic diagram of ICP, ion sampling interface, and vacuum system: (1) analyte aerosol from nebulizer; (2) ICP torch and load coil; (3) shielding box; (4) skimmer with plasma plume shown streaming through central hole; (5) sampler cone with extraction orifice (detailed diagram in Figure 2); (6) electrostatic ion lens assembly; (7) quadrupole mass analyzer; (8) channeltron electron multiplier; (9) pumping port to slide valve and diffusion pump (first pumping stage); (10) pumping port to slide valve, liquid nitrogen baffle, and diffusion pump (second pumping stage).

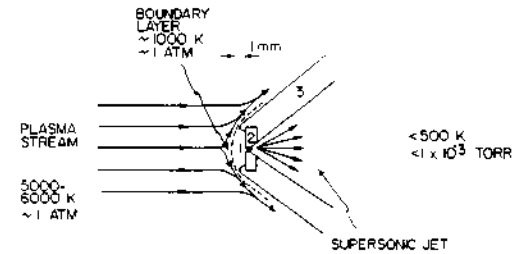

Figure 2. Cross-sectional diagram of sampler tip: (1) sampling orifice (50 μm diameter); (2) molybdenum disk containing orifice; (3) copper cone with spun copper seal to retain molybdenum disk.

zation, and ionization of analyte species occurred as in conventional ICPs (*27–29*). The torch was enclosed in a grounded, copper-lined shielding box.

Plasma Sampling Interface. The function of the interface was to extract a small fraction of plasma gas, along with its ions, into the vacuum system. The extraction was performed in two steps with the skimmer and sampler shown in Figure 1. The axial channel region of the ICP flowed through the central hole of the water-cooled, stainless steel skimmer, forming a well-defined plume. Analyte species derived from the sample aerosol streamed through the skimmer hole with the plume, while the outer portions of the vortex of the ICP were deflected outside the skimmer. The plume, still near atmospheric pressure, next impinged on the sampler, which consisted of a water-cooled copper cone mounted on the vacuum system. Plume particles (atoms, ions, and electrons) were extracted through a 50 μm diameter orifice drilled through the center of a molybdenum disk. The disk was mounted in the tip of the sampler behind a retaining copper lip as shown in Figure 2. The copper lip held the disk firmly in position, served as a vacuum seal, and provided thermal contact between the disk and the cooled sampler cone.

The stainless steel skimmer glowed orange hot (~1000 K) when immersed in the ICP. The tip of the sampler glowed red hot (~800 K) when thrust inside the skimmer. These elevated temperatures greatly inhibited the condensation of analyte-derived solids on either the skimmer or sampler tip. When such condensation became extensive, ion sampling was unstable, i.e., solid deposits plugged the sampling orifice or the ICP arced sporadically to the skimmer and sampler. Maximum count rates for analyte ions were obtained when the sampler tip was thrust inside the skimmer about 2 mm behind the skimmer tip.

A typical sampler operated in a stable fashion for nebulization of dilute (<150 μg/mL) analyte solutions for 8–10 h before sampling conditions deteriorated due to gradual condensation of solid on the tip of the sampler. The sampler was readily cleaned by immersing it in an ultrasonically agitated water bath for a few minutes. An individual sampler remained useful for a total of 50–100 h. During this time the disk gradually became pitted and discolored, and the orifice developed an irregular cross section.

A Teflon gasket and nylon bolts were used to retain the cooling flange and to isolate it electrically from the vacuum system. The skimmer and sampler were each grounded through separate inductive–capacitive filters (*36*). This grounding scheme reduced RF interference in the ion gauges, counting electronics, and recording equipment.

Vacuum System. The sampler cone and orifice assembly were mounted on a two-stage, differentially pumped vacuum system of welded stainless steel construction. The first stage was evacuated by an oil diffusion pump (1600 L s^{-1}, Lexington Vacuum Division, Varian Associates, Lexington, MD). The electrostatic ion lens was mounted in the first stage. As shown in Table I, the first-stage pressure was sufficiently low for ion collection and beam formation but too high for mass spectrometer operation. A second stage of differential pumping was therefore required. The ions were directed through a 3 mm diameter × 8 mm long aperture into the second stage, which housed the quadrupole mass spectrometer. The second stage was pumped by a second 1600 L s^{-1} oil diffusion pump equipped with a liquid nitrogen cooled baffle. Both pumping stations were provided with slide valves to permit rapid venting for sampler installation or modification of internal components.

Electrostatic Ion Lens System. An ion lens system was used to collect positive ions from the supersonic jet of sampled gas while neutral particles were pumped away. The ions were then focused and transmitted to the mass analyzer. As shown in Figure 1, the lens system consisted of a set of coaxial, sequential cylinders, each biased at a particular dc voltage. Maximum ion signals were obtained at the voltages specified in Table I (*35*). The shapes, width, resolution, and symmetry of the ion peaks were unaffected by the voltage settings on the ion optical elements. The cylindrical section of the first element was made of no. 16 mesh screen to provide fast pumping of neutral species from the ion collection and collimation region. A 4.6 mm diameter solid metal disk was positioned in the center of the first element. This disk acted as an optical baffle, i.e., it blocked the line of sight from the ICP through the sampling orifice, lens system, and quadrupole axis, and thus helped to prevent optical radiation from the ICP from reaching the electron multiplier.

Mass Analyzer. The quadrupole mass analyzer (originally supplied as a residual gas analyzer) was modified as follows. First, the filaments, grid, and reflector of the electron impact ionizer were removed; the focus plate was retained as the quadrupole entrance aperture. The latter was aligned visually with the center of the lens system by shimming under the rod mounting bracket. Second, the rods were biased below ground by connecting separate dc supplies into the dc rod driver circuit. The mass analyzer had a mass range of 1–300 amu with resolution sufficient to resolve adjacent masses unless one peak was much more intense than the adjacent one. Because the transmission of the mass analyzer dropped significantly as the transmitted mass increased, the observation of relatively low analyte masses was emphasized in this feasibility study.

Electron Multiplier and Pulse Counting Electronics. The Channeltron electron multiplier detector as supplied with the mass analyzer was operated in the pulse counting mode. Although this multiplier had a much lower gain than those designed specifically for pulse counting, it still performed adequately for the following reasons. First, there was no evidence of loss of gain or pulse overlap at count rates up to at least 5×10^4 counts/s. The multiplier therefore had a linear dynamic range of at least 5×10^4. At −4 kV the threshold setting on the pulse counting equipment could be set over a broad range (0.2–30 mV) without attenuating the observed count rate. The pulses were conducted from the multiplier anode to a preamplifier–discriminator–counter system. The counting threshold was set just above the height of RF noise pulses from the ICP.

Mass Spectra, Analytical Calibration Curves, and Detection Limits. The reference blank solution and the matrix for the reference solutions used for calibration consisted of 1% (volume) nitric acid, prepared by diluting doubly distilled, concentrated nitric acid with deionized water. The reference calibration solutions were prepared by appropriate dilution of stock solutions. The stock solutions were prepared by dissolving pure metals or reagent grade salts in dilute nitric acid.

Mass spectra were acquired in the scanning mode as described in Table I. Individual points for analytical calibration curves were obtained in the integration mode. The average total count for the reference blank solution at the mass of interest was evaluated first, followed by the average total count for each reference calibration solution, in ascending order of concentration. The average total count for the reference blank was then subtracted from the average total count for each reference standard solution before plotting. The detection limit was calculated as the analyte concentration required to give an average net count equal to twice the standard deviation observed at the mass of interest for the blank solution, $2\sigma_b$.

RESULTS AND DISCUSSION

Boundary Layer Formation. As the flowing plasma plume approached the sampler, the plume gas was deflected around the blunt sampler tip. As shown in Figure 2, an aerodynamically stagnant layer of gas formed between the flowing plume and the sampler tip (*10*, *15*, *16*, *38–40*). Formation of a space–charge sheath or electrical double layer in contact with the sampler was also probable (*40–44*). This composite boundary layer was in thermal contact with the relatively cool sampler. Thus, the temperatures in the boundary layer were intermediate between the plume and sampler temperatures. The boundary layer extended across the sampler tip and was visibly unbroken by the gas flow drawn into the sampling orifice. Ion extraction into the vacuum system therefore occurred only after transport through the boundary layer, which would take 1–2 ms and involve up to ~10^6 collisions (*35*).

Such collisions in a medium temperature environment probably facilitated ion–electron recombination, ion neutralization at the sampler walls, charge exchange, ion–neutral attachment, nucleation and condensation of solid deposits, or other reactions (*10*, *16*, *38*). The metal surface of the orifice disk may have catalyzed some of these reactions occurring in the boundary layer or just inside the channel-like orifice (*15*). Also, collisions leading to clustering, ion–electron recombination, or charge exchange occurred in the supersonically expanding jet of extracted gas (*10*, *11*). The effects of these reactions are described below.

Mass Spectra of Reference Solutions. The mass spectrum of the major positive ions from the ICP plume observed during nebulization of a reference blank solution is shown in Figure 3. The two most intense peaks corresponded to Ar^+ (40 amu) and ArH^+ (41 amu). A comparable peak for H^+ (1 amu) was evident, with its low mass edge obscured by "zero blast", i.e., ions anomalously transmitted through the quadrupole field region at the beginning of a scan because the low applied potentials led to very weak fields within the rod structure (*2*).

The major ions observed in the mass spectrum of the reference blank solution are identified in Table II. All of the major ions have been observed previously by other investigators in the mass spectra of flames and plasmas (*5*, *17*, *18*,

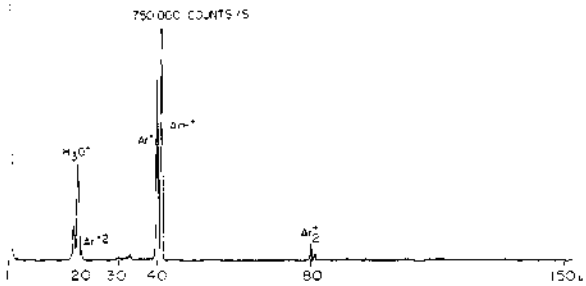

Figure 3. Positive ion mass spectrum of reference blank solution (1% HNO_3 in deionized distilled water). Vertical scale is linear with count rate; base peak count rate is indicated. The background ranged from 30 to 100 counts/s.

Table II. Major Ions Observed in Mass Spectrum of Reference Blank Solution

mass	ion(s)[a]	rel count rate[b] ArH^+ = 100	rel count rate[b] $^{55}Mn^+$ = 100
16	O^+	0.4	6
17	HO^+, NH_3^+	1	15
18	H_2O^+, NH_4^+	12	180
19	H_3O^+	40	600
20	Ar^{2+}	4	60
30	NO^+	4	60
32	O_2^+	2	30
33	$(O_2^+)\cdot H$	4	60
36	$^{36}Ar^+$	0.8	12
37	$^{36}ArH^+$ $(H_3O^+)\cdot H_2O$	1	15
40	$^{40}Ar^+$	75	1125
41	$^{40}ArH^+$ $(Na^+)\cdot H_2O$	100	1500
80	Ar_2^+	8	120
81	$(ArH^+)\cdot Ar$	3	45

[a] Possible ions at same mass number are listed in decreasing order of likelihood or probable intensity. [b] $ArH^+ \approx 750\,000$ counts/s; $^{55}Mn^+ \approx 50\,000$ counts/s at 50 μg/mL solution concentration.

20, *22*, *23*) or as analogous cluster species formed during supersonic jet expansions. Of the major ions only Ar^+ has been identified in analytical ICPs by optical spectrometry, and even that identification is tentative or disputed (*30*, *45*). The existence of an intense peak due to ArH^+, along with the observation of other cluster ions such as H_3O^+ (19 amu) and Ar_2^+ (80 amu) indicated that some clustering reactions occurred during ion extraction. Some minor ions (≤1000 counts/s) were observed at times at 2, 45–48, 50, 54–59, 68–70, 73, and 76 amu. Many of these were also formed during the extraction process, e.g., $O_2^+\cdot H_2O$ at 50 amu. Despite the opportunities for complicating reactions described above, the mass spectrum of the reference blank solution had usefully clear mass regions from 2 to 13 amu, from 21 to 29 amu, and from 42 amu up.

Because there was no ion source inside the vacuum system, the residual gas was not ionized. Ions derived from pump oil were not observed. Thus, a major background contribution from ionization of residual gas in conventional ion sources was not observed with the plasma ion source (*22*, *23*).

The count rate obtained for the reference blank spectrum at those masses free of major or minor ions was 30–100 counts/s, well above the dark current count rate characteristic of the electron multiplier (≤1 count/s). This background count rate was the same at all masses and was independent of the ion lens voltages and mass spectrometer operating conditions. Apparently, this background was caused by vacuum UV photons striking the electron multiplier. These

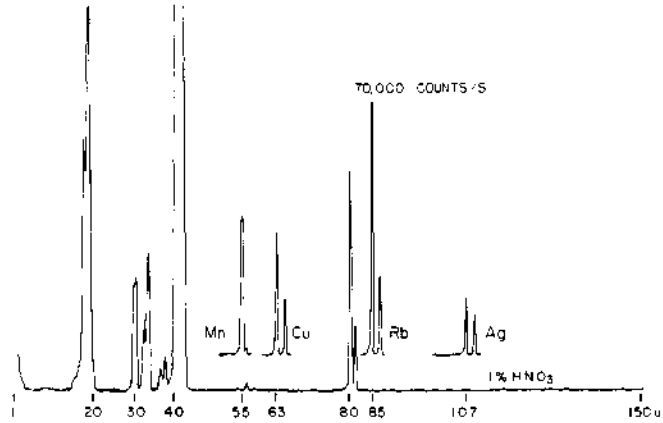

Figure 4. Reference blank spectrum (bottom); superimposed spectra are from 50 μg/mL solutions of the indicated element in 1% HNO_3. Vertical scale sensitivity is 10 times that of Figure 3.

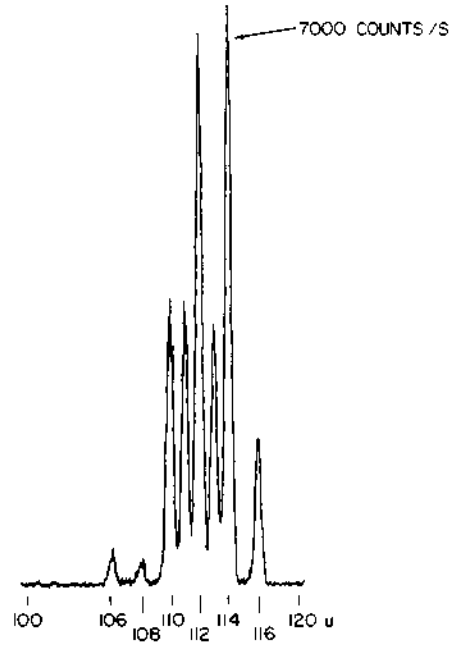

Figure 5. Mass spectrum of Cd at 50 μg/mL in 1% HNO_3.

photons probably were radiated directly from the ICP and also from the decay of metastable argon atoms within the vacuum system. Although the direct line-of-sight from the orifice through the quadrupole field region was blocked by a disklike baffle (Figure 1) and the multiplier was offset from the quadrupole axis, numerous photons still struck the multiplier. The background count rate (photons + minor ions, if present) at each mass of interest of the reference blank solution was reproducible during a 5–10-h period, and integration data for reference standards were adequately corrected by subtraction of the reference blank spectrum.

The recorded peaks of monatomic, singly charged positive ions from solutions of Mn, Cu, Rb, and Ag are shown superimposed on the reference blank spectrum in Figure 4. The metal ion spectra are plotted on the same mass and count rate scales as the reference blank spectrum but are displaced vertically by a change in the recorder zero. As shown in the figure, the accepted relative abundances of the isotopes of Cu, Rb, and Ag were observed. The mass spectrum of Cd is shown in Figure 5; again, the count rates for the various isotopes corresponded to the accepted relative isotopic abundances. The peaks were symmetrical and nearly triangular, as expected for quadrupole mass analysis of ions having a low kinetic energy spread. The least abundant Cd isotope ($^{108}Cd^+$, 0.88%) was clearly detected. For the elements shown in Figures 4

Table III. Relative Isotopic Abundance Determination of Naturally Occurring Copper Isotopes, 2.5 μg/mL Cu in 1% HNO_3

isotope	N^a	σ	$N^{1/2}$	% abundance determined	% abundance accepted
$^{63}Cu^+$	19786	740	143	69.9 ± 1.1	69.1
$^{65}Cu^+$	8505	546	98	30.1 ± 1.1	30.9

[a] N = background subtracted average count, obtained in integration mode as described in Apparatus and Procedures section. Uncertainties are indicated at 95% confidence level for 15 determinations, counting time 10 s for each determination.

and 5, and for most of the elements studied, only monatomic, singly charged ions (M^+) were observed. Several elements were detected as a distribution of M^+ and MO^+ ions, e.g., Ti, As, and Y. The only doubly charged analyte ions observed were Ba^{2+} and Sr^{2+}, i.e., from the two elements with the lowest second ionization energies. Also, no Cu^+ or Mo^+ ions were observed from the orifice assembly. Thus, the mass spectra obtained were remarkably simple, which facilitated use of a low-resolution mass analyzer.

Isotopic Abundance Determinations. The utility of the ICP-MS approach for the direct determination of isotopic abundances of elemental constituents in solutions is illustrated further by the data shown in Table III. The agreement with the accepted values of the relative abundances of $^{63}Cu^+$ and $^{65}Cu^+$ was within the estimated uncertainty in the determined values. The absolute standard deviation of the count was approximately 5 times greater than the square root of the average count, which indicated that the uncertainty in the count was significantly greater than the uncertainty expected from counting statistics. This increased uncertainty was undoubtedly due to instability of some instrumental parameter; instability in nebulizer efficiency and ion extraction efficiency through the boundary layer were likely culprits. Thus the precision of the isotopic ratio determinations in Table III is expected to improve with continued development of the ICP-MS technique.

These isotope ratio determinations were performed directly on a trace level of copper in solution. Also, the total time for the determination of both isotopes was 5 min, including the time required for sample interchange, nebulizer equilibration, and adjustment of the mass transmitted by the mass analyzer. Thus, 100 isotopic ratio determinations could easily be performed in a single day, indicating the potential of the ICP-MS approach for rapid isotopic abundance determinations of trace levels of elements in large numbers of solutions.

Analytical Calibration Curves and Detection Limits. The analytical calibration curves shown in Figure 6 which were obtained in the integration mode, show a useful working range of 3 to 4 orders of magnitude. These data were obtained from reference solutions containing only one element.

When the plasma plume was first moved into contact with the sampler, the count rates of all the ions increased rapidly. After about 1 h this rate of increase tapered off so that the calibration data could be obtained. The Co and Mn curves in Figure 6 show replicate determinations at the 0.02 μg/mL level. For Co and Mn the point labeled by the arrow was determined first. The unlabeled points at 0.02 μg/mL were determined after the calibration data at higher concentrations were obtained, i.e., after about 30 min. This small positive deviation was not caused by memory; instead it reflected the general tendency of the count rates of all the ions to increase slowly with time (~20% every hour) in the absence of orifice plugging. This gradual increase was not accompanied by any discernible increase in orifice diameter. Some subtle phenomena related to the plasma sampling process apparently caused the number of extracted ions to increase with time. This increase should not affect isotope ratio measurements provided they are performed by rapid, repetitive scanning or peak switching techniques. For determination of elemental concentrations, normalization of the ion count rate to an internal standard ion or to a total beam monitor signal should provide internal compensation for the increasing ion signals.

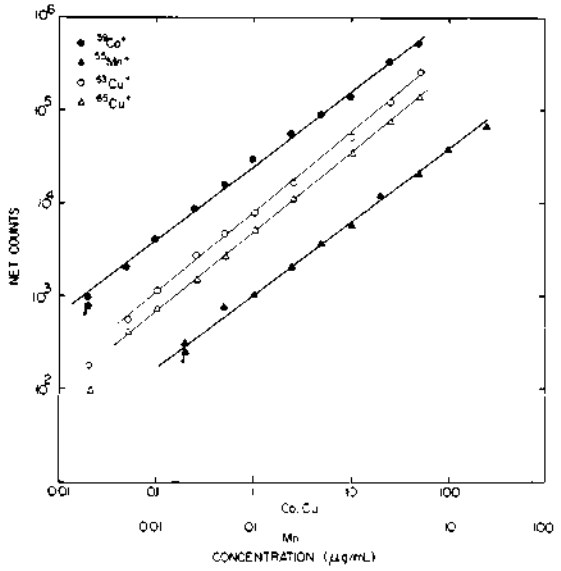

Figure 6. Analytical calibration curves obtained in integration mode. Read bottom scale for Mn curve.

Table IV. Detection Limits Obtained

element	ion detected	% abundance	detection limit ($2\sigma_b$) μg/mL	detection limit ($2\sigma_b$) ppma[a]
Mg	$^{24}Mg^+$	78.6	0.006	0.004
Cr	$^{52}Cr^+$	83.8	0.002	0.0007
	$^{53}Cr^+$	9.6	0.01	0.003
Mn	$^{55}Mn^+$	100	0.003	0.001
Co	$^{59}Co^+$	100	0.006	0.002
Cu	$^{63}Cu^+$	69.1	0.009	0.002
	$^{65}Cu^+$	30.9	0.02	0.005
Rb	$^{85}Rb^+$	72.2	0.008	0.002
	$^{87}Rb^+$	27.8	0.02	0.004
As	$^{75}AsO^+$	100 (^{75}As)	0.06	0.01
Y	$^{89}YO^+$	100 (^{89}Y)	0.04	0.008

[a] ppma = DL(μg/mL) × (18/(atomic weight)).

The detection limits obtained for selected elements are listed in Table IV. The detection limits for the major isotopes of Cr, Cu, and Rb were lower than those for the corresponding minor isotopes by factors approximately equal to the relative isotopic abundances. Because the reference blank spectrum had minor peaks (<1000 counts/s) at 54, 56, and 59 amu, the standard deviation of the reference blank count rate increased in the order 52 amu (photons) < 55 amu (photons + ions from peak edges at 54 and 56 amu) < 59 amu (photons + minor ions). Thus the detection limits were degraded in the same order, i.e., $^{52}Cr^+ < ^{55}Mn^+ < ^{59}Co^+$, although the net counts at these masses were similar for equimolar solutions of these three elements. It is clearly desirable to reduce both the number and count rates of minor ions in the reference blank spectrum and the count rate of the photon background.

The detection limits listed in Table IV were obtained with a sampler that provided more AsO^+ and YO^+ than As^+ and Y^+ ions; hence the oxide ions were used for the determinations of the detection limits of these two elements. Useful analytical calibration curves for As and Y were obtained up to at least

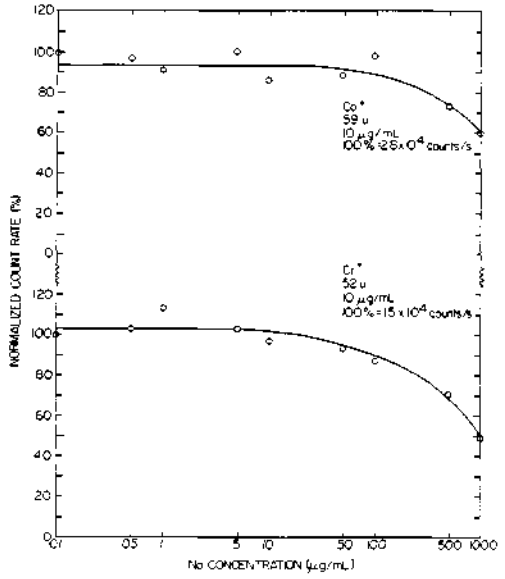

Figure 7. Effect of Na concomitant concentration on count rates of $^{52}Cr^+$ and $^{59}Co^+$, integration mode, 10 s count time, ~5 count periods averaged for each point.

50 μg/mL for either the metal or metal oxide ion. Although formation of metal oxide ions was not desirable, these ions were still useful analytically. Also, metal oxide ion formation is not expected to cause serious mass spectral interferences, because most of the elements are not detected as oxide ions, and the masses and isotopic distribution of MO^+ ions are predictable for those elements with a high probability of oxide formation.

The ICP-MS detection limits in Table IV were poorer, i.e., larger numbers, than the CAP-MS detection limits by factors of 10–100. This discrepancy is largely accounted for by the longer integration time (30 s), larger orifice diameter (75 μm), and much lower background levels and background standard deviations obtained in the CAP-MS study. Indeed, the standard deviation of the background in the CAP-MS study was so low (~1 count/s) that the conventional definition of detection limit was considered inappropriate (*22*, *23*). The CAP-MS detection limits were superior to those characteristic of all other techniques for trace elemental analysis. Unfortunately, these powers of detection were of little analytical value because of severe interelement interference effects (*26*).

The ICP-MS detection limits in Table IV represent potentially useful powers of detection, which can undoubtedly be enhanced by experimental improvements in ion extraction and transmission efficiency and optical baffling of the electron multiplier. Furthermore, the ICP-MS approach should be less susceptible to interelement interference effects than CAP-MS because of the superior sample injection, vaporization, and atomization capabilities and higher electron number density of the ICP (*27–29*, *32*). This expectation is partially demonstrated below.

Ionization Type Interelement Effects. As mentioned above, the ICP as an atomization–excitation source for atomic emission spectrometry is relatively free from ionization interferences caused by easily ionizable elements in solution. For example, the intensities of certain emission lines of excited ions of Ca, Cr, and Cd show little dependence on Na concentration from 0 to 7000 μg/mL (*32*, *33*). In the present work, the count rates of mass resolved analyte ions were suppressed to a somewhat greater extent in the presence of Na as shown in Figure 7. Each point plotted in this figure was normalized to a reference count rate for the same solution concentration of the analyte ion in the absence of Na. Because solute concentrations ≥150 μg/mL gradually clogged the orifice with condensed solid, the reference count rate gradually decreased and was therefore determined repeatedly. The arbitrary nature of this correction procedure, coupled with a significant long-term drift in aerosol intensity produced by the ultrasonic transducer, led to the scatter of the points shown in Figure 7. These plots exhibited a shape similar to those observed for atomic emission spectrometry by Larson et al. (*32*, *33*). Because of the ultrasonic nebulizer used in the present work, 1000 μg/mL Na corresponded roughly to 10 000 μg/mL Na in Larson's work, which was performed with a pneumatic nebulizer (*36*).

The magnitude of suppression of analyte ionization shown in Figure 7 is approximately twice as large as that observed by atomic emission spectrometry by Larson et al. (*32*) if the latter data are adjusted for the approximately tenfold difference in nebulization efficiency. This difference may be rationalized as follows. In the present work, ion extraction occurs through an unbroken boundary layer that is somewhat cooler than the unperturbed plasma. Ion–electron recombination or electron loss to the sampler wall may occur at a significant rate in this layer, leading to an effective electron number density (n_e) in the vicinity of the orifice that is less than that prevalent in the unperturbed plasma. For this lower value of n_e, the "extra" electrons contributed by the ionization of Na should be more significant, causing a proportionately greater increase in the total n_e near the orifice. Thus, the greater suppression of analyte ionization observed in the present work may be a characteristic of the boundary layer rather than the unperturbed plasma. A strict comparison of the magnitudes of the ionization suppressions observed in the present work with those observed from the ICP by atomic emission spectrometry is therefore not necessarily valid.

To place the ionization type interelement effect measured in the present work into perspective, we note that the degree of suppression of analyte ionization was far less severe than that observed for the capillary arc plasma–mass spectrometric approach (*26*) or for flames and other plasmas that have been used as atomization sources in atomic emission or absorption spectrometry (*31*, *33*). Furthermore, the >100 μg/mL Na range, where ionization suppression was significant, represented the analytical equivalent of determining the Co and Cr content of NaCl. Thus, analytical calibrations established for the determination of Co and Cr in a deionized water matrix would have yielded analytical results only ~12% lower if the sample calibrations were used for the analysis of a NaCl sample prepared as a solution of approximately 100 μg/mL Na. Even only approximate matching of the total concentration of easily ionizable elements in reference calibration solutions and samples would essentially eliminate analytical bias caused by ionization type interferences, including samples in which these elements (e.g., Na or K) represent varying major fractions of the total metal content.

Solid Deposition in the Sampling Orifice. Solid condensation in or near the orifice remains an operational problem. As mentioned above, normalization of analyte ion count rates either to an internal standard ion or to a beam monitor signal should correct for the gradual decrease in extraction efficiency of analyte ions caused by progressive solid condensation expected from solutions such as hard water. However, progressive deposition of sample material does restrict the useful life of orifices exposed to solutions whose total solute concentrations are above approximately 150 μg/mL. Thus, biological fluids such as urine or blood serum would require a dilution factor of several hundred before analyses of such solutions could be performed for more than about 1 h. The consequent deterioration in powers of detection for analyte elements may not be acceptable for various applications.

Sample deposition in the orifice is primarily caused by the formation of involatile metal compounds in the relatively cool, stagnant gas of the boundary layer shown in Figure 2. Potential solutions to the troublesome deposition of sample material in the orifice undoubtedly lie in the geometry and operating conditions of the sampler tip, which govern boundary layer formation. For example, solid deposition should be less significant in orifices of diameter >50 μm, which would also extract more ions into the vacuum system. A more streamlined, conical orifice assembly should deflect the plasma stream smoothly around the cone tip, instead of allowing a stagnant layer of gas to build up outside the extraction orifice (Figure 2) (*10*, *11*, *15*, *16*, *38*, *40*). Such refinements are expected to relax the compromise between powers of detection, dilution factors, and orifice lifetimes, thus facilitating application of the ICP-MS approach to elemental and isotopic determinations in samples of total solute content greater than 150 μg/mL.

ACKNOWLEDGMENT

The contributions of Tom Johnson and Garry Wells of the Ames Laboratory machine shop are gratefully acknowledged.

LITERATURE CITED

(1) Ahearn, A. J., Ed. "Trace Analysis by Mass Spectrometry"; Academic Press: New York, 1972; Chapter 1.
(2) Dawson, P. H., Ed. "Quadrupole Mass Spectrometry and Its Applications"; Elsevier: New York, 1976; p 323.
(3) Drawin, H. W. In "Plasma Diagnostics"; Lochte-Holtgreven, W., Ed.; Wiley: New York, 1968; Chapter 13.
(4) Fristrom, R. M. *Int. J. Mass Spectrom. Ion Phys.* **1975**, *16*, 15–32.
(5) Goodings, J. M.; Bohme, D. K.; Ng, C. W. *Combust. Flame* **1979**, *36*, 27–43.
(6) Hasted, J. B. *Int. J. Mass Spectrom. Ion Phys.* **1975**, *16*, 3–14.
(7) Hastie, J. W. *Int. J. Mass Spectrom. Ion Phys.* **1975**, *16*, 89–100.
(8) Hayhurst, A. N.; Mitchell, F. R. G.; Telford, N. R. *Int. J. Mass Spectrom. Ion Phys.* **1971**, *7*, 177–187.
(9) Hayhurst, A. N.; Telford, N. R. *Combust. Flame* **1977**, *28*, 67–80.
(10) Hayhurst, A. N.; Kittelson, D. B.; Telford, N. R. *Combust. Flame* **1977**, *28*, 123–135, 137–143.
(11) Burdett, N. A.; Hayhurst, A. N. *Chem. Phys. Lett.* **1977**, *48*, 95–99; *Combust. Flame* **1979**, *34*, 119–134.
(12) Horning, E. C.; Horning, M. G.; Carroll, D. L.; Dzidic, J.; Stillwell, R. N. *Anal. Chem.* **1973**, *45*, 936–943; **1975**, *47*, 1308–1312, 2369–2373; **1976**, *48*, 1763–1768; *J. Chromatogr.* **1974**, *99*, 13–21.
(13) Knewstubb, P. F. "Mass Spectrometry and Ion-Molecule Reactions"; Cambridge University: London, 1969; Chapter 2.3.
(14) Milne, T. A.; Greene, F. T. *Adv. Chem. Ser.* **1968**, *No. 72*, Chapter 5.
(15) Morley, C. *Vacuum* **1974**, *24*, 581–584.
(16) Pertel, R. *Int. J. Mass Spectrom. Ion Phys.* **1975**, *16*, 39–52.
(17) Prokopenko, S. M. J.; Laframboise, J. G.; Goodings, J. M. *J. Phys. D* **1972**, *5*, 2152–2160; **1974**, *7*, 355–362, 563–568; **1975**, *8*, 135–140.
(18) Rowe, B. *Int. J. Mass Spectrom. Ion Phys.* **1975**, *16*, 209–223.
(19) Siegel, M. W.; Fite, W. L. *J. Phys. Chem.* **1976**, *80*, 2871–2881.
(20) Vasile, M. J.; Smolinsky, G. *Int. J. Mass Spectrom. Ion Phys.* **1973**, *12*, 133–146; **1975**, *18*, 179–192; **1976**, *21*, 263–277.
(21) Jones, J. L.; Dahlquist, R. L.; Hoyt, R. E. *Appl. Spectrosc.* **1971**, *25*, 628–635.
(22) Gray, A. L. *Proc. Soc. Anal. Chem.* **1974**, *11*, 182–183; *Anal. Chem.* **1975**, *47*, 600–601; *Analyst (London)* **1975**, *100*, 289–299.
(23) Gray, A. L. In "Dynamic Mass Spectrometry"; Price, D., Todd, J. F. J., Eds.; Heyden: London, 1975; Vol. 4, Chapter 10.
(24) Applied Research Laboratories, Ltd., British Patent 1 261 596, 1969; U.S. Patent 3 944 826, 1976.
(25) Anderson, F. J.; Gray, A. L. *Proc. Anal. Div. Chem. Soc.* **1976**, *13*, 284–287.
(26) Gray, A. L. In "Dynamic Mass Spectrometry"; Price, D., Todd, J. F. J., Eds.; Heyden: London, 1978; Vol. 5, Chapter 8.
(27) Barnes, R. M. *CRC Crit. Rev. Anal. Chem.* **1978**, *7*, 203–296.
(28) Fassel, V. A. *Science* **1978**, *202*, 183–191; *Anal. Chem.* **1979**, *51*, 1290A–1308A; *Pure Appl. Chem.* **1977**, *49*, 1533–1545.
(29) Fassel, V. A.; Kniseley, R. N. *Anal. Chem.* **1974**, *46*, 1110A–1120A, 1155A–1164A.
(30) Winge, R. K.; Peterson, V. J.; Fassel, V. A. *Appl. Spectrosc.* **1979**, *33*, 206–219.
(31) Rubeska, I.; Rains, T. C. In "Flame Emission and Atomic Absorption Spectrometry"; Dean, J. A., Rains, T. C., Eds.; Marcel Dekker: New York, 1969; Vol. 1, Chapters 11 and 12.
(32) Larson, G. F.; Fassel, V. A.; Scott, R. H.; Kniseley, R. N. *Anal. Chem.* **1975**, *47*, 238–243.
(33) Larson, G. F.; Fassel, V. A. *Anal. Chem.* **1976**, *48*, 1161–1166.
(34) Kalnicky, D. J.; Fassel, V. A.; Kniseley, R. N. *Appl. Spectrosc.* **1977**, *31*, 137–150.
(35) Houk, R. S. Ph.D. Dissertation, Iowa State University, Ames, Iowa, 1980; Report IS-T-989; U.S. Department of Energy, Washington, DC, 1980.
(36) Olson, K. W.; Haas, W. J., Jr.; Fassel, V. A. *Anal. Chem.* **1977**, *49*, 632–637.
(37) Veillon, C.; Margoshes, M. *Spectrochim. Acta, Part B* **1968**, *23B*, 553–555.
(38) Biordi, J. C.; Lazzara, C. P.; Papp, J. F. *Combust. Flame* **1974**, *23*, 73–82.
(39) Reed, T. B. *J. Appl. Phys.* **1963**, *34*, 2266–2269.
(40) Clements, R. M.; Smy, P. R. *Combust. Flame* **1977**, *29*, 33–41.
(41) Boyd, R. L. F. *Proc. Phys. Soc. London, Sect. B* **1951**, *64*, 795–804.
(42) Oliver, B. M.; Clements, R. M. *J. Phys. D* **1975**, *8*, 914–921.
(43) Smy, P. R. *Adv. Phys.* **1976**, *25*, 517–553.
(44) Böhme, D. K.; Goodings, J. M. *J. Appl. Phys.* **1966**, *37*, 362–366, 4261–4268.
(45) Robin, J. *Analusis* **1978**, *6*, 89–97; *ICP Inf. Newsl.* **1979**, *4*, 495–509.

RECEIVED for review November 12, 1979. Resubmitted June 19, 1980. Accepted August 19, 1980. Presented in part at the Federation of Analytical Chemistry and Spectroscopy Societies 6th Annual Meeting, Philadelphia, PA, Sept 1979, and at the Pittsburgh Conference on Analytical Chemistry and Applied Spectroscopy, Atlantic City, NJ, March 1980. This work was supported by the U.S. Environmental Protection Agency and was performed at the Ames Laboratory, U.S. Department of Energy, Contract No. W-7405-Eng-82, under Interagency Agreement EPA-IAG-D-X0147-1.

TUTORIAL

A Beginner's Guide to ICP-MS

Part XII – A Review of Interferences

Robert Thomas

We have previously covered the major instrumental components of an ICP mass spectrometer; now let's turn our attention to the technique's most common interferences and what methods are used to compensate for them. Although interferences are reasonably well understood in inductively coupled plasma–mass spectrometry (ICP-MS), it can often be difficult and time-consuming to compensate for them, particularly in complex sample matrices. Having prior knowledge of the interferences associated with a particular set of samples will often dictate the sample preparation steps and the instrumental methodology used to analyze them.

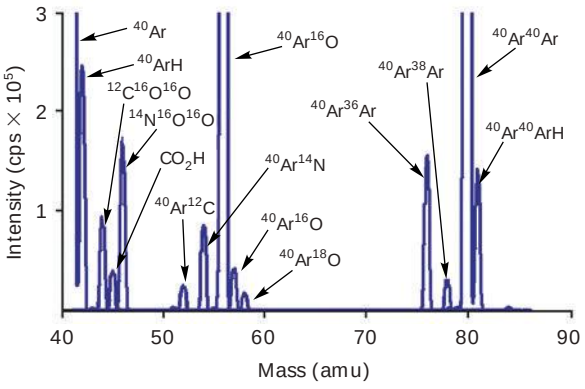

Figure 1. Mass spectrum of deionized water from mass 40 to mass 85.

Robert Thomas has more than 30 years of experience in trace element analysis. He is the principal of his own freelance writing and consulting company, Scientific Solutions, based in Gaithersburg, MD. He can be contacted by e-mail at thomasrj@bellatlantic.net or via his web site at www.scientificsolutions1.com.

Interferences in ICP-MS are generally classified into three major groups — spectral, matrix, and physical. Each of them has the potential to be problematic in its own right, but modern instrumentation and good software, combined with optimized analytical methodologies, has minimized their negative impact on trace element determinations by ICP-MS. Let us take a look at these interferences in greater detail and describe the different approaches used to compensate for them.

Spectral Interferences

Spectral overlaps are probably the most serious types of interferences seen in ICP-MS. The most common type is known as a polyatomic or molecular spectral interference, which is produced by the combination of two or more atomic ions. They are caused by a variety of factors, but are usually associated with either the plasma and nebulizer gas used, matrix components in the solvent and sample, other analyte elements, or entrained oxygen or nitrogen from the surrounding air. For example, in the argon plasma, spectral overlaps caused by argon ions and combinations of argon ions with other species are very common. The most abundant isotope of argon is at mass 40, which dramatically interferes with the most abundant isotope of calcium at mass 40, whereas the combination of argon and oxygen in an aqueous sample generates the $^{40}Ar^{16}O$ interference, which has a significant impact on the major isotope of Fe at mass 56. The complexity of these kinds of spectral problems can be seen in Figure 1, which shows a mass spectrum of deionized water from mass 40 to mass 90.

Additionally, argon can also form polyatomic interferences with elements found in the acids used to dissolve the sample. For example in a hydrochloric acid medium, ^{40}Ar combines with the most abundant chlorine isotope at 35 amu to form $^{40}Ar^{35}Cl$, which interferes with the only isotope of arsenic at mass 75, while in an organic solvent ma-

Relative Abundance of the Natural Isotopes

Isotope		%		%		%	Isotope		%		%		%	Isotope		%		%		%	Isotope		%		%		%
1	H	99.985					61					Ni	1.140	121					Sb	57.36	181	Ta	99.988				
2	H	0.015					62					Ni	3.634	122	Sn	4.63	Te	2.603			182			W	26.3		
3			He	0.000137			63	Cu	69.17					123			Te	0.908	Sb	42.64	183			W	14.3		
4			He	99.999863			64			Zn	48.6	Ni	0.926	124	Sn	5.79	Te	4.816	Xe	0.10	184	Os	0.02	W	30.67		
5							65	Cu	30.83					125			Te	7.139			185					Re	37.40
6					Li	7.5	66			Zn	27.9			126			Te	18.95	Xe	0.09	186	Os	1.58	W	28.6		
7					Li	92.5	67			Zn	4.1			127	I	100					187	Os	1.6			Re	62.60
8							68			Zn	18.8			128			Te	31.69	Xe	1.91	188	Os	13.3				
9	Be	100					69					Ga	60.108	129					Xe	26.4	189	Os	16.1				
10			B	19.9			70	Ge	21.23	Zn	0.6			130	Ba	0.106	Te	33.80	Xe	4.1	190	Os	26.4			Pt	0.01
11			B	80.1			71					Ga	39.892	131					Xe	21.2	191			Ir	37.3		
12					C	98.90	72	Ge	27.66					132	Ba	0.101			Xe	26.9	192	Os	41.0			Pt	0.79
13					C	1.10	73	Ge	7.73					133			Ce	100			193			Ir	62.7		
14	N	99.643					74	Ge	35.94	Se	0.89			134	Ba	2.417			Xe	10.4	194					Pt	32.9
15	N	0.366					75					As	100	135	Ba	6.592					195					Pt	33.8
16			O	99.762			76	Ge	7.44	Se	9.36			136	Ba	7.854	Ce	0.19	Xe	8.9	196	Hg	0.15			Pt	25.3
17			O	0.038			77			Se	7.63			137	Ba	11.23					197			Au	100		
18			O	0.200			78	Kr	0.35	Se	23.78			138	Ba	71.70	Ce	0.25	La	0.0902	198	Hg	9.97			Pt	7.2
19					F	100	79					Br	50.69	139					La	99.9098	199	Hg	16.87				
20	Ne	90.48					80	Kr	2.25	Se	49.61			140			Ce	88.48			200	Hg	23.10				
21	Ne	0.27					81					Br	49.31	141					Pr	100	201	Hg	13.18				
22	Ne	9.25					82	Kr	11.6	Se	8.73			142	Nd	27.13	Ce	11.08			202	Hg	29.86				
23			Na	100			83	Kr	11.5					143	Nd	12.18					203					Tl	29.524
24					Mg	78.99	84	Kr	57.0	Sr	0.56			144	Nd	23.80	Sm	3.1			204	Hg	6.87	Pb	1.4		
25					Mg	10.00	85					Rb	72.165	145	Nd	8.30					205					Tl	70.476
26					Mg	11.01	86	Kr	17.3	Sr	9.86			146	Nd	17.19					206			Pb	24.1		
27	Al	100					87			Sr	7.00	Rb	27.835	147			Sm	15.0			207			Pb	22.1		
28			Si	92.23			88			Sr	82.58			148	Nd	5.76	Sm	11.3			208			Pb	52.4		
29			Si	4.67			89					Y	100	149			Sm	13.8			209	Bi	100				
30			Si	3.10			90	Zr	51.45					150	Nd	5.64	Sm	7.4			210						
31					P	100	91	Zr	11.22					151					Eu	47.8	211						
32	S	95.02					92	Zr	17.15	Mo	14.84			152	Gd	0.20	Sm	26.7			212						
33	S	0.75					93					Nb	100	153					Eu	52.2	213						
34	S	4.21					94	Zr	17.38	Mo	9.25			154	Gd	2.18	Sm	22.7			214						
35			Cl	75.77			95			Mo	15.92			155	Gd	14.80					215						
36	S	0.02			Ar	0.337	96	Zr	2.80	Mo	16.68	Ru	5.52	156	Gd	20.47	Dy	0.06			216						
37			Cl	24.23			97			Mo	9.55			157	Gd	15.65					217						
38					Ar	0.063	98			Mo	24.13	Ru	1.88	158	Gd	24.84	Dy	0.10			218						
39	K	93.2581					99					Ru	12.7	159					Tb	100	219						
40	K	0.0117	Ca	96.941	Ar	99.600	100			Mo	9.63	Ru	12.6	160	Gd	21.86	Dy	2.34			220						
41	K	6.7302					101					Ru	17.0	161			Dy	18.9			221						
42			Ca	0.647			102	Pd	1.02			Ru	31.6	162	Er	0.14	Dy	25.5			222						
43			Ca	0.135			103			Rh	100			163			Dy	24.9			223						
44			Ca	2.086			104	Pd	11.14			Ru	18.7	164	Er	1.61	Dy	28.2			224						
45					Sc	100	105	Pd	22.33					165					Ho	100	225						
46	Ti	8.0	Ca	0.004			106	Pd	27.33	Cd	1.25			166	Er	33.6					226						
47	Ti	7.3					107					Ag	51.839	167	Er	22.95					227						
48	Ti	73.8	Ca	0.187			108	Pd	26.46	Cd	0.89			168	Er	26.8	Yb	0.13			228						
49	Ti	5.5					109					Ag	48.161	169					Tm	100	229						
50	Ti	5.4	V	0.250	Cr	4.345	110	Pd	11.72	Cd	12.49			170	Er	14.9	Yb	3.05			230						
51			V	99.750			111			Cd	12.80			171			Yb	14.3			231	Pa	100				
52					Cr	83.789	112	Sn	0.97	Cd	24.13			172			Yb	21.9			232	Th	100				
53					Cr	9.501	113			Cd	12.22	In	4.3	173			Yb	16.12			233						
54	Fe	5.8			Cr	2.365	114	Sn	0.65	Cd	28.73			174			Yb	31.8	Hf	0.162	234	U	0.0055				
55			Mn	100			115	Sn	0.34			In	95.7	175	Lu	97.41					235	U	0.7200				
56	Fe	91.72					116	Sn	14.53	Cd	7.49			176	Lu	2.59	Yb	12.7	Hf	5.206	236						
57	Fe	2.2					117	Sn	7.68					177					Hf	18.606	237						
58	Fe	0.28			Ni	68.077	118	Sn	24.23					178					Hf	27.297	238	U	99.2745				
59			Co	100			119	Sn	8.59					179					Hf	13.629							
60					Ni	26.223	120	Sn	32.59	Te	0.096			180	Ta	0.012	W	0.13	Hf	35.100							

Figure 2. Relative isotopic abundances of the naturally occurring elements, showing all the potential isobaric interferences.

trix, argon and carbon combine to form $^{40}Ar^{12}C$, which interferes with ^{52}Cr, the most abundant isotope of chromium. Sometimes, matrix or solvent species need no help from argon ions and combine to form spectral interferences of their own. A good example is in a sample that contains sulfuric acid. The dominant sulfur isotope ^{32}S combines with two oxygen ions to form a $^{32}S^{16}O^{16}O$ molecular ion, which interferes with the major isotope of Zn at mass 64. In the analysis of samples containing high concentrations of sodium, such as seawater, the most abundant isotope of Cu at mass 63 cannot be used because of interference from the $^{40}Ar^{23}Na$ molecular ion. There are many more examples of these kinds of polyatomic and molecular interferences (1). Table I represents some of the most common ones seen in ICP-MS.

Oxides, Hydroxides, Hydrides, and Doubly Charged Species

Another type of spectral interference is produced by elements in the sample combining with H, ^{16}O, or ^{16}OH (either from water or air) to form molecular hydride (H), oxide (^{16}O), and hydroxide (^{16}OH) ions, which occur at 1, 16, and 17 mass units higher than its mass (2). These interferences are typically produced in the cooler zones of the plasma, immediately before the interface region. They are usually more serious when rare earth or refractory-type elements are present in the sample, because many of them readily form molecular species (particularly oxides), which create spectral overlap problems on other elements in the same group. Associated with oxide-based spectral overlaps are doubly charged spectral interferences. These are species that are formed when an ion is generated with a double positive charge, as opposed to a normal single charge, and produces a peak at half its mass. Like the formation of oxides, the level of doubly charged species is related to the ionization conditions in the plasma and can usually be minimized by careful optimization of the nebulizer gas flow, rf power, and sampling position within the plasma. It can also be impacted by the severity of the secondary discharge present at the interface (3), which was described in greater detail in Part IV of the series (4). Table II shows a selected group of elements, that readily form oxides, hydroxides, hydrides, and doubly charged species, together with the analytes that are affected by them.

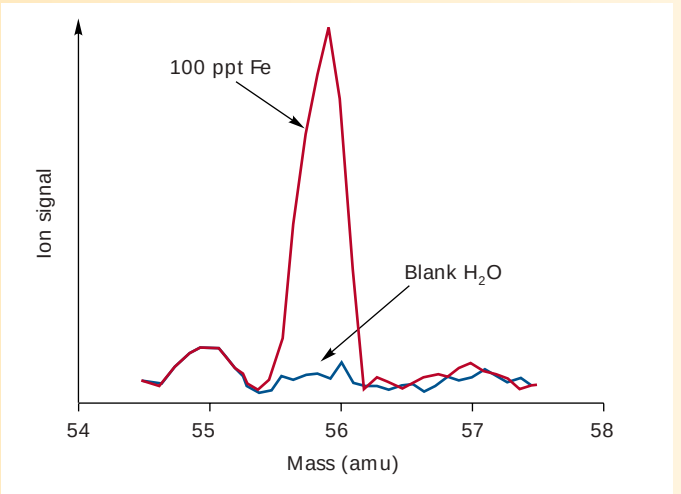

Figure 3. Spectral scan of 100 ppt ^{56}Fe and deionized water using cool plasma conditions.

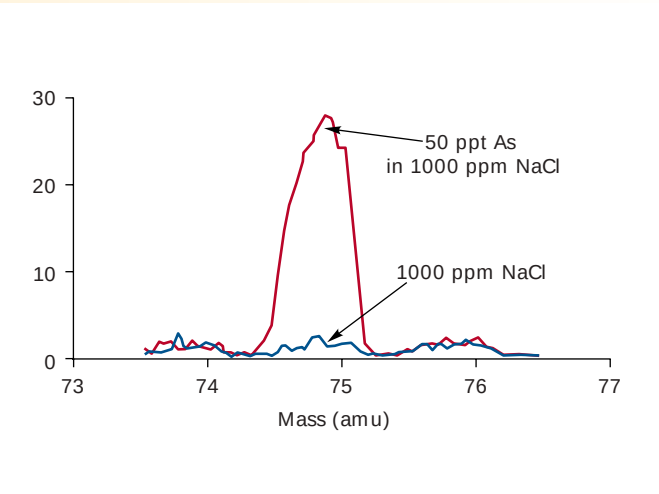

Figure 4. Reduction of the $^{40}Ar^{35}Cl$ interference makes it possible to determine low ppt levels of monoisotopic ^{75}As in a high chloride matrix using dynamic reaction cell technology.

Table I. Some common plasma, matrix, and solvent-related polyatomic spectral interferences seen in ICP-MS.

Element/ Isotope	Matrix/ solvent	Interference
^{39}K	H_2O	^{38}ArH
^{40}Ca	H_2O	^{40}Ar
^{56}Fe	H_2O	$^{40}Ar^{16}O$
^{80}Se	H_2O	$^{40}Ar^{40}Ar$
^{51}V	HCl	$^{35}Cl^{16}O$
^{75}As	HCl	$^{40}Ar^{35}Ci$
^{28}Si	HNO_3	$^{14}N^{14}N$
^{44}Ca	HNO_3	$^{14}N^{14}N^{16}O$
^{55}Mn	HNO_3	$^{40}Ar^{15}N$
^{48}Ti	H_2SO_4	$^{32}S^{16}O$
^{52}Cr	H_2SO_4	$^{34}S^{18}O$
^{64}Zn	H_2SO_4	$^{32}S^{16}O^{16}O$
^{63}Cu	H_3PO_4	$^{31}P^{16}O^{16}O$
^{24}Mg	Organics	$^{12}C^{12}C$
^{52}Cr	Organics	$^{40}Ar^{12}C$
^{65}Cu	Minerals	$^{48}Ca^{16}OH$
^{64}Zn	Minerals	$^{48}Ca^{16}O$
^{63}Cu	Seawater	$^{40}Ar^{23}Na$

Isobaric Interferences

The final classification of spectral interferences is called "isobaric overlaps," produced mainly by different isotopes of other elements in the sample that create spectral interferences at the same mass as the analyte. For example, vanadium has two isotopes at 50 and 51 amu. However, mass 50 is the only practical isotope to use in the presence of a chloride matrix, because of the large contribution from the $^{16}O^{35}Cl$ interference at mass 51. Unfortunately mass 50 amu, which is only 0.25% abundant, also coincides with isotopes of titanium and chromium, which are 5.4% and 4.3% abundant, respectively. This makes the determination of vanadium in the presence of titanium and chromium very difficult unless mathematical corrections are made. Figure 2 — the relative abundance of the naturally occurring isotopes — shows all the naturally occuring isobaric spectral overlaps possible in ICP-MS (5).

Ways to Compensate for Spectral Interferences

Let us look at the different approaches used to compensate for spectral interferences. One of the very first ways used to get around severe matrix-derived spectral interferences was to remove the matrix somehow. In the early days, this involved precipitating the matrix with a complexing agent and then filtering off the precipitate. However, this has been more recently carried out by automated matrix removal and analyte preconcentration techniques using chromatography-type equipment. In fact, this method is preferred for carrying out trace metal determinations in seawater because of the matrix and spectral problems associated with such high concentrations of sodium and magnesium chloride (6).

Mathematical Correction Equations

Another method that has been successfully used to compensate for isobaric interferences and some less severe polyatomic overlaps (when no alternative isotopes are available for quantitation) is to use mathematical interference correction equations. Similar to interelement corrections (IECs) in ICP–optical emission spectroscopy, this method works on the principle of measuring the intensity of the interfering isotope or interfering species at another mass, which ideally is free of any interferences. A correction is then applied by knowing the ratio of the intensity of the interfering species at the analyte mass to its intensity at the alternate mass.

Let's take a look at a real-world example of this type of correction. The most sensitive isotope for cadmium is at mass 114. However, there is also a minor isotope of tin at mass 114. This means that if there is any tin in the sample, quantitation using ^{114}Cd can only be carried out if a correction is made for ^{114}Sn. Fortunately Sn has a total of 10 isotopes, which means that at least one of them will probably be free of a spectral interference. Therefore, by measuring the intensity of Sn at one of its most abundant isotopes (typically ^{118}Sn) and ratioing it to ^{114}Sn, a correction is made in the method software in the following manner:

Table II. Some elements that readily form oxides, hydroxides, or hydrides and doubly charged species in the plasma and the analyte affected by the potential interference.

Oxide/hydroxide/ hydride doubly charged species	Analyte
$^{40}Ca^{16}O$	^{56}Fe
$^{48}Ti^{16}O$	^{64}Zn
$^{98}Mo^{16}O$	^{114}Cd
$^{138}Ba^{16}O$	^{154}Sm, ^{154}Gd
$^{139}La^{16}O$	^{155}Gd
$^{140}Ce^{16}O$	^{156}Gd, ^{156}Dy
$^{40}Ca^{16}OH$	^{57}Fe
$^{31}P^{18}O^{16}OH$	^{66}Zn
^{79}BrH	^{80}Se
$^{31}P^{16}O_2H$	^{64}Zn
$^{138}Ba^{2+}$	^{69}Ga
$^{139}La^{2+}$	^{69}Ga
$^{140}Ce^{2+}$	^{70}Ge, ^{70}Zn

Total counts at mass 114 = $^{114}Cd + ^{114}Sn - (0.0268)*(^{118}Sn)$.

Therefore ^{114}Cd = total counts at mass 114 − ^{114}Sn

To find out the contribution from ^{114}Sn, it is measured at the interference-free isotope of ^{118}Sn and a correction of the ratio of $^{114}Sn/^{118}Sn$ is applied:

Which means ^{114}Cd = counts at mass 114 = $(^{114}Sn/^{118}Sn) \times (^{118}Sn)$

Now the ratio $(^{114}Sn/^{118}Sn)$ is the ratio of the natural abundances of these two isotopes (0.65%/24.23%) and is always constant

Therefore ^{114}Cd = mass 114 − (0.65%/24.23%) × (^{118}Sn)

or ^{114}Cd = mass 114 − (0.0268) × (^{118}Sn)

An interference correction for ^{114}Cd would then be entered in the software as:

This is a relatively simple example, but explains the basic principles of the process. In practice, especially in spectrally complex samples, corrections often have to be made to the isotope being used for the correction — these corrections are in addition to the analyte mass, which makes the mathematical equation far more complex.

This approach can also be used for some less severe polyatomic-type spectral interferences. For example, in the determination of V at mass 51 in diluted brine (typically 1000 ppm NaCl), there is a substantial spectral interference from $^{35}Cl^{16}O$ at mass 51. By measuring the intensity of the $^{37}Cl^{16}O$ at mass 53, which is free of any interference, a correction can be applied in a similar way to the previous example.

Cool/Cold Plasma Technology

If the intensity of the interference is large, and analyte intensity is extremely

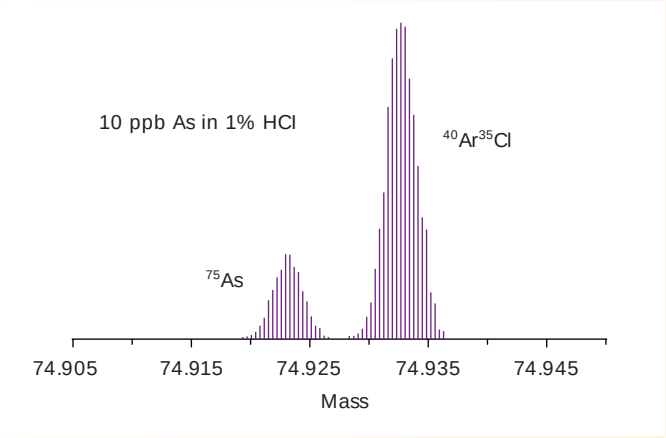

Figure 5 (above). Separation of ^{75}As from $^{40}Ar^{35}Cl$ using the high resolving power (10,000) of a double-focusing magnetic sector instrument (Courtesy of Thermo Finnigan).

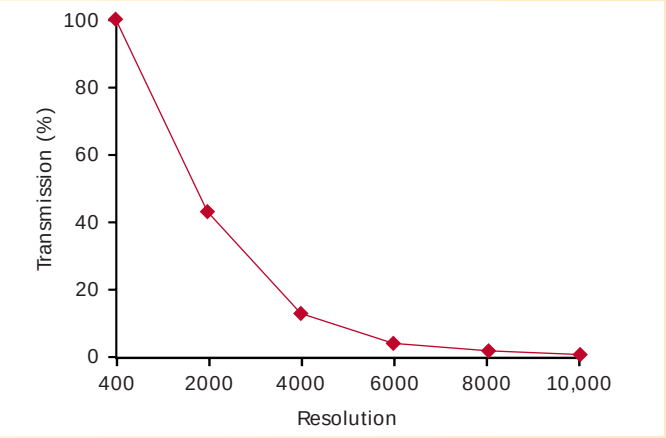

Figure 6 (upper right). The transmission characteristics of a magnetic sector ICP mass spectrometer decreases as the resolving power increases.

low, mathematical equations are not ideally suited as a correction method. For that reason, alternative approaches have to be considered to compensate for the interference. One such approach, which has helped to reduce some of the severe polyatomic overlaps, is to use cold/cool plasma conditions. This technology, which was reported in the literature in the late 1980s, uses a low-temperature plasma to minimize the formation of certain argon-based polyatomic species (7).

Under normal plasma conditions (typically 1000–1400 W rf power and 0.8–1.0 L/min of nebulizer gas flow), argon ions combine with matrix and solvent components to generate problematic spectral interferences such as ^{38}ArH, ^{40}Ar, and $^{40}Ar^{16}O$, which impact

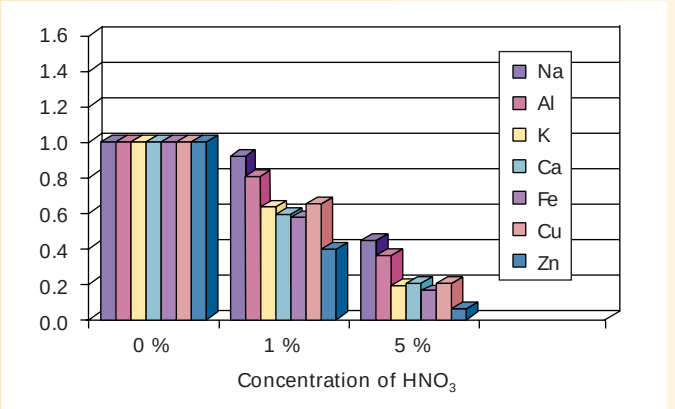

Figure 7. Matrix suppression caused by increasing concentrations of HNO_3, using cool plasma conditions (rf power: 800 W, nebulizer gas: 1.5 L/min).

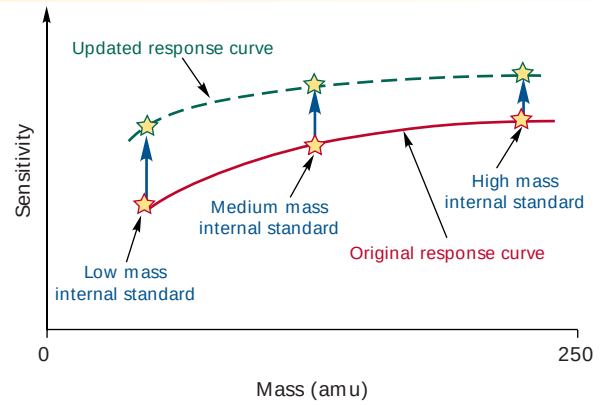

Figure 8. The analyte response curve is updated across the full mass range, based on the intensities of low, medium, and high mass internal standards.

the detection limits of a small number of elements including K, Ca, and Fe. By using cool plasma conditions (500–800 W rf power and 1.5–1.8 L/min nebulizer gas flow), the ionization conditions in the plasma are changed so that many of these interferences are dramatically reduced. The result is that detection limits for this group of elements are significantly enhanced (8).

An example of this improvement is seen in Figure 3, which shows a spectral scan of 100 ppt of ^{56}Fe (its most sensitive isotope) using cool plasma conditions. It can be clearly seen that there is virtually no contribution from $^{40}Ar^{16}O$, as indicated by the extremely low background for deionized water, resulting in single-figure parts-per-trillion (ppt) detection limits for iron. Under normal plasma conditions, the $^{40}Ar^{16}O$ intensity is so large that it would completely overlap the ^{56}Fe peak.

Cool plasma conditions are limited to a small group of elements in simple aqueous solutions that are prone to argon-based spectral interferences. It offers very little benefit for the majority of the other elements, because its ionization temperature is significantly lower than a normal plasma. In addition, it is often impractical for the analysis of complex samples, because of severe signal suppression caused by the matrix.

Collision/Reaction Cells

These limitations have led to the development of collision and reaction cells, which use ion–molecule collisions and reactions to cleanse the ion beam of harmful polyatomic and molecular interferences before they enter the mass analyzer. Collision/reaction cells are showing enormous potential to eliminate spectral interferences and make available isotopes that were previously unavailable for quantitation. For example, Figure 4 shows a spectral scan of 50 ppt As in 1000 ppm NaCl, together with 1000 ppm NaCl at mass 75, using a dynamic reaction cell with hydrogen/argon mixture as the reaction gas. It can be seen that there is insignificant contribution from the $^{40}Ar^{35}Cl$ interference, as indicated by the NaCl baseline. The capability of this type of reaction cell to virtually eliminate the $^{40}Ar^{35}Cl$ interference now makes it possible to determine low ppt levels of mono-isotopic ^{75}As in a high chloride matrix — previously not achievable by conventional interference correction methods (9). For a complete review of the benefits of collision/reaction cells for ICP-MS, refer to part 9 of this series (10).

High Resolution Mass Analyzers

The best and probably most efficient way to remove spectral overlaps is to resolve them away using a high resolution mass spectrometer (11). During the past 10 years this approach, particularly with double-focusing magnetic sector mass analyzers, has proved to be invaluable for separating many of the problematic polyatomic and molecular interferences seen in ICP-MS, without the need to use cool plasma conditions or collision/reaction cells. Figure 5 shows 10 ppb of ^{75}As resolved from the $^{40}Ar^{35}Cl$ interference in a 1% hydrochloric acid matrix, using normal, hot plasma conditions and a resolution setting of 10,000.

However, even though their resolving capability is far more powerful than quadrupole-based instruments, there is a sacrifice in sensitivity if extremely high resolution is used, as shown in Figure 6. This can often translate into a degradation in detection capability for some elements, compared to other spectral interference correction approaches. You will find an overview of the benefits of magnetic sector technology for ICP-MS in part VII of this series (12).

Matrix Interferences

Let's now take a look at the other class of interference in ICP-MS — suppression of the signal by the matrix itself. There are basically two types of matrix-induced interferences. The first and simplest to overcome is often called a sample transport effect and is a physical suppression of the analyte signal, brought on by the matrix components. It is caused by the sample's impact on droplet formation in the nebulizer or droplet-size selection in the spray chamber. In the case of organic matrices, it is usually caused by a difference in sample viscosities of the solvents being aspirated. In some matrices, signal suppression is caused not so much

by sample transport effects, but by its impact on the ionization temperature of the plasma discharge. This is exemplified when different concentrations of acids are aspirated into a cool plasma. The ionization conditions in the plasma are so fragile that higher concentrations of acid result in severe suppression of the analyte signal. Figure 7 shows the sensitivity for a selected group of elements in varying concentrations of nitric acid in a cool plasma (13).

Internal Standardization

The classic way to compensate for a physical interference is to use internal standardization. With this method of correction, a small group of elements (usually at the parts-per-billion level) are spiked into the samples, calibration standards, and blank to correct for any variations in the response of the elements caused by the matrix. As the intensity of the internal standards change, the element responses are updated every time a sample is analyzed. The following criteria are typically used for selecting the internal standards:

- They are not present in the sample
- The sample matrix or analyte elements do not spectrally interfere with them
- They do not spectrally interfere with the analyte masses
- They should not be elements that are considered environmental contaminants
- They are usually grouped with analyte elements of a similar mass range. For example, a low mass internal standard is grouped with the low mass analyte elements and so on up the mass range
- They should be of a similar ionization potential to the groups of analyte elements so they behave in a similar manner in the plasma
- Some of the common ones reported to be good candidates include ^{9}Be, ^{45}Sc, ^{59}Co, ^{74}Ge, ^{89}Y, ^{103}Rh, ^{115}In, ^{169}Tm, ^{175}Lu, ^{187}Re, and ^{232}Th.

A simplified representation of internal standardization is seen in Figure 8, which shows updating the analyte response curve across the full mass range, based on the intensities of low, medium, and high mass internal standards. It should also be noted that internal standardization is also used to compensate for long-term signal drift produced by matrix components slowly blocking the sampler and skimmer cone orifices. Even though total dissolved solids are kept below <0.2% in ICP-MS, this can still produce instability of the analyte signal over time with some sample matrices.

Space-Charge Interferences

Many of the early researchers reported that the magnitude of signal suppression in ICP-MS increased with decreasing atomic mass of the analyte ion (14). More recently it has been suggested that the major cause of this kind of suppression is the result of poor transmission of ions through the ion optics due to matrix-induced space charge effects (15). This has the effect of defocusing the ion beam, which leads to poor sensitivity and detection limits, especially when trace levels of low mass elements are being determined in the presence of large concentrations of high mass matrices. Unless any compensation is made, the high-mass matrix element will dominate the ion beam, pushing the lighter elements out of the way. Figure 9 shows the classic space charge effects of a uranium (major isotope ^{238}U) matrix on the determination of ^{7}Li, ^{9}Be, ^{24}Mg, ^{55}Mn, ^{85}Rb, ^{115}In, ^{133}Cs, ^{205}Tl, and ^{208}Pb. The suppression of low mass elements such as Li and Be is significantly higher than with high mass elements such as Tl and Pb in the presence of 1000 ppm uranium.

There are a number of ways to compensate for space charge matrix suppression in ICP-MS. Internal standardization has been used, but unfortunately doesn't address the fundamental cause of the problem. The most common approach used to alleviate or at least reduce space charge effects is to apply voltages to the individual ion lens components. This is achieved in a number of ways but, irrespective of the design of the ion focusing system, its main function is to reduce matrix-based suppression effects by steering as many of the analyte ions through to the mass analyzer while rejecting the maximum number of matrix ions. Space charge effects and different designs of ion optics were described in greater detail in part V of this series (16).

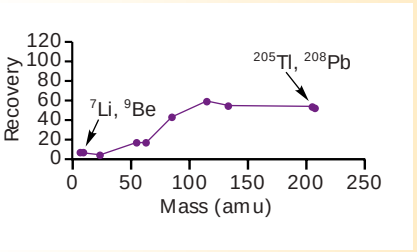

Figure 9. Space charge matrix suppression caused by 1000 ppm uranium is significantly higher on low mass elements Li and Be than it is with the high mass elements Tl and Pb.

References

1. G. Horlick and S.N. Tan, *Appl. Spectrosc.* **40,** 4 (1986).
2. G. Horlick and S.N. Tan, *Appl. Spectrosc.* **40,** 4 (1986).
3. D.J. Douglas and J.B. French, *Spectrochim. Acta* **41B**(3), 197 (1986).
4. R. Thomas, *Spectroscopy* **16**(7), 26–34, (2001).
5. "Isotopic Composition of the Elements," *Pure Applied Chemistry* **63**(7), 991–1002, (IUPAC, 1991).
6. S.N. Willie, Y. Iida, and J.W. McLaren, *Atom. Spectrosc.* **19**(3), 67 (1998).
7. S.J. Jiang, R.S. Houk, and M.A. Stevens, *Anal. Chem.* **60,** 1217 (1988).
8. S.D. Tanner, M. Paul, S.A. Beres, and E.R. Denoyer, *Atom. Spectrosc.* **16**(1), 16 (1995).
9. K.R. Neubauer and R.E. Wolf, "Determination of Arsenic in Chloride Matrices," *PerkinElmer Instruments Application Note* (PerkinElmer Instruments, Shelton, CT, 2000).
10. R. Thomas, *Spectroscopy* **17**(2), 42–48, (2002).
11. R. Hutton, A. Walsh, D. Milton, and J. Cantle, *ChemSA* **17,** 213–215 (1992).
12. R. Thomas, *Spectroscopy* **16**(11), 22–27, (2001).
13. J.M. Collard, K. Kawabata, Y. Kishi, and R. Thomas, *Micro,* January, 2002.
14. J.A. Olivares and R.S Houk, *Anal. Chem.* **58,** 20 (1986).
15. S.D. Tanner, D.J. Douglas, and J.B. French, *Appl. Spectrosc.* **48,** 1373, (1994).
16. R. Thomas, *Spectroscopy* **16**(9), 38–46, (2001). ■

Table of Isotopic Masses and Natural Abundances

This table lists the mass and percent natural abundance for the stable nuclides. The mass of the longest lived isotope is given for elements without a stable nuclide. Nuclides marked with an asterisk (*) in the abundance column indicate that it is not present in nature or that a meaningful natural abundance cannot be given. The isotopic mass data is from G. Audi, A. H. Wapstra *Nucl. Phys A*. **1993**, *565*, 1-65 and G. Audi, A. H. Wapstra *Nucl. Phys A*. **1995**, *595*, 409-480. The percent natural abundance data is from the 1997 report of the IUPAC Subcommittee for Isotopic Abundance Measurements by K.J.R. Rosman, P.D.P. Taylor *Pure Appl. Chem.* **1999**, *71*, 1593-1607.

Z	Name	Symbol	Mass of Atom (u)	% Abundance
1	Hydrogen	^{1}H	1.007825	99.9885
	Deuterium	^{2}H	2.014102	0.0115
	Tritium	^{3}H	3.016049	*
2	Helium	^{3}He	3.016029	0.000137
		^{4}He	4.002603	99.999863
3	Lithium	^{6}Li	6.015122	7.59
		^{7}Li	7.016004	92.41
4	Beryllium	^{9}Be	9.012182	100
5	Boron	^{10}B	10.012937	19.9
		^{11}B	11.009305	80.1
6	Carbon	^{12}C	12.000000	98.93
		^{13}C	13.003355	1.07
		^{14}C	14.003242	*
7	Nitrogen	^{14}N	14.003074	99.632
		^{15}N	15.000109	0.368
8	Oxygen	^{16}O	15.994915	99.757
		^{17}O	16.999132	0.038
		^{18}O	17.999160	0.205
9	Fluorine	^{19}F	18.998403	100
10	Neon	^{20}Ne	19.992440	90.48
		^{21}Ne	20.993847	0.27
		^{22}Ne	21.991386	9.25
11	Sodium	^{23}Na	22.989770	100
12	Magnesium	^{24}Mg	23.985042	78.99
		^{25}Mg	24.985837	10.00
		^{26}Mg	25.982593	11.01
13	Aluminum	^{27}Al	26.981538	100
14	Silicon	^{28}Si	27.976927	92.2297
		^{29}Si	28.976495	4.6832
		^{30}Si	29.973770	3.0872
15	Phosphorus	^{31}P	30.973762	100
16	Sulphur	^{32}S	31.972071	94.93
		^{33}S	32.971458	0.76
		^{34}S	33.967867	4.29
		^{36}S	35.967081	0.02
17	Chlorine	^{35}Cl	34.968853	75.78
		^{37}Cl	36.965903	24.22
18	Argon	^{36}Ar	35.967546	0.3365
		^{38}Ar	37.962732	0.0632
		^{40}Ar	39.962383	99.6003
19	Potassium	^{39}K	38.963707	93.2581
		^{40}K	39.963999	0.0117
		^{41}K	40.961826	6.7302
20	Calcium	^{40}Ca	39.962591	96.941
		^{42}Ca	41.958618	0.647
		^{43}Ca	42.958767	0.135
		^{44}Ca	43.955481	2.086
		^{46}Ca	45.953693	0.004
		^{48}Ca	47.952534	0.187
21	Scandium	^{45}Sc	44.955910	100
22	Titanium	^{46}Ti	45.952629	8.25
		^{47}Ti	46.951764	7.44
		^{48}Ti	47.947947	73.72
		^{49}Ti	48.947871	5.41
		^{50}Ti	49.944792	5.18
23	Vanadium	^{50}V	49.947163	0.250
		^{51}V	50.943964	99.750
24	Chromium	^{50}Cr	49.946050	4.345
		^{52}Cr	51.940512	83.789
		^{53}Cr	52.940654	9.501
		^{54}Cr	53.938885	2.365
25	Manganese	^{55}Mn	54.938050	100
26	Iron	^{54}Fe	53.939615	5.845
		^{56}Fe	55.934942	91.754

Z	Name	Symbol	Mass of Atom (u)	% Abundance
		^{57}Fe	56.935399	2.119
		^{58}Fe	57.933280	0.282
27	Cobalt	^{59}Co	58.933200	100
28	Nickel	^{58}Ni	57.935348	68.0769
		^{60}Ni	59.930791	26.2231
		^{61}Ni	60.931060	1.1399
		^{62}Ni	61.928349	3.6345
		^{64}Ni	63.927970	0.9256
29	Copper	^{63}Cu	62.929601	69.17
		^{65}Cu	64.927794	30.83
30	Zinc	^{64}Zn	63.929147	48.63
		^{66}Zn	65.926037	27.90
		^{67}Zn	66.927131	4.10
		^{68}Zn	67.924848	18.75
		^{70}Zn	69.925325	0.62
31	Gallium	^{69}Ga	68.925581	60.108
		^{71}Ga	70.924705	39.892
32	Germanium	^{70}Ge	69.924250	20.84
		^{72}Ge	71.922076	27.54
		^{73}Ge	72.923459	7.73
		^{74}Ge	73.921178	36.28
		^{76}Ge	75.921403	7.61
33	Arsenic	^{75}As	74.921596	100
34	Selenium	^{74}Se	73.922477	0.89
		^{76}Se	75.919214	9.37
		^{77}Se	76.919915	7.63
		^{78}Se	77.917310	23.77
		^{80}Se	79.916522	49.61
		^{82}Se	81.916700	8.73
35	Bromine	^{79}Br	78.918338	50.69
		^{81}Br	80.916291	49.31
36	Krypton	^{78}Kr	77.920386	0.35
		^{80}Kr	79.916378	2.28
		^{82}Kr	81.913485	11.58
		^{83}Kr	82.914136	11.49
		^{84}Kr	83.911507	57.00
		^{86}Kr	85.910610	17.30
37	Rubidium	^{85}Rb	84.911789	72.17
		^{87}Rb	86.909183	27.83

Z	Name	Symbol	Mass of Atom (u)	% Abundance
38	Strontium	^{84}Sr	83.913425	0.56
		^{86}Sr	85.909262	9.86
		^{87}Sr	86.908879	7.00
		^{88}Sr	87.905614	82.58
39	Yttrium	^{89}Y	88.905848	100
40	Zirconium	^{90}Zr	89.904704	51.45
		^{91}Zr	90.905645	11.22
		^{92}Zr	91.905040	17.15
		^{94}Zr	93.906316	17.38
		^{96}Zr	95.908276	2.80
41	Niobium	^{93}Nb	92.906378	100
42	Molybdenum	^{92}Mo	91.906810	14.84
		^{94}Mo	93.905088	9.25
		^{95}Mo	94.905841	15.92
		^{96}Mo	95.904679	16.68
		^{97}Mo	96.906021	9.55
		^{98}Mo	97.905408	24.13
		^{100}Mo	99.907477	9.63
43	Technetium	^{98}Tc	97.907216	*
44	Ruthenium	^{96}Ru	95.907598	5.54
		^{98}Ru	97.905287	1.87
		^{99}Ru	98.905939	12.76
		^{100}Ru	99.904220	12.60
		^{101}Ru	100.905582	17.06
		^{102}Ru	101.904350	31.55
		^{104}Ru	103.905430	18.62
45	Rhodium	^{103}Rh	102.905504	100
46	Palladium	^{102}Pd	101.905608	1.02
		^{104}Pd	103.904035	11.14
		^{105}Pd	104.905084	22.33
		^{106}Pd	105.903483	27.33
		^{108}Pd	107.903894	26.46
		^{110}Pd	109.905152	11.72
47	Silver	^{107}Ag	106.905093	51.839
		^{109}Ag	108.904756	48.161
48	Cadmium	^{106}Cd	105.906458	1.25
		^{108}Cd	107.904183	0.89
		^{110}Cd	109.903006	12.49
		^{111}Cd	110.904182	12.80

Z	Name	Symbol	Mass of Atom (u)	% Abundance
		^{112}Cd	111.902757	24.13
		^{113}Cd	112.904401	12.22
		^{114}Cd	113.903358	28.73
		^{116}Cd	115.904755	7.49
49	Indium	^{113}In	112.904061	4.29
		^{115}In	114.903878	95.71
50	Tin	^{112}Sn	111.904821	0.97
		^{114}Sn	113.902782	0.66
		^{115}Sn	114.903346	0.34
		^{116}Sn	115.901744	14.54
		^{117}Sn	116.902954	7.68
		^{118}Sn	117.901606	24.22
		^{119}Sn	118.903309	8.59
		^{120}Sn	119.902197	32.58
		^{122}Sn	121.903440	4.63
		^{124}Sn	123.905275	5.79
51	Antimony	^{121}Sb	120.903818	57.21
		^{123}Sb	122.904216	42.79
52	Tellurium	^{120}Te	119.904020	0.09
		^{122}Te	121.903047	2.55
		^{123}Te	122.904273	0.89
		^{124}Te	123.902819	4.74
		^{125}Te	124.904425	7.07
		^{126}Te	125.903306	18.84
		^{128}Te	127.904461	31.74
		^{130}Te	129.906223	34.08
53	Iodine	^{127}I	126.904468	100
54	Xenon	^{124}Xe	123.905896	0.09
		^{126}Xe	125.904269	0.09
		^{128}Xe	127.903530	1.92
		^{129}Xe	128.904779	26.44
		^{130}Xe	129.903508	4.08
		^{131}Xe	130.905082	21.18
		^{132}Xe	131.904154	26.89
		^{134}Xe	133.905395	10.44
		^{136}Xe	135.907220	8.87
55	Cesium	^{133}Cs	132.905447	100
56	Barium	^{130}Ba	129.906310	0.106
		^{132}Ba	131.905056	0.101
		^{134}Ba	133.904503	2.417
		^{135}Ba	134.905683	6.592
		^{136}Ba	135.904570	7.854
		^{137}Ba	136.905821	11.232
		^{138}Ba	137.905241	71.698
57	Lanthanum	^{138}La	137.907107	0.090
		^{139}La	138.906348	99.910
58	Cerium	^{136}Ce	135.907144	0.185
		^{138}Ce	137.905986	0.251
		^{140}Ce	139.905434	88.450
		^{142}Ce	141.909240	11.114
59	Praseodymium	^{141}Pr	140.907648	100
60	Neodymium	^{142}Nd	141.907719	27.2
		^{143}Nd	142.909810	12.2
		^{144}Nd	143.910083	23.8
		^{145}Nd	144.912569	8.3
		^{146}Nd	145.913112	17.2
		^{148}Nd	147.916889	5.7
		^{150}Nd	149.920887	5.6
61	Promethium	^{145}Pm	144.912744	*
62	Samarium	^{144}Sm	143.911995	3.07
		^{147}Sm	146.914893	14.99
		^{148}Sm	147.914818	11.24
		^{149}Sm	148.917180	13.82
		^{150}Sm	149.917271	7.38
		^{152}Sm	151.919728	26.75
		^{154}Sm	153.922205	22.75
63	Europium	^{151}Eu	150.919846	47.81
		^{153}Eu	152.921226	52.19
64	Gadolinium	^{152}Gd	151.919788	0.20
		^{154}Gd	153.920862	2.18
		^{155}Gd	154.922619	14.80
		^{156}Gd	155.922120	20.47
		^{157}Gd	156.923957	15.65
		^{158}Gd	157.924101	24.84
		^{160}Gd	159.927051	21.86
65	Terbium	^{159}Tb	158.925343	100
66	Dysprosium	^{156}Dy	155.924278	0.06
		^{158}Dy	157.924405	0.10
		^{160}Dy	159.925194	2.34
		^{161}Dy	160.926930	18.91
		^{162}Dy	161.926795	25.51
		^{163}Dy	162.928728	24.90

Z	Name	Symbol	Mass of Atom (u)	% Abundance
		^{164}Dy	163.929171	28.18
67	Holmium	^{165}Ho	164.930319	100
68	Erbium	^{162}Er	161.928775	0.14
		^{164}Er	163.929197	1.61
		^{166}Er	165.930290	33.61
		^{167}Er	166.932045	22.93
		^{168}Er	167.932368	26.78
		^{170}Er	169.935460	14.93
69	Thulium	^{169}Tm	168.934211	100
70	Ytterbium	^{168}Yb	167.933894	0.13
		^{170}Yb	169.934759	3.04
		^{171}Yb	170.936322	14.28
		^{172}Yb	171.936378	21.83
		^{173}Yb	172.938207	16.13
		^{174}Yb	173.938858	31.83
		^{176}Yb	175.942568	12.76
71	Lutetium	^{175}Lu	174.940768	97.41
		^{176}Lu	175.942682	2.59
72	Hafnium	^{174}Hf	173.940040	0.16
		^{176}Hf	175.941402	5.26
		^{177}Hf	176.943220	18.60
		^{178}Hf	177.943698	27.28
		^{179}Hf	178.945815	13.62
		^{180}Hf	179.946549	35.08
73	Tantalum	^{180}Ta	179.947466	0.012
		^{181}Ta	180.947996	99.988
74	Tungsten	^{180}W	179.946706	0.12
		^{182}W	181.948206	26.50
		^{183}W	182.950224	14.31
		^{184}W	183.950933	30.64
		^{186}W	185.954362	28.43
75	Rhenium	^{185}Re	184.952956	37.40
		^{187}Re	186.955751	62.60
76	Osmium	^{184}Os	183.952491	0.02
		^{186}Os	185.953838	1.59
		^{187}Os	186.955748	1.96
		^{188}Os	187.955836	13.24
		^{189}Os	188.958145	16.15
		^{190}Os	189.958445	26.26
		^{192}Os	191.961479	40.78
77	Iridium	^{191}Ir	190.960591	37.3
		^{193}Ir	192.962924	62.7
78	Platinum	^{190}Pt	189.959930	0.014
		^{192}Pt	191.961035	0.782
		^{194}Pt	193.962664	32.967
		^{195}Pt	194.964774	33.832
		^{196}Pt	195.964935	25.242
		^{198}Pt	197.967876	7.163
79	Gold	^{197}Au	196.966552	100
80	Mercury	^{196}Hg	195.965815	0.15
		^{198}Hg	197.966752	9.97
		^{199}Hg	198.968262	16.87
		^{200}Hg	199.968309	23.10
		^{201}Hg	200.970285	13.18
		^{202}Hg	201.970626	29.86
		^{204}Hg	203.973476	6.87
81	Thallium	^{203}Tl	202.972329	29.524
		^{205}Tl	204.974412	70.476
82	Lead	^{204}Pb	203.973029	1.4
		^{206}Pb	205.974449	24.1
		^{207}Pb	206.975881	22.1
		^{208}Pb	207.976636	52.4
83	Bismuth	^{209}Bi	208.980383	100
84	Polonium	^{209}Po	208.982416	*
85	Astatine	^{210}At	209.987131	*
86	Radon	^{222}Rn	222.017570	*
87	Francium	^{223}Fr	223.019731	*
88	Radium	^{226}Ra	226.025403	*
89	Actinium	^{227}Ac	227.027747	*
90	Thorium	^{232}Th	232.038050	100
91	Protactinium	^{231}Pa	231.035879	100
92	Uranium	^{234}U	234.040946	0.0055
		^{235}U	235.043923	0.7200
		^{238}U	238.050783	99.2745

Z	Name	Symbol	Mass of Atom (u)	% Abundance
93	Neptunium	^{237}Np	237.048167	*
94	Plutonium	^{244}Pu	244.064198	*
95	Americium	^{243}Am	243.061373	*
96	Curium	^{247}Cm	247.070347	*
97	Berkelium	^{247}Bk	247.070299	*
98	Californium	^{251}Cf	251.079580	*
99	Einsteinium	^{252}Es	252.082972	*
100	Fermium	^{257}Fm	257.095099	*
101	Mendelevium	^{258}Md	258.098425	*
102	Nobelium	^{259}No	259.101024	*
103	Lawrencium	^{262}Lr	262.109692	*
104	Rutherfordium	^{263}Rf	263.118313	*
105	Dubnium	^{262}Db	262.011437	*
106	Seaborgium	^{266}Sg	266.012238	*
107	Bohrium	^{264}Bh	264.012496	*
108	Hassium	^{269}Hs	269.001341	*
109	Meitnerium	^{268}Mt	268.001388	*
110	Ununnilium	^{272}Uun	272.001463	*
111	Unununium	^{272}Uuu	272.001535	*
112	Ununbium	^{277}Uub	(277)	*
114	Ununquadium	^{289}Uuq	(289)	*
116	Ununhexium	^{289}Uuh	(289)	*
118	Ununoctium	^{293}Uuo	(293)	*

A Table of Polyatomic Interferences in ICP-MS

Thomas W. May and Ray H. Wiedmeyer
U.S. Geological Survey, Biological Resources Division
Columbia Environmental Research Center
4200 New Haven Road, Columbia, MO 65201 USA

Spectroscopic interferences are probably the largest class of interferences in ICP-MS and are caused by atomic or molecular ions that have the same mass-to-charge as analytes of interest. Current ICP-MS instrumental software corrects for all known atomic "isobaric" interferences, or those caused by overlapping isotopes of different elements, but does not correct for most polyatomic interferences. Such interferences are caused by polyatomic ions that are formed from precursors having numerous sources, such as the sample matrix, reagents used for preparation, plasma gases, and entrained atmospheric gases.

A prior knowledge of polyatomic interferences cited in the literature for a particular analyte mass may be helpful to the analyst for selecting reagents and conditions that would preclude or at least reduce the possibility of their formation. A good perspective of known polyatomic interferences is difficult because of the number of affected masses, the number of interferences themselves, and the number of literature references in which they are reported. In a review of the ICP-MS literature, reported polyatomic interferences were consolidated to produce a table that may serve as a useful tool for the ICP-MS analyst. For quick reference, the masses are arranged in alphabetical order by elemental symbol. This list of interferences is not intended to be complete, but does cover those more frequently reported.

A Table of Polyatomic Interferences in ICP-MS

Isotope	Abundance	Interference	Reference
^{107}Ag	51.8	$^{91}Zr^{16}O^+$	(6)(9)
^{109}Ag	48.2	$^{92}Zr^{16}O^1H^+$	(9)
^{27}Al	100.	$^{12}C^{15}N^+$, $^{13}C^{14}N^+$, $^{14}N^2$ spread, $^1H^{12}C^{14}N^+$	(11)(18)(29)
^{75}As	100.	$^{40}Ar^{35}Cl^+$, $^{59}Co^{16}O^+$, $^{36}Ar^{38}Ar^1H^+$, $^{38}Ar^{37}Cl^+$, $^{36}Ar^{39}K$, $^{43}Ca^{16}O_2$, $^{23}Na^{12}C^{40}Ar$, $^{12}C^{31}P^{16}O_2{}^+$	(2)(9)(15)(19)(22)(33)(34) (35)
^{197}Au	100.	$^{181}Ta^{16}O^+$	(9)
^{11}B	80.09	^{12}C spread	(18)
^{130}Ba	0.106	$^{98}Ru^{16}O_2{}^+$	(32)
^{132}Ba	0.101	$^{100}Ru^{16}O_2{}^+$	(32)
^{134}Ba	2.417	$^{102}Ru^{16}O_2{}^+$	(32)
^{136}Ba	7.854	$^{104}Ru^{16}O_2{}^+$	(32)
^{209}Bi	100.	$^{193}Ir^{16}O^+$	(32)
^{79}Br	50.54	$^{40}Ar^{39}K^+$, $^{31}P^{16}O_3{}^+$, $^{38}Ar^{40}Ar^1H^+$	(19)(22)
^{81}Br	49.46	$^{32}S^{16}O_3{}^1H^+$, $^{40}Ar^{40}Ar^1H^+$, $^{33}S^{16}O_3{}^+$	(19)(22)
^{40}Ca	96.97	$^{40}Ar^+$	(4)(22)
^{42}Ca	0.64	$^{40}Ar^1H_2$	(12)(22)
^{43}Ca	0.145	$^{27}Al^{16}O^+$	(21)
^{44}Ca	2.06	$^{12}C^{16}O_2$, $^{14}N_2{}^{16}O^+$, $^{28}Si^{16}O^+$	(12)(22)(29)
^{46}Ca	0.003	$^{14}N^{16}O_2{}^+$, $^{32}S^{14}N^+$	(22)
^{48}Ca	0.19	$^{33}S^{15}N^+$, $^{34}S^{14}N^+$, $^{32}S^{16}O^+$	(22)
^{110}Cd	12.5	$^{39}K_2{}^{16}O^+$	(6)
^{111}Cd	12.8	$^{95}Mo^{16}O^+$, $^{94}Zr^{16}O^1H^+$, $^{39}K_2{}^{16}O_2{}^1H^+$	(1)(6)
^{112}Cd	24.1	$^{40}Ca_2{}^{16}O_2$, $^{40}Ar_2{}^{16}O_2$, $^{96}Ru^{16}O^+$	(6)(32)
^{113}Cd	12.22	$^{96}Zr^{16}O^1H^+$, $^{40}Ca_2{}^{16}O_2{}^1H^+$, $^{40}Ar_2{}^{16}O_2{}^1H^+$, $^{96}Ru^{17}O^+$	(1)(6)(32)
^{114}Cd	28.7	$^{98}Mo^{16}O^+$, $^{98}Ru^{16}O^+$	(6)(32)
^{116}Cd	7.49	$^{100}Ru^{16}O^+$	(32)

Atomic Spectroscopy
Vol. 19(5), Sep./Oct. 1998

A Table of Polyatomic Interferences in ICP-MS (cont'd)

Isotope	Abundance	Interference	Reference
^{35}Cl	75.77	$^{16}O^{18}O^{1}H^{+}$, $^{34}S^{1}H^{+}$, $^{35}Cl^{+}$	(22)
^{37}Cl	24.23	$^{36}Ar^{1}H^{+}$, $^{36}S^{1}H^{+}$, $^{37}Cl^{+}$	(22)
^{59}Co	100.	$^{43}Ca^{16}O^{+}$, $^{42}Ca^{16}O^{1}H^{+}$, $^{24}Mg^{35}Cl^{+}$, $^{36}Ar^{23}Na^{+}$, $^{40}Ar^{18}O^{1}H^{+}$, $^{40}Ar^{19}F^{+}$	(5)(8)(9)(13)(19)(22)(29)(34)
^{50}Cr	4.35	$^{34}S^{16}O^{+}$, $^{36}Ar^{14}N^{+}$, $^{35}Cl^{15}N^{+}$ $^{36}S^{14}N^{+}$, $^{32}S^{18}O^{+}$, $^{33}S^{17}O^{+}$	(2)(15)(22)
^{52}Cr	83.76	$^{35}Cl^{16}O^{1}H^{+}$, $^{40}Ar^{12}C^{+}$, $^{36}Ar^{16}O^{+}$, $^{37}Cl^{15}N^{+}$ $^{34}S^{18}O^{+}$, $^{36}S^{16}O^{+}$, $^{38}Ar^{14}N^{+}$, $^{36}Ar^{15}N^{1}H^{+}$, $^{35}Cl^{17}O^{+}$	(1)(2)(9)(15)(18) (19)(22)(29)(35)
^{53}Cr	9.51	$^{37}Cl^{16}O^{+}$, $^{38}Ar^{15}N^{+}$, $^{38}Ar^{14}N^{1}H^{+}$, $^{36}Ar^{17}O^{+}$, $^{36}Ar^{16}O^{1}H^{+}$, $^{35}Cl^{17}O^{1}H^{+}$, $^{35}Cl^{18}O^{+}$, $^{36}S^{17}O^{+}$, $^{40}Ar^{13}C^{+}$	(1)(22)(29)(34)
^{54}Cr	2.38	$^{37}Cl^{16}O^{1}H^{+}$, $^{40}Ar^{14}N^{+}$, $^{38}Ar^{15}N^{1}H^{+}$, $^{36}Ar^{18}O^{+}$, $^{38}Ar^{16}O^{+}$, $^{36}Ar^{17}O^{1}H^{+}$, $^{37}Cl^{17}O^{+}$, $^{19}F_{2}{}^{16}O^{+}$	(2)(22)(29)(34)
^{133}Cs	100.	$^{101}Ru^{16}O_{2}{}^{+}$	(32)
^{63}Cu	69.1	$^{31}P^{16}O_{2}{}^{+}$, $^{40}Ar^{23}Na^{+}$, $^{47}Ti^{16}O^{+}$, $^{23}Na^{40}Ca^{+}$, $^{46}Ca^{16}O^{1}H^{+}$, $^{36}Ar^{12}C^{14}N^{1}H^{+}$, $^{14}N^{12}C^{37}Cl^{+}$, $^{16}O^{12}C^{35}Cl^{+}$	(2)(9)(19)(28)(29)
65Cu	30.9	$^{49}Ti^{16}O^{+}$, $^{32}S^{16}O_{2}{}^{1}H^{+}$, $^{40}Ar^{25}Mg^{+}$, $^{40}Ca^{16}O^{1}H^{+}$, $^{36}Ar^{14}N_{2}{}^{1}H^{+}$, $^{32}S^{33}S^{+}$, $^{32}S^{16}O^{17}O^{+}$, $^{33}S^{16}O_{2}{}^{+}$, $^{12}C^{16}O^{37}Cl^{+}$, $^{12}C^{18}O^{35}Cl^{+}$, $^{31}P^{16}O^{18}O^{+}$	(5)(15)(17)(21)(22)(29)(34)
^{163}Dy	24.97	$^{147}Sm^{16}O^{+}$	(27)(38)
^{166}Er	33.6	$^{160}Nd^{16}O$, $^{150}Sm^{16}O$	(38)
^{167}Er	22.94	$^{151}Eu^{16}O^{+}$	(27)
^{151}Eu	47.82	$^{135}Ba^{16}O^{+}$	(23)(27)
^{153}Eu	52.2	$^{137}Ba^{16}O^{+}$	(9)(38)
^{54}Fe	5.82	$^{37}Cl^{16}O^{1}H^{+}$, $^{40}Ar^{14}N$, $^{38}Ar^{15}N^{1}H^{+}$, $^{36}Ar^{18}O^{+}$, $^{38}Ar^{16}O^{+}$, $^{36}Ar^{17}O^{1}H^{+}$, $^{36}S^{18}O^{+}$, $^{35}Cl^{18}O^{1}H^{+}$, $^{37}Cl^{17}O$	(15)(18)(22)(29)(36)
^{56}Fe	91.66	$^{40}Ar^{16}O^{+}$, $^{40}Ca^{16}O^{+}$, $^{40}Ar^{15}N^{1}H^{+}$, $^{38}Ar^{18}O^{+}$, $^{38}Ar^{17}O^{1}H^{+}$ $^{37}Cl^{18}O^{1}H^{+}$	(3)(22)(29)
^{57}Fe	2.19	$^{40}Ar^{16}O^{1}H^{+}$, $^{40}Ca^{16}O^{1}H^{+}$, $^{40}Ar^{17}O^{+}$, $^{38}Ar^{18}O^{1}H^{+}$, $^{38}Ar^{19}F^{+}$	(8)(9)(21)(22)(29)(34)
^{58}Fe	0.33	$^{40}Ar^{18}O^{+}$, $^{40}Ar^{17}O^{1}H^{+}$	(22)
^{69}Ga	60.16	$^{35}Cl^{16}O^{18}O^{+}$, $^{35}Cl^{17}O_{2}{}^{+}$, $^{37}Cl^{16}O_{2}{}^{+}$, $^{36}Ar^{33}S^{+}$, $^{33}S^{18}O_{2}{}^{+}$, $^{34}S^{17}O^{18}O^{+}$, $^{36}S^{16}O^{17}O^{+}$, $^{33}S^{36}S^{+}$	(22)
^{71}Ga	39.84	$^{35}Cl^{18}O_{2}{}^{+}$, $^{37}Cl^{16}O^{18}O^{+}$, $^{37}Cl^{17}O_{2}{}^{+}$, $^{36}Ar^{35}Cl^{+}$, $^{36}S^{17}O^{18}O^{+}$, $^{38}Ar^{33}S^{+}$	(22)
^{155}Gd	14.8	$^{139}La^{16}O^{+}$	(3)
^{157}Gd	15.68	$^{138}B^{19}F^{+}$, $^{141}Pr^{16}O^{+}$	(26)(27)
^{70}Ge	20.51	$^{40}Ar^{14}N^{16}O^{+}$, $^{35}Cl^{17}O^{18}O^{+}$, $^{37}Cl^{16}O^{17}O^{+}$, $^{34}S^{18}O_{2}{}^{+}$, $^{36}S^{16}O^{18}O^{+}$, $^{36}S^{17}O_{2}{}^{+}$, $^{34}S^{36}S^{+}$, $^{36}Ar^{34}S^{+}$, $^{38}Ar^{32}S^{+}$, $^{35}Cl_{2}{}^{+}$	(22)(30)
^{72}Ge	27.4	$^{36}Ar_{2}{}^{+}$, $^{37}Cl^{17}O^{18}O^{+}$, $^{35}Cl^{37}Cl^{+}$, $^{36}S^{18}O_{2}{}^{+}$, $^{36}S_{2}{}^{+}$, $^{36}Ar^{36}S^{+}$ $^{56}Fe^{16}O^{+}$, $^{40}Ar^{16}O_{2}{}^{+}$, $^{40}Ca^{16}O_{2}{}^{+}$, $^{40}Ar^{32}S^{+}$	(22)(28)
^{73}Ge	7.76	$^{36}Ar_{2}{}^{1}H^{+}$, $^{37}Cl^{18}O_{2}{}^{+}$, $^{36}Ar^{37}Cl^{+}$, $^{38}Ar^{35}Cl^{+}$, $^{40}Ar^{33}S^{+}$	(22)
^{74}Ge	36.56	$^{40}Ar^{34}S^{+}$, $^{36}Ar^{38}Ar^{+}$, $^{37}Cl^{37}Cl^{+}$, $^{38}Ar^{36}S^{+}$	(22)
^{76}Ge	7.77	$^{36}Ar^{40}Ar^{+}$, $^{38}Ar^{38}Ar^{+}$, $^{40}Ar^{36}S^{+}$	(22)
^{177}Hf	18.5	$^{161}Dy^{16}O^{+}$	(27)
^{165}Ho	100.	$^{149}Sm^{16}O$	(27)

A Table of Polyatomic Interferences in ICP-MS (cont'd)

Isotope	Abundance	Interference	Reference
^{113}In	4.3	$^{96}Ru^{17}O^+$	(32)
^{39}K	93.08	$^{38}Ar^1H^+$	(22)(29)
^{40}K	0.01	$^{40}Ar^+$	(22)
^{41}K	6.91	$^{40}Ar^1H^+$	(22)
^{78}Kr	0.35	$^{38}Ar^{40}Ar^+$	(22)
^{80}Kr	2.27	$^{40}Ar_2^+$, $^{32}S^{16}O_3^+$	(22)
^{82}Kr	11.56	$^{40}Ar^{40}Ar^1H_2^+$, $^{34}S^{16}O_3^+$, $^{33}S^{16}O_3{}^1H^+$	(22)
^{83}Kr	11.55	$^{34}S^{16}O_3{}^1H^+$	(22)
^{84}Kr	56.9	$^{36}S^{16}O_3^+$	(22)
^{175}Lu	97.41	$^{159}Tb^{16}O^+$	(27)(38)
^{24}Mg	78.7	$^{12}C_2^+$	(29)
^{25}Mg	10.13	$^{12}C_2{}^1H^+$	(29)
^{26}Mg	11.17	$^{12}C^{14}N^+$, $^{12}C_2{}^1H_2^+$, $^{12}C^{13}C^1H^+$	(29)
^{55}Mn	100.	$^{40}Ar^{14}N^1H^+$, $^{39}K^{16}O^+$, $^{37}Cl^{18}O^+$, $^{40}Ar^{15}N^+$, $^{38}Ar^{17}O^+$, $^{36}Ar^{18}O^1H^+$ $^{38}Ar^{16}O^1H^+$, $^{37}Cl^{17}O^1H^+$, $^{23}Na^{32}S^+$, $^{36}Ar^{19}F^+$	(2)(9)(11)(19)(22)(29)(34) (35)
^{94}Mo	9.3	$^{39}K_2{}^{16}O^+$	(11)
^{95}Mo	15.9	$^{40}Ar^{39}K^{16}O^+$, $^{79}Br^{16}O^+$	(11)
^{96}Mo	16.7	$^{39}K^{41}K^{16}O^+$, $^{79}Br^{17}O^+$	(11)
^{97}Mo	9.6	$^{40}Ar_2{}^{16}O^1H^+$, $^{40}Ca_2{}^{16}O^1H^+$, $^{40}Ar^{41}K^{16}O^+$, $^{81}Br^{16}O^+$	(6)(11)
^{98}Mo	24.1	$^{81}Br^{17}O^+$, $^{41}K_2O^+$	(6)(11)
^{144}Nd	23.80	$^{96}Ru^{16}O_3^+$	(32)
^{146}Nd	17.19	$^{98}Ru^{16}O_3^+$	(32)
^{148}Nd	5.76	$^{100}Ru^{16}O^{3+}$	(32)
^{150}Nd	5.64	$^{102}Ru^{16}O_3^+$	(32)
^{58}Ni	67.77	$^{23}Na^{35}Cl^+$, $^{40}Ar^{18}O^+$, $^{40}Ca^{18}O^+$, $^{40}Ca^{17}O^1H^+$, $^{42}Ca^{16}O^+$, $^{29}Si_2^+$, $^{40}Ar^{17}O^1H^+$, $^{23}Na^{35}Cl^+$	(9)(16)(18)(19)(20)(22)(29)
^{60}Ni	26.16	$^{44}Ca^{16}O^+$, $^{23}Na^{37}Cl^+$, $^{43}Ca^{16}O^1H^+$	(3)(13)(26)(29)
^{61}Ni	1.25	$^{44}Ca^{16}O^1H^+$, $^{45}Sc^{16}O^+$	(1)(25)
^{62}Ni	3.66	$^{46}Ti^{16}O^+$, $^{23}Na^{39}K^+$, $^{46}Ca^{16}O^+$	(1)(9)(25)
^{64}Ni	1.16	$^{32}S^{16}O_2^+$, $^{32}S_2^+$	(22)(29)
^{31}P	100.	$^{14}N^{16}O^1H^+$, $^{15}N^{15}N^1H^+$, $^{15}N^{16}O^+$, $^{14}N^{17}O^+$, $^{13}C^{18}O^+$, $^{12}C^{18}O^1H^+$	(3)(22)(29)
^{206}Pb	24.1	$^{190}Pt^{16}O^+$	(32)
^{207}Pb	22.1	$^{191}Ir^{16}O^+$	(32)
^{208}Pb	52.4	$^{192}Pt^{16}O^+$	(32)
^{105}Pd	22.3	$^{40}Ar^{65}Cu^+$	(9)
^{103}Rh	100.	$^{40}Ar^{63}Cu^+$	(9)(26)
^{101}Ru	17.0	$^{40}Ar^{61}Ni^+$, $^{64}Ni^{37}Cl^+$	(9)
^{32}S	95.02	$^{16}O_2^+$, $^{14}N^{18}O^+$, $^{15}N^{17}O^+$, $^{14}N^{17}O^1H^+$, $^{15}N^{16}O^1H^+$, $^{32}S^+$ $^{14}N^{16}O^1H_2^+$	(9)(22)(29)
^{33}S	0.75	$^{15}N^{18}O^+$, $^{14}N^{18}O^1H^+$, $^{15}N^{17}O^1H^+$, $^{16}O^{17}O^+$, $^{16}O_2{}^1H^+$, $^{33}S^+$, $^{32}S^1H^+$	(22)(29)
^{34}S	4.21	$^{15}N^{18}O^1H^+$, $^{16}O^{18}O^+$, $^{17}O_2^+$, $^{16}O^{17}O^1H^+$, $^{34}S^+$, $^{33}S^1H^+$	(22)(29)
^{121}Sb	57.36	$^{105}Pd^{16}O^+$	(32)

Atomic Spectroscopy
Vol. 19(5), Sep./Oct. 1998

A Table of Polyatomic Interferences in ICP-MS (cont'd)

Isotope	Abundance	Interference	Reference
^{123}Sb	47.6	$^{94}Zr^{16}O_2$	(1)
^{45}Sc	100.	$^{12}C^{16}O_2{}^1H^+$, $^{28}Si^{16}O^1H^+$, $^{29}Si^{16}O^+$, $^{14}N_2{}^{16}O^1H^+$, $^{13}C^{16}O_2{}^+$	(2)(9)(22)(29)
^{74}Se	0.87	$^{37}Cl^{37}Cl^+$, $^{36}Ar^{38}Ar^+$, $^{38}Ar^{36}S^+$, $^{40}Ar^{34}S^+$	(9)(22)(35)
^{76}Se	9.02	$^{40}Ar^{36}Ar^+$, $^{38}Ar^{38}Ar^+$	(2)(10)(22)(35)
^{77}Se	7.58	$^{40}Ar^{37}Cl^+$, $^{36}Ar^{40}Ar^1H^+$, $^{38}Ar_2{}^1H^+$, $^{12}C^{19}F^{14}N^{16}O_2{}^+$	(2)(15)(19)(22)(34)
^{78}Se	23.52	$^{40}Ar^{38}Ar^+$, $^{38}Ar^{40}Ca^+$	(2)(24)(35)
^{80}Se	49.82	$^{40}Ar_2{}^+$, $^{32}S^{16}O_3{}^+$	(7)(19)(22)
^{82}Se	9.19	$^{12}C^{35}Cl_2{}^+$, $^{34}S^{16}O_3{}^+$, $^{40}Ar_2{}^1H_2{}^+$	(9)(11)(22)
^{28}Si	92.21	$^{14}N_2{}^+$, $^{12}C^{16}O^+$	(21)(22)(29)
^{29}Si	4.7	$^{14}N^{15}N^+$, $^{14}N_2{}^1H^+$, $^{13}C^{16}O^+$, $^{12}C^{17}O^+$, $^{12}C^{16}O^1H^+$	(22)(29)
^{30}Si	3.09	$^{15}N_2{}^+$, $^{14}N^{15}N^1H^+$, $^{14}N^{16}O^+$, $^{12}C^{18}O^+$, $^{13}C^{17}O^+$, $^{13}C^{16}O^1H^+$, $^{12}C^{17}O^1H^+$, $^{14}N_2{}^1H_2{}^+$, $^{12}C^{16}O^1H_2{}^+$	(22)(29)(31)
^{144}Sm	3.1	$^{96}Ru^{16}O_3{}^+$	(32)
^{147}Sm	15.0	$^{99}Ru^{16}O_3{}^+$	(32)
^{148}Sm	11.3	$^{100}Ru^{16}O_3{}^+$	(32)
^{149}Sm	13.8	$^{101}Ru^{16}O_3{}^+$	(32)
^{150}Sm	7.4	$^{102}Ru^{16}O_3{}^+$	(32)
^{152}Sm	26.7	$^{104}Ru^{16}O_3{}^+$	(32)
^{112}Sn	0.97	$^{96}Ru^{16}O^+$	(32)
^{115}Sn	0.34	$^{99}Ru^{16}O^+$	(32)
^{116}Sn	14.53	$^{100}Ru^{16}O^+$	(32)
^{117}Sn	7.68	$^{101}Ru^{16}O^+$	(32)
^{118}Sn	24.23	$^{102}Ru^{16}O^+$, $^{102}Pd^{16}O^+$	(32)
^{119}Sn	8.59	$^{103}Rh^{16}O^+$	(32)
^{120}Sn	32.59	$^{104}Ru^{16}O^+$, $^{104}Pd^{16}O^+$	(32)
^{122}Sn	4.63	$^{106}Pd^{16}O^+$	(32)
^{124}Sn	5.79	$^{108}Pd^{16}O^+$	(32)
^{84}Sr	0.56	$^{36}S^{16}O_3{}^+$	(22)
^{86}Sr	9.86	$^{85}Rb^1H^+$	(26)(27)
^{181}Ta	99.988	$^{165}Ho^{16}O^+$	(27)
^{159}Tb	100.	$^{143}Nd^{16}O^+$	(27)(38)
^{122}Te	2.603	$^{106}Pd^{16}O^+$	(32)
^{124}Te	4.816	$^{108}Pd^{16}O^+$	(32)
^{126}Te	18.95	$^{110}Pd^{16}O^+$	(32)
^{128}Te	31.69	$^{96}Ru^{16}O_2{}^+$	(32)
^{130}Te	33.80	$^{98}Ru^{16}O_2{}^+$	(32)
^{46}Ti	7.99	$^{32}S^{14}N^+$, $^{14}N^{16}O_2{}^+$, $^{15}N_2{}^{16}O^+$	(3)(22)(29)
^{47}Ti	7.32	$^{32}S^{14}N^1H^+$, $^{30}Si^{16}O^1H^+$, $^{32}S^{15}N^+$, $^{33}N^{14}N^+$, $^{33}S^{14}N^+$, $^{15}N^{16}O_2{}^+$, $^{14}N^{16}O_2{}^1H^+$, $^{12}C^{35}Cl^+$, $^{31}P^{16}O^+$	(3)(9)(22)(29)(37)
^{48}Ti	73.98	$^{32}S^{16}O^+$, $^{34}S^{14}N^+$, $^{33}S^{15}N^+$, $^{14}N^{16}O^{18}O^+$, $^{14}N^{17}N_2{}^+$, $^{12}C_4{}^+$, $^{36}Ar^{12}C^+$	(3)(18)(19)(22)(29)
^{49}Ti	5.46	$^{32}S^{17}O^+$, $^{32}S^{16}O^1H^+$, $^{35}Cl^{14}N^+$, $^{34}S^{15}N^+$, $^{33}S^{16}O^+$, $^{14}N^{17}O_2{}^1H^+$, $^{14}N^{35}Cl^+$, $^{36}Ar^{13}C^+$, $^{36}Ar^{12}C^1H^+$, $^{12}C^{37}Cl^+$, $^{31}P^{18}O^+$	(3)(22)(29)(37)

A Table of Polyatomic Interferences in ICP-MS (cont'd)

Isotope	Abundance	Interference	Reference
^{50}Ti	5.25	$^{32}S^{18}O^+$, $^{32}S^{17}O^1H^+$, $^{36}Ar^{14}N^+$, $^{35}Cl^{15}N^+$, $^{36}S^{14}N^+$, $^{33}S^{17}O^+$ $^{34}S^{16}O^+$, $^1H^{14}N^{35}Cl^+$, $^{34}S^{15}O^1H^+$	(3)(22)(29)
^{203}Tl	29.5	$^{187}Re^{16}O^+$, $^{186}W^{16}O^1H^+$	(3)
^{169}Tm	100.	$^{153}Eu^{16}O^+$	(27)
^{50}V	0.24	$^{34}S^{16}O^+$, $^{36}Ar^{14}N^+$, $^{35}Cl^{15}N^+$, $^{36}S^{14}N^+$, $^{32}S^{18}O^+$, $^{33}S^{17}O^+$	(2)(22)(29)
^{51}V	99.76	$^{34}S^{16}O^1H^+$, $^{35}Cl^{16}O^+$, $^{38}Ar^{13}C^+$, $^{36}Ar^{15}N^+$, $^{36}Ar^{14}N^1H^+$, $^{37}Cl^{14}N^+$, $^{36}S^{15}N^+$, $^{33}S^{18}O^+$, $^{34}S^{17}O^+$	(2)(3)(14)(15)(19)(22) (29)(35)
^{182}W	26.41	$^{166}Er^{16}O^+$	(27)
^{172}Yb	21.9	$^{156}Gd^{16}O^+$	(38)
^{173}Yb	16.13	$^{157}Gd^{16}O^+$	(27)
^{64}Zn	48.89	$^{32}S^{16}O_2^+$, $^{48}Ti^{16}O^+$, $^{31}P^{16}O_2{}^1H^+$, $^{48}Ca^{16}O^+$, $^{32}S_2^+$, $^{31}P^{16}O^{17}O^+$ $^{34}S^{16}O_2^+$, $^{36}Ar^{14}N_2^+$	(2)(9)(11)(15)(19)(22)(34) (35)
^{66}Zn	27.81	$^{50}Ti^{16}O^+$, $^{34}S^{16}O_2^+$, $^{33}S^{16}O_2{}^1H^+$, $^{32}S^{16}O^{18}O^+$, $^{32}S^{17}O_2^+$, $^{33}S^{16}O^{17}O^+$, $^{32}S^{34}S^+$, $^{33}S_2^+$	(9)(11)(15)(22)
^{67}Zn	4.11	$^{35}Cl^{16}O_2^+$, $^{33}S^{34}S^+$, $^{34}S^{16}O_2{}^1H^+$, $^{32}S^{16}O^{18}O^1H^+$, $^{33}S^{34}S^+$, $^{34}S^{16}O^{17}O^+$, $^{33}S^{16}O^{18}O^+$, $^{32}S^{17}O^{18}O^+$, $^{33}S^{17}O_2^+$, $^{35}Cl^{16}O_2^+$	(1)(9)(11)(15)(22) (35)
^{68}Zn	18.57	$^{36}S^{16}O_2^+$, $^{34}S^{16}O^{18}O^+$, $^{40}Ar^{14}N_2^+$, $^{35}Cl^{16}O^{17}O^+$, $^{34}S_2^+$, $^{36}Ar^{32}S^+$, $^{34}S^{17}O_2^+$, $^{33}S^{17}O^{18}O^+$, $^{32}S^{18}O_2^+$, $^{32}S^{36}S^+$	(11)(15)(22) (35)
^{70}Zn	0.62	$^{35}Cl^{35}Cl^+$, $^{40}Ar^{14}N^{16}O^+$, $^{35}Cl^{17}O^{18}O^+$, $^{37}Cl^{16}O^{17}O^+$, $^{34}S^{18}O_2^+$, $^{36}S^{16}O^{18}O^+$, $^{36}S^{17}O_2^+$, $^{34}S^{36}S^+$, $^{36}Ar^{34}S^+$, $^{38}Ar^{32}S^+$	(9)(22)

REFERENCES

1. J.W. McLaren, D. Beauchemin, and S.S. Berman, "Application of isotope dilution inductively coupled plasma masss spectrometry to the analysis of marine sediments." *Anal. Chem.* 59 (4), 610–613 (1987).
2. J.E. Longbottom, T.D. Martin, K.W. Edgell, S.E. Long, M.R. Plantz, and B.E. Warden, "Determination of trace elements in water by inductively coupled-plasma spectrometry: collaborative study." *J. AOAC* 77 (4), 1004-1023 (1994).
3. J.M. Corey and J.A. Caruso, "Electrothermal vaporization for sample introduction in plasma source spectrometry. Critical reviews in *Anal. Chem.* 23 (5), 397–439 (1992).
4. D. Beauchemin, J.W. McLauren, S.N. Willie, and S.S. Berman, "Determination of trace metals in marine biological reference materials by inductively coupled plasma mass spectrometry." *Anal. Chem.* 60 (7); 687–691 (1988).
5. A. Stroh and U. Völlkopf, "Effects of Ca on instrument stability in the trace element determination of Ca-rich soils using ICP-MS." *At. Spectrosc.* 14 (3); 76–79 (1993).
6. E.S. Beary and P.J. Paulsen, "Selective application of chemical separations to isotope dilution inductively coupled plasma mass spectrometric analyses of standard reference materials." *Anal. Chem.* 65 (11); 1602–1608 (1993).
7. V. Balaram, "Characterization of trace elements in environmental samples by ICP-MS." At. Spectrosc. 14 (6); 174–179 (1993).
8. J.W. McLarean, J.W.H. Lam, S.S. Berman, K. Akatsuka, and M.A. Azeredo, "On-line method for the analysis of sea-water for trace elements by inductively coupled plasma mass spectrometry." *J. Anal. At.. Spectrom.* 8, pp 279–286 (1993).
9. H. Evans and J. Giglio, "Interferences in inductively coupled plasma mass spectrometry - A Review." *J. Anal. At. Spectrom*. 8, 1–18 (1993).
10. L. Ebdon, A. Fisher, and P. Worsfold, "Determination of arsenic, chromium, selenium, and vanadium in biological samples by inductively coupled plasma mass spectrometry using on-line elimination of interference and preconcentration by flow injection." *J. Anal. At.. Spectrom.* 9, 611–614 (1994).
11. C. Vandecasteele, H. Vanhoe, and R. Dams, "Inductively coupled plasma mass spectrometry of biological samples." *J. Anal. At. Spectrom.*. 8, 781–786 (1993).
12. L. Ebdon, A. Fisher, H. Handley, and P. Jones, "Determination of trace metals in concentrated brines using inductively coupled plasma mass spectrometry on-line preconcentration and matrix elimi-

nation with flow injection." *J. Anal. At.. Spectrom.* 8, 979–981 (1993).

13. H. Vanhoe and R. Dams, "Use of inductively coupled plasma mass spectrometry for the determination of ultra-trace elements in human serum." *J. Anal. At.. Spectrom.* 9, 23–31 (1994).
14. G. Xiao and D. Beauchemin, "Reduction of matrix effects and mass discrimination in inductively coupled plasma mass spectrometry with optimized argon-nitrogen plasmas." *J. Anal. At.. Spectrom.* 9, 509–518 (1994).
15. J. Gossens and R. Dams, "Anion exchange for the elimination of spectral interference caused by chlorine and sulfur in inductively coupled plasma mass spectrometry." *J. Anal. At. Spectrom*. 7, 1167–1171 (1992).
16. J.W. McLaren, A.P. Mykytiuk, S.N. Willie, and S.S. Berman, S.S. "Determination of trace metals in seawater by inductively coupled plasma mass spectrometry with preconcentration on silica-immobilized 8-hydroxyquinoline." *Anal. Chem.* 57, 2907–2911 (1985).
17. Kuang-Shie Huang and Shiuh-Jen Jiang.. "Determination of trace levels of metal ions in water samples by inductively coupled plasma mass spectrometry after on-line preconcentration on SO3-oxine cellulose." *Fres. J. Anal. Chem.* 347, 238–242 (1993).
18. M-A. Vaughan,A.D. Baines, and D.M. Templeton, "Multielement analysis of biological samples by ICPMS II. Rapid survey method for profiling trace elements in body fluids." *Clin. Chem.* 37, 210–215 (1991).
19. H. Vanhoe, "A review of the capabilities of ICP-MS for trace element analysis in body fluids and tissues." *J. Trace Elem. Electrolytes Health Dis.* 7, 131-139 (1993).
20. M.R. Plantz, J.S. Fritz, F.F. Smith, and R.S. Honk, "Separation of trace metal complexes for analysis of samples of high salt content by inductively coupled plasma mass spectrometry." *Anal. Chem.* 61, 149–153 (1989).
21. J.K. Friel, C.S. Skinner, S.E. Jackson, and H.P. Longerich, "Analysis of biological reference materials, prepared by microwave dissolution, using inductively coupled plasma mass spectrometry." *Analyst* 115, 269-273 (1990).
22. S.H. Tan and G. Horlick, "Background spectral features in inductively coupled plasma/mass spectrometry." *Appl. Spectrosc.* 40, 445–460 (1986).
23. A. Stroh, F. Bea, and P.G. Montero, "Ultratrace-level determination of rare earth elements, thorium, and uranium in ultramafic rocks by ICP-MS." *At. Spectrosc.*1, 7–11 (1995).
24. U. Völlkopf and K. Barnes, "Rapid multielement analysis of urine." *At. Spectrosc.* 16 (1), 19–21 (1995).
25. D.M. Templeton, S.X. Xu, and L. Stuhne-Sekalee, "Isotope-specific analysis of Ni by ICP-MS: applications of stable isotope tracers to biokinetic studies." *Science of Total Envir.* 148, 253–262 (1994).
26. H.P. Longerich, G.A. Jenner, B.J. Fryer, and S.E. Jackson, "Inductively coupled plasma-mass spectrometric analysis of geological samples: a critical evaluation based on case studies." *Chem. Geol.* 83, 105–118 (1990).
27. G.A. Jenner, H.P. Longerich, S.E. Jackson,and B.J. Fryer, "ICP-MS - a powerful tool for high-precision trace-element analysis in earth sciences: evidence from analysis of selected U.S.G.S. reference samples." *Chem. Geol.* 83, 133–148 (1990).
28. E.S. Beary, P.J. Paulsen, and J.D. Fassett, "Sample preparation approaches for isotope dilution inductively coupled plasma mass spectrometric certification of reference materials." *J. Anal. At. Spectrom.* 9, 1363–1369 (1994).
29. N.M. Reed, R.O. Cairns, and R.C. Hutton, "Characterization of polyatomic ion interferences in inductively coupled plasma mass spectrometry using a high resolution mass spectrometer." *J Anal. At. Specrom.* 9, 88–896 (1994).
30. W. Tittes, N. Jakubowski, D. Stuwer, and G. Tolg," Reduction of some selected spectral interferences in inductively coupled plasma mass spectrometry." *J. Anal. At.. Spectrom.* 9, 1015–1020 (1994).
31. H. Kuss, D. Bossmann, and M. Muller, M. "Silicon determination in steel by ICP-MS." *At.. Spectrosc.* July/Aug, 148–150 (1994).
32. S.M. Graham and R.V.O. Robert, "The analysis of high-purity noble metals and their salts by ICP-MS." *Talanta* 41 (8), 1369-1375 (1994).
33. M.J. Campbell, C. Demesmay, and M. Olle, "Determination of total arsenic concentrations in biological matrices by inductively coupled plasma mass spectrometry." *J. Anal. At. Spectrom.* 9, 1379–1384 (1994).
34. I. Platzner, J.V. Sala, F. Mousty, P.R. Trincherini, and A.L. Polettini, "Signal enhancement and reduction of interferences in inductively coupled plasma mass spectrometry with an argon-trifluoromethane mixed aerosol carrier gas." *J. Anal. At. Spectrom.* 9, 719–726 (1994).
35. F. Laborda, M.J. Baxter, H.M. Crews, and J. Dennis, "Reduction of polyatomic interferences in inductively coupled plasma mass spectrometry by selection of instrumental parameters and using an argon-nitrogen plasma: Effect on multi-element analyses." *J. Anal. At. Spectrom.* 9, 727–736 (1994).
36. ELAN 6000 Training Manual, The Perkin-Elmer Corporation, Norwalk, CT USA, pp 1–11 (1995).
37. L. Yu, R. Koirtyohann, M. Rueppel, A. Skipor, and J. Jacobs, "Simultaneous determination of aluminum, titanium, vanadium in serum by electrothermal vaporization-inductively coupled plasma mass spectrometry." *J. Anal. At. Spectrom.* 1, 69–74 (1997).
38. Zhang Shuzhan and Shan Xiaoquan."The determination of rare earth elements in soil by inductively coupled plasma mass spectrometry." *At. Spectrosc.* 18 (5),140–144 (1997).